Handbook of Heterogeneous Catalysis

8 Volumes

Volume 3

Edited by
Gerhard Ertl, Helmut Knözinger, Ferdi Schüth,
and Jens Weitkamp

Second, Completely Revised and Enlarged Edition

WILEY-VCH

WILEY-VCH Verlag GmbH & Co. KGaA

5
Elementary Steps and Mechanisms

5.1
Chemisorption

5.1.1
Principles of Chemisorption

*Hans-Joachim Freund**

5.1.1.1 Introduction

The term "chemisorption" was coined in order to classify the interaction between a particle in the gas phase and a solid surface – that is, the result of the adsorption process [1]. If the interaction leads to the formation of a chemical bond, then the adsorbate formed is referred to as being "chemisorbed". Where chemical bond formation is not important, the process is classified as "physisorption". There are several conceptual problems with such a differentiation, which are briefly addressed in this chapter, and which indicate that a more detailed examination of the entire process of adsorbate formation is needed before a reliable classification may be carried out. In fact, as it turns out, for a conclusive classification one would need the full theoretical and experimental understanding of the system under investigation. Such an approach must include the static aspects (i.e., the energies involved) as well as the dynamic aspects (i.e., the processes involved in the formation of the adsorptive interactions).

Irving Langmuir, in 1916, introduced and investigated the idea that there can exist strong, short-range forces between adsorbates and a substrate [2, 3]. Previously, it was generally believed that more or less unspecified long-range forces (we would today call this physisorption) draw gases towards a solid. Langmuir, shortly after the introduction of the concept of an ordered lattice for the arrangement of the atomic constituents of a bulk solid by von Laue [4], considered an arrangement of atoms at the surface, a surface lattice that defines a specific density of adsorption sites. Atoms from a gas phase, for example, striking the surface may either bounce back into the gas phase or establish a bond to one of these sites. This process is equivalent to the formation of a surface chemical bond and was termed chemisorption [5–7]. Chemisorption lowers the free energy of the closed system containing the uncovered, "clean" surface and atoms or molecules from the gas phase. This lowering in energy can be measured via calorimetry or (less well-defined) by a Clausius–Clapeyron analysis of isostere data. It was therefore tempting to differentiate chemisorption with respect to physisorption via the energy that is deliberated in bond formation [1]. Such a definition involves a limiting energy, which separates chemisorption and physisorption regimes, and this was put in the neighborhood of 40 kJ mol^{-1} [1]. Clearly, such a definition is rather artificial, and today one generally disregards this type of differentiation solely on the basis of the enthalpy of formation. Today, the accepted definition of chemisorption is independent of thermochemical data and rests on the concept of a short-range chemical bond, which only forms when there is direct intermingling of the substrate and the adsorbate charge densities. In order then to differentiate between chemisorption and physisorption, one must understand the electronic structure of the system [6, 8]. Experimentally, this means that we cannot rest the definition on a single measurement of the heat of adsorption, but rather on an as-complete-as-possible spectroscopic characterization of the surface interacting with the adsorbate in comparison with the same measurements of the separated systems.

The interaction between say a gas phase, containing molecules AB, and a surface is discussed by considering various aspects of the process of AB–surface bond formation. We cover the dynamic aspects connected with the sticking of AB such as its dependence on the population of internal and external degrees of freedom of AB in the collision, mobility on the surface

* Corresponding author.

References see page 1410

Handbook of Heterogeneous Catalysis, 2nd Ed.
Edited by G. Ertl, H. Knözinger, F. Schüth, and J. Weitkamp

ISBN: 978-3-527-31241-2

(i.e., surface diffusion, etc.), and the energetics – which will be the starting point – all as a function of the surface coverage. We shall discuss associative versus dissociative chemisorption and its dependences on surface structure. Consideration of coadsorption and cooperativity in the adsorption process is as important as invoking the structure of the adsorbate, as well as the restructuring of the surface as it interacts with an adsorbate.

Some brief comments will also be made as to how chemisorption changes as a function of gas pressure.

5.1.1.2 Thermodynamics and Energetics

At this point, it is important to differentiate between macroscopic and microscopic surface phenomena. *Surface phenomena* can be treated macroscopically by chemical thermodynamics, in which atomic concepts are not necessary. Accordingly, the thermodynamic relationships can be derived on the basis of pressure, volume, surface area, composition, and temperature, which can be measured in a straightforward manner. Historically, therefore, the thermodynamic approach was pursued first. Before discussing the atomic aspects of the energy content of an adsorbate phase, we shall briefly summarize the important thermodynamic aspects – noting, however, that this cannot be a comprehensive treatment. For the latter, the reader is referred to the literature [1, 7, 9–12].

Consider an adsorbate phase consisting of n_a moles of a non-volatile adsorbent (surface) and n_s moles of an adsorbate (gas phase). They are assigned internal energy U, entropy S, and volume V. The surface A of the adsorbent is assumed to be proportional to the adsorbent volume. The Gibbs fundamental equation for the full system is then

$$dG = -SdT + VdP + \mu_a dn_a + \mu_s dn_s \tag{1}$$

For the pure adsorbent,

$$dG^o = -S_a dT + V_a dP + \mu_a^o dn_a \tag{2}$$

Consequently, for the interacting adsorbate–adsorbent system, the difference $dG^s = dG - dG^o$ gives

$$dG^s = -S_s dT + V_s dP + \Phi dn_a + \mu_a dn_s \tag{3}$$

where $S_s = S - S_a$, $V_s = V - V_a$, and $\Phi = \mu_a - \mu_a^o$. Using the above-mentioned proportionality between adsorbent volume and adsorbent surface,

$$\Phi dn_a = f\Phi dA \tag{4}$$

where f is a proportionality factor, the surface tension ϕ is given by

$$f\Phi = \varphi = \left(\frac{\partial G^s}{\partial A}\right)_{T,P,n} \tag{5}$$

which has the dimension of a two-dimensional pressure. This leads to the final equation

$$dG^s = -S_s dT + V_s dP + \varphi dA + \mu_s dn_s \tag{6}$$

This equation refers to a system where the adsorbate resides on a truly inert substrate. In other words, Eq. (6) can only rigorously be applied to weakly interacting physisorbate systems. For chemisorbates, this equation is not strictly applicable because the thermodynamic parameters of adsorbate and adsorbent cannot be separated.

Bearing this restriction in mind, and assuming that the adsorbate phase is in equilibrium with the gas phase, a Clausius–Clapeyron analysis yields

$$\left(\frac{\partial 1nP}{\partial T}\right) = \frac{(S_g - S_s)}{RT} = \frac{(h_g - h_s)}{RT^2} = -\frac{\Delta h_{ads}}{RT^2} \tag{7}$$

where we have changed to molar quantities s, v, and the enthalpy h. The slope of a semilogarithmic plot of the equilibrium pressure versus the inverse temperature at constant ϕ yields the adsorption enthalpy, Δh_{ads}, released upon adsorption of 1 mole of gas. The problem, of course, arises because the surface tension is difficult to determine in general. However, the problem may be circumvented by considering the so-called surface coverage Θ instead:

$$\Theta = \frac{n_s}{n_a} \tag{8}$$

and resorting to partial molar quantities, e.g.,

$$\tilde{v}_s = \left(\frac{\partial v}{\partial n_s}\right)_{T,P,n_a} \tag{9}$$

Then, a similar Clausius–Clapeyron analysis leads to

$$\left(\frac{\partial 1nP}{\partial T}\right)_\Theta = \frac{(S_g - \tilde{S}_s)}{RT} = \frac{(h_g - \tilde{h}_s)}{RT^2} = \frac{-q_{st}}{RT^2} \tag{10}$$

where q_{st} is the isosteric heat of adsorption. This quantity can be measured quite easily because constant coverage is not too difficult to establish experimentally. However, q_{st} represents the difference between molar enthalpy in the gas phase and partial molar enthalpy in the adsorbed phase – a quantity not easily connected to microscopic considerations.

In order to see directly how the isosteric heat of adsorption is measured, Eq. (10) is written in the form

$$\frac{dP}{P} = \left(\frac{-q_{st}}{RT^2}\right) dT \tag{11}$$

and integrated over a reasonably small pressure and temperature interval so that we can assume the isosteric heat to be constant. This yields

$$1n\left(\frac{P_1}{P_2}\right) = \frac{q_{st}}{R}\left(\frac{1}{T_1} - \frac{1}{T_2}\right) \tag{12}$$

for two pairs of temperatures and pressures that produce the same surface coverage. For true equilibrium conditions, a straight line with negative slope should be obtained for the semilogarithmic plot, which in turn yields the isosteric heat of adsorption. Repeating this procedure for various coverages allows the coverage dependence of the heat of adsorption to be determined. It is clear that the isosteric heat is a differential quantity, in contrast to the equilibrium heat of adsorption. Both are, of course, isothermal quantities. From the differential heats of adsorption the integral heat of adsorption can be obtained as

$$Q_{\text{integr}} = \int_o^{ns} q_{st}\, dn_s \tag{13}$$

In the following, we present an example of isosteric heat determination [13]. Figure 1 shows, in the upper panel, a set of four isotherms for the physisorption system Xe/Ni(100). The second panel contains the data set in the upper panel as a plot of p_{Xe} versus reciprocal temperature for various values of Θ_{Xe}. From the shape of the individual straight lines the isosteric heat has been determined and plotted in the third panel as a function of Θ_{Xe}. From the plot we see that the isosteric heat slowly varies with coverage, the decrease indicating repulsive interactions.

As mentioned above, the application of an isosteric heat analysis to a chemisorption system is rather problematic, because inherently the analysis starts from the assumption of truly separable subsystems. Therefore, for such systems it is more appropriate to resort to a direct calorimetric measurement of the adsorption enthalpy. Until very recently, it has only been possible to undertake such measurements for thin-film systems [1, 14–19]. The reason for this was that the increase in temperature

References see page 1410

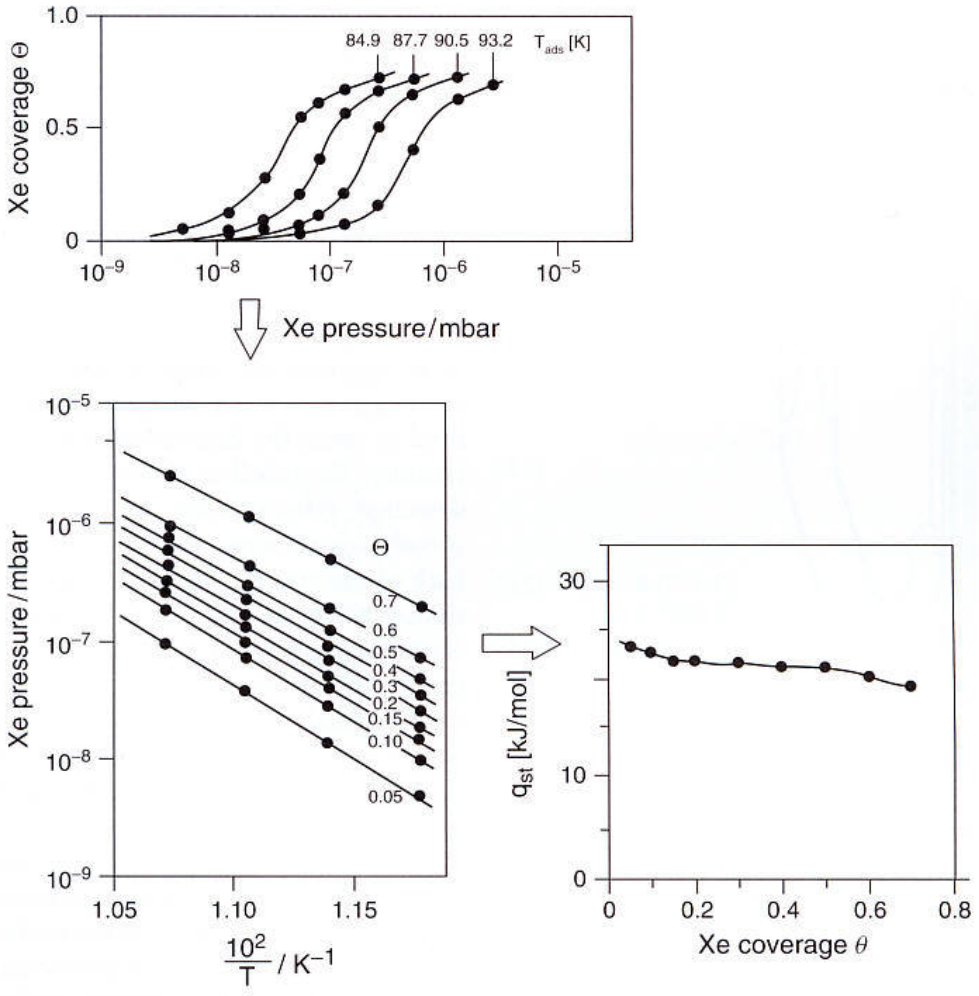

Fig. 1 Determination of the isosteric heat of adsorption from the measurement of adsorption isotherms for the system Xe/Ni(100) [13].

of the calorimeter depends on the heat capacity of the system and the absolute number of adsorbed particles. The most complete set of data for such thin-film systems has been reported by Wedler and coworkers [1, 20]. These authors used the so-called "spherical calorimeter" shown in Fig. 2 [17]. Briefly, the calorimeter sphere is located inside an ultrahigh-vacuum (UHV) glass recipient, and temperatures change of less than 10^{-5} K are registered with a thermometer connected to the calorimeter sphere. The metal film is evaporated onto the sphere and gas admitted. The change in temperature measured by the thermometer surrounding the calorimeter sphere upon gas exposure is plotted versus time (see Fig. 3). The heat of adsorption is determined from the integral of the T versus t curve. The example here is the adsorption of H_2 onto a Pd film [21]. Converting the temperature–time curve into a heat of adsorption yields 88 kJ mol^{-1} [21].

The heats of adsorption for various adsorbate systems on different substrates determined via isosteric heat measurement as well as calorimetric measurements are assembled in Table 1. In some cases, the heat of adsorption for one system has been measured using different techniques. This allows an estimation of the error involved in

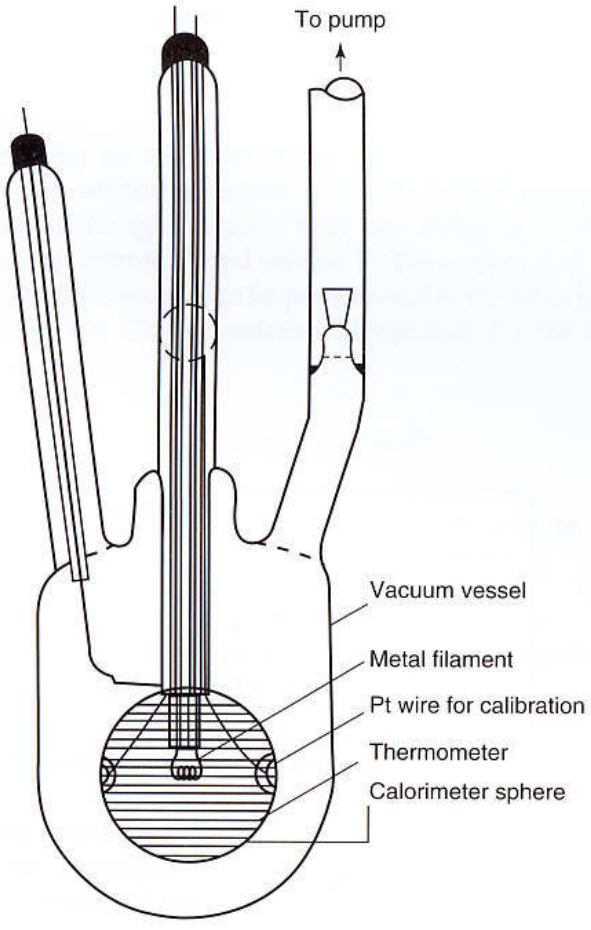

Fig. 2 Schematic diagram of the spherical calorimeter [19].

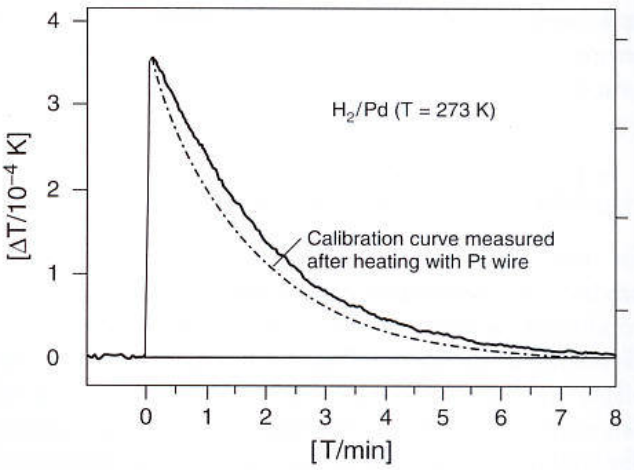

Fig. 3 Temperature–time curve of a calorimetric measurement for the system H_2/Pd [21].

using those values based on different measurements. It is clear that the value for CO adsorption on Fe, for example, is considerably higher than values for other CO-adsorbate systems. In order to judge this, it must be understood that, at room temperature, CO partly dissociates on polycrystalline Fe and this contributes to the observed calorimetric value. This is a useful reminder that consecutive processes must be considered in calorimetric measurements.

King and coworkers have recently extended calorimetric measurements to single-crystal surfaces by applying molecular beam techniques in combination with IR radiation emission measurements (Fig. 4) [22–26]. There are three important parts of the experiment. First, there is a molecular beam source to provide accurate determination of coverage. Second, the sample consists of an unsupported single-crystal thin film to reduce the thermal mass to a minimum. Finally, an IR detector is used to sense the heat radiated as the gas adsorbs. Very recently, Campbell et al. have proposed an alternative detection system based on the use of one or several pyroelectric ribbons which are gently pressed against the back of the crystal. When the surface of the pyroelectric ribbon touching the crystal changes temperature, an electric voltage builds up which can be measured with great accuracy (see inset in Fig. 4). Even thicker (≈75 μm) single crystals may be used [27, 28]. In order to reduce white noise, the experiments are performed using a pulsed molecular beam, which must be capable of producing a significant enthalpy change per pulse upon adsorption. In Table 1, a set of results is included which are compared with those from other thermodynamic measurements. It is interesting to note that the results for the single-crystal surfaces are situated in the region of those determined for the polycrystalline films, indicating that the latter consist of many crystallites exposing low-index planes.

Tab. 1 Enthalpies of adsorption

Adsorbate	*Substrate*	*q/kJ mol^{-1}*		*Remarks*	*Reference*
CO	Ni(111)	111	(±5)	WF	[71]
		130		Microcalorimetry	[22]
	Ni(100)	125	(0 ± 5)	WF	[287]
		115		TDS	[288]
		119		TDS	[289]
		138		TDS	[290]
		109		Isosteric E_{ad}	[291]
		123		Isosteric E_{ad}	[287]
		130		Isosteric E_{ad}	[292]
		134		Isosteric E_{ad}	[293]
		123		Microcalorimetry	[22]
	Ni(110)	133		Microcalorimetry	[22]
	Pd(100)	150	(±5)	WF	[58]
		161	(±8)	WF, TDS, LEED	[72]
	Pd(111)	142	(±3)	WF	[96]
	Ru(0001)	160	(±10)	WF	[294]
	Ru(1010)	157	(±10)	Contact-pot., TDS	[295]
	Cu(106)	58	(±10)	WF	[296]
	Fe(111)	325		273 K (dissociative)	[297]
	Fe(111)	200		195 K (partially diss.)	[297]
	Fe(111)	100		(not dissociative)	[20]
CO/K	Ni(100)	190		Microcalorimetry	[23]
CO_2	Fe	300		195 K (dissociative)	[297]
H_2	Ni(100)	96.3	(±5)	WF	[73]
	Ni(110)	90.0	(±5)	WF	[73]
	Ni(111)	96.3	(±5)	WF	[73]
		85	(±5)		[298]
	Ni	75 · · · 176			[1]
	Pd(111)	88	(±5)	WF	[299]
	Pd(110)	103	(±5)	WF	[300]
	Pd(100)	102	(±5)	WF	[299]
	Rh(110)	92	(±5)	WF, TDS	[301]
	Ru(1010)	80	(±5)		[302]
	Co(1010)	80	(±5)		[303]
	Ta	188.1			[1]
	W	188.1			[1]
	Cr	188.1			[1]
	Fe	133.8			[1]
	Fe	100		Dissociative (273 K)	[20]
	Fe	97	(±3)		[297]
	Pd	80/96			[21]
Na	W	133.8			[1]
Cs		267.5			[1]
O	Ni(100)	532	(±5)	IR (300 K)	
		≈432		IR (100 K)	
		532	(±5)		[22]
	Ni(111)	470	(±15)		[22]
	Ni(110)	498	(±5)		[22]
O_2/CO	Fe(111)	490		273 K	[20]

TDS, thermal desorption spectroscopy; WF, work function.

The free enthalpy of adsorption is determined by the enthalpy, as well as the entropy of adsorption. The entropy of adsorption – which is the quotient of the reversibly exchanged heat and the temperature – may be calculated from the equilibrium heat of adsorption, if the surface tension is known, or from the isosteric heat of adsorption. One prerequisite is knowledge of the corresponding equilibrium gas pressure. Some typical values for the

References see page 1410

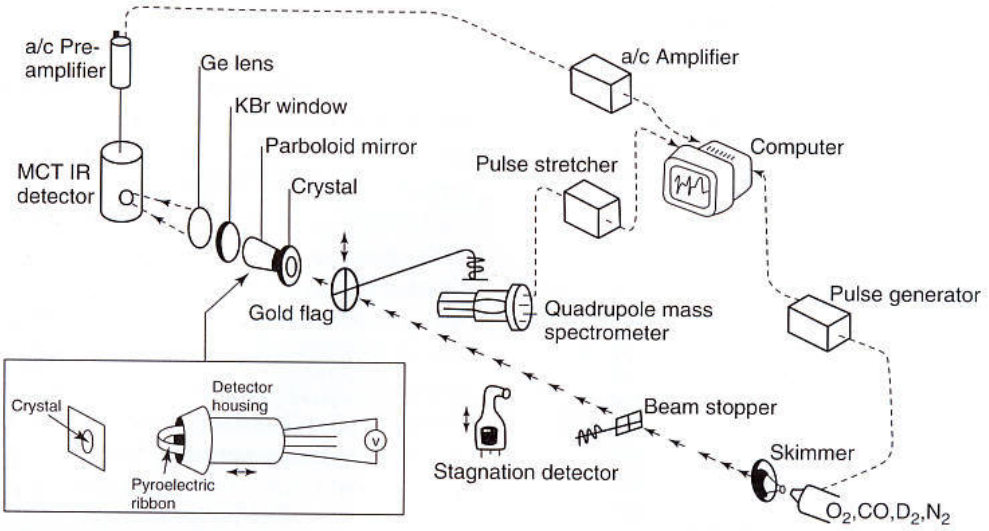

Fig. 4 Schematic diagram of the set-up for microcalorimetric measurements on single crystals [24].

Tab. 2 Entropies of adsorption

Adsorbate	*Substrate*	ΔS^0_{ad}/J K^{-1} mol^{-1}	*References*
Xe	Ni(100)	≈56	[13, 300]
	Pd(100)	≈58	[304]
H	Pd(100)	≈263	[300]
N_2	Ni(100)	≤550	[305]
	Ni(110)	112 (±5)	[306]

entropy of adsorption of several adsorbate systems are listed in Table 2.

The number of values available is much smaller than for the enthalpies of adsorption. The interpretation of entropies is considerably more involved than the interpretation of enthalpies. Often, the observed values – and, in particular, the coverage dependencies – cannot be reconciled on the basis of theoretical predictions. It appears that the predictions as to how the various degrees of freedom of the adsorbate contribute are not yet sufficiently accurate enough. However, in most cases large entropy values are found when the mobility of the adsorbate was expected or known (from other methods) to be large.

The most popular method by which to deduce the heat of adsorption of an adsorbate system is thermal desorption spectrometry (TDS) [29–33]. A schematic set-up for a TDS measurement is shown in Fig. 5 [34]. The sample is heated resistively and the temperature monitored using a thermocouple. If the sample is a single crystal it responds rather rapidly to heating, so that relatively high heating rates may be used. The concentration of desorbing species is measured with a quadrupole mass spectrometer (QMS). Pumping capacity is important in thermal desorption, because readsorption of the desorbing species back onto

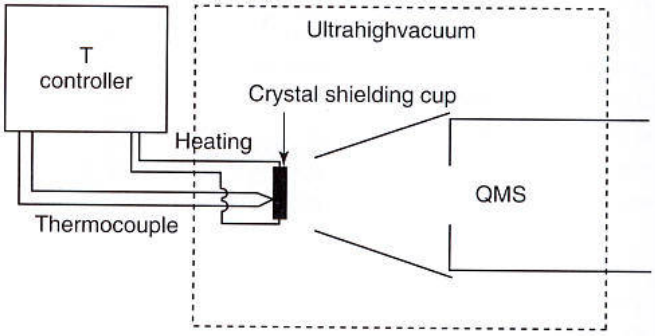

Fig. 5 Schematic diagram of the experimental set-up for a thermal desorption experiment.

the surface is excluded only if the pumping capacity is high enough. If the pumping speed is infinitely high we can ignore readsorption and the change in adsorbate coverage per unit time; then, a measure for the desorption rate (r_{des}), is given by the Wigner–Polanyi equation [7, 35]:

$$r_{des} = -\frac{d\Theta}{d_t} = k_{des}\Theta^n = \nu(\Theta)\Theta^n \exp\left\{-\frac{E_{des}(\Theta)}{RT}\right\} \tag{14}$$

where $T = T_o + \beta t$. This is the basis for the analysis of thermal desorption spectra.

Figure 6 shows, schematically, a set of TDS spectra for various initial coverages Θ_o and a given heating rate, β [7, 34]. The first step is the integration of the spectra starting from the highest temperature (i.e., coverage $\Theta = 0$) to a given coverage Θ' (e.g., 0.15). This yields a pair of (r, T) values for each initial coverage larger than $\Theta' = 0.15$. A plot of $\ln r$ versus $1/T$ yields $E_{des}(\Theta')$ from the slope and ν (Θ') from the intercept, which is given by $n\ln\Theta' + \ln\nu(\Theta')$, if the order n of the

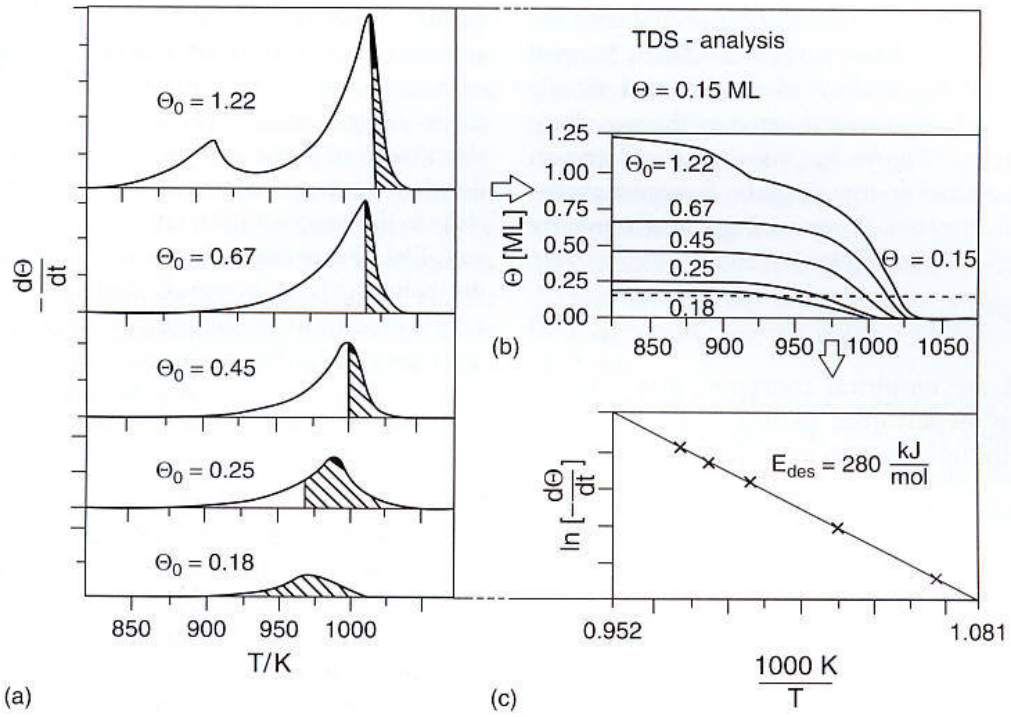

Fig. 6 Determination of the desorption energy E_{des} from a model-independent analysis of thermal desorption data. The analysis is carried out for an artificially chosen coverage of $\Theta = 0.15$: (a) TDS data; (b) integration of the TDS data to give Θ versus T plots; (c) plot of $\ln d\Theta/dt$ versus $1/T$ to determine E_{des} according to Eq. (14). The basis for the diagram are data for Ag/Ru(0001) [34].

desorption reaction is known. However, for coverages above 0.1, the second term is much larger than the first, so the latter may be neglected without large errors. It should be noted that there are methods to determine the order rigorously. This analysis, called the "complete analysis", was first proposed by King in 1975 [31]. The pre-exponential factor $\nu(\Theta)$ can be regarded as representing the frequency of attempts of the adsorbed particle to escape the chemisorptive potential. The values determined vary by at least four orders of magnitude, from 10^{12} to 10^{16} s^{-1} [7]. If we adopt the simplest picture and set $\nu(\Theta)$ equal to the frequency of vibration of the adsorbed particle, then values near 10^{13} s^{-1} are expected. The problems become even more involved if we consider the number of successful attempts – that is, after multiplication of $\nu(\Theta)$ by the exponential in Eq. (14). Here, the activation energy for desorption $E_{des}(\Theta)$ comes into play; both $\nu(\Theta)$ and $E_{des}(\Theta)$ depend on coverage. These coverage dependencies partly compensate each other for certain systems in the sense that high values of $\nu(\Theta)$ are associated with large values of E_{des} [7]. This point must be considered when dealing with predictions and interpretations of desorption rates. It is, therefore, important to resort to a complete or close-to-complete analysis of desorption data. Simplified analyses were published much earlier, with the most popular version being the so-called Redhead analysis; this is based on the peak maximum temperature observed in a thermal desorption spectrum [30]:

$$E_{des} = RT_{max}[\ln(\nu T_{max}/\beta) - 3.46] \quad (15)$$

It results in reliable values only for first-order desorption and provided that a reliable value for υ is available. The Redhead equation can be directly derived from the Wigner–Polanyi equation by determining the temperature derivative of the rate, and realizing that it must vanish at the peak maximum temperature [7]. Additional procedures have been reported in the literature [34, 36, 37]. In connection with the initial question concerning the heat of adsorption, it must be realized that the desorption energy may be directly related to the heat of adsorption if adsorption is a non-activated process. In other words, the adsorption process is, in energetic terms, continuously "downhill". A detailed understanding, however, necessitates an understanding of the dynamics of adsorption.

A connection exists between the phenomenological view of the energetics from the standpoint of thermodynamics, and the microscopic view of adsorbate energetics. In this context the question as to whether a process is activated or non-activated may already have been answered.

This approach goes back to Lennard-Jones, who discussed adsorption energetics in a landmark paper in 1932 when applying a quasi-one-dimensional approach [38].

References see page 1410

Neglect for the moment all problems connected with the question as to how a gas-phase particle is actually trapped in a bound state at the surface of a solid, and simply consider the interaction potential between the gas-phase particle and a surface. Figure 7(a) shows the well-known Lennard-Jones potential energy diagram. It represents the superposition of attractive (longer range) and repulsive (short range) forces according to

$$E(z) = -Az^{-6} + Bz^{-12} \tag{16}$$

where A and B are empirical constants, and z is the distance between the adsorbed particle and the surface. In order to describe this interaction on the basis of *ab initio* quantum mechanical calculations it would be necessary to consider a semi-infinitive solid interacting with an atom or a molecule. This can be done in favorable, simple cases using a variety of approaches [39–42]. The most prominent of these – at least for metal surfaces – is the density functional approach, with which one can come close to the exact solution [39, 41]. Another approach is the so-called "embedded cluster *ab initio*" approach, where the solid surface is represented by a cluster of atoms, augmented by an embedding scheme to represent more accurately the infinite extension of the two-dimensional (2-D) system [42]. Assume for the moment that this problem has been solved. Then, the potential energy curve in Fig. 7(a) represents the case where the particle incident from the gas phase "sees" a continuously "downhill" energy change until it reaches the equilibrium position at z_o. (Note that, for the present, the dynamics of the trapping process is being neglected.) In such a case the desorption energy, as determined from thermal desorption data, is equivalent to the heat of adsorption. It is this situation that is often considered for associative molecular adsorption. However, the situation becomes more difficult if either a molecule which is associatively adsorbed may assume different adsorption geometries on the surface, or the molecule may dissociate upon adsorption and – to increase complexity – may do so via a molecularly adsorbed precursor state. Figures 7b and c show schematically the corresponding quasi-one-dimensional (1-D) potential energy diagrams. In Fig. 7(b) there is a second minimum in the potential energy diagram representing the two possible adsorption geometries. It is already clear that, in this case, the use of such a quasi-1-D diagram becomes very problematic because only a single spatial coordinate is used to represent the molecule–surface interaction. Therefore, such a situation calls for a multidimensional potential energy diagram (we will return to this more general requirement later). For the moment, however, Fig. 7(b) already allows us to visualize the transformation between the two inequivalent molecular adsorption geometries as an activated process. It is immediately clear that a desorption experiment will probe this more complicated potential energy curve, and thus a simple interpretation of the measured desorption energy as the heat of adsorption will not be possible in general.

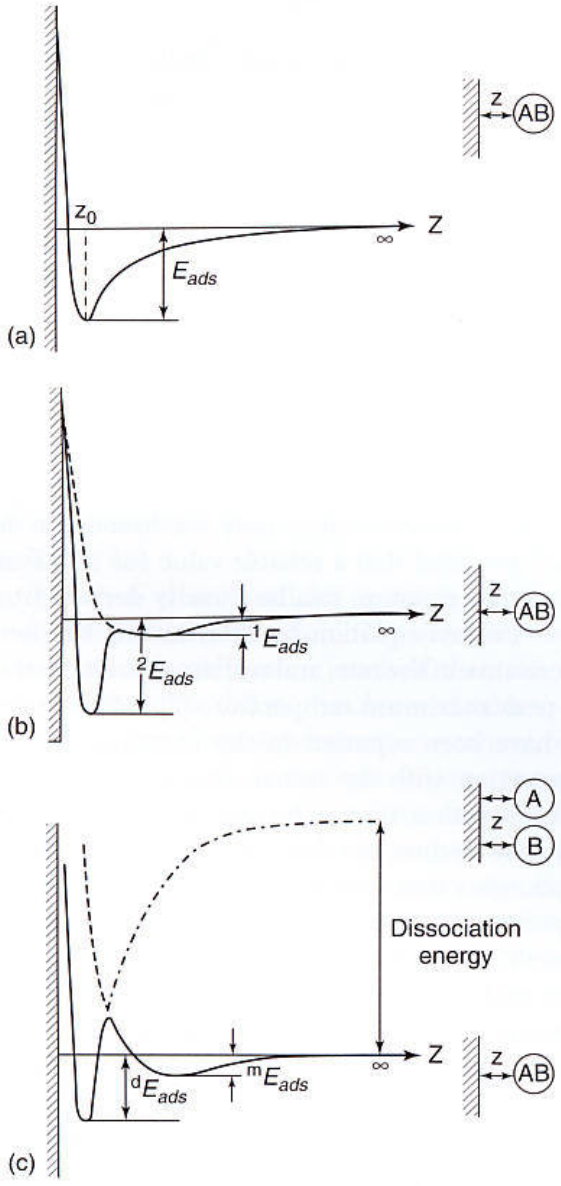

Fig. 7 Schematic potential energy diagrams for a molecule AB approaching a surface. (a) Associative chemisorption (E_{ads}); (b) associative chemisorption ($^2E_{ads}$) with precursor ($^1E_{ads}$); (c) dissociative chemisorption ($^dE_{ads}$) with molecular precursor ($^mE_{ads}$).

The situation becomes even more complicated if, upon interaction with the surface, the molecule dissociates. This is depicted in Fig. 7(c). In this case it is necessary to consider two intersecting potential energy curves which refer to two different zero-energy levels, namely the diatomic molecule being infinitely separated from the surface for the associative interaction, as well as the two constituent atoms being infinitely separated from the surface. The difference between the reference levels, of

course, represents the heat of formation of the diatomic molecule in the gas phase. In this case, the above-mentioned difficulty with the quasi-1-D representation becomes particularly clear, in the sense that here the coordinate representing the separation between the two constituent atoms has not been considered at all. Nevertheless, it can be seen that there may be a rather large activation energy between the molecularly adsorbed precursor and the dissociatively adsorbed atoms, which is very crudely represented by the energy near the crossing point with respect to the potential energy minimum of the molecular precursor. Clearly, the point of intersection may be situated well above the reference level corresponding to the infinitely separated molecule and surface, which in turn has strong consequences for the ability to populate the dissociative adsorbate. As will become clearer when considering multidimensional potential energy surfaces in such a situation, the molecule must have a certain impact energy to be able to surmount the activation barrier. Whether this impact energy should be represented by translational degrees of freedom or internal (rotational or vibrational) degrees of freedom cannot be concluded on the basis of the quasi-1-D potential energy surface. However, it is already fully transparent that the shape of the potential energy surfaces will determine the kinetics as well as the dynamics of the system, and thus the probability to chemisorb. Experimentally, we measure (for example) the sticking probability of a particle from the gas phase into a particular adsorbate channel by probing the number of adsorbed species as a function of gas pressure and surface temperature. In other words, a relatively complex scenario is condensed into basically a single number. As shown in the next section, it is far from easy to resolve the details.

Before tackling the problem of sticking, it is valuable to consider (as alluded to above) the potential energy diagrams that allow the incorporation of some essential additional features such as simultaneous motion along several coordinates (often normal coordinates). Clearly, the situation becomes very complicated as soon as many such coordinates come into play. Consider therefore, for simplicity, the most simple case of a hydrogen molecule interacting with a transition metal surface. In recent years, this problem has been treated experimentally as well as theoretically in great detail, so that a clear picture of the factors influencing the activation process has emerged. A good review for the case of H_2/Cu can be found in Ref. [43].

Figures 8a and b show potential energy diagrams for such a system [44]. The potential energy is plotted as equipotential lines in a coordinate system where the ordinate represents the surface–molecule (center of mass) distance, and the abscissa the interatomic distance of the diatomic molecule (in this case, the hydrogen molecule). Denoting the intermolecular distance in the molecule by x and the distance of the center of gravity of the bond to the surface by y, small x values are found for large y values, indicating the intact bond between the hydrogen atoms. As the molecule moves closer to the surface (i.e., y decreases), x finally increases to large values that are characteristic of the bond-breaking process. It is the exact position of the barrier, indicated by the letter B at the top of the saddle point in the potential energy diagram, that now governs the dynamics of the process. Two different situations are depicted. In Fig. 8a the activation barrier is located in the entrance channel. A molecule entering the entrance channel with sufficiently high translational energy can surmount the barrier, as indicated by the trajectory. However, it may well move up the wall before it can follow the bend (as if on a "bobsleigh" course) and the system will consequently come out the exit channel vibrationally excited (i.e., the hydrogen surface modes are

References see page 1410

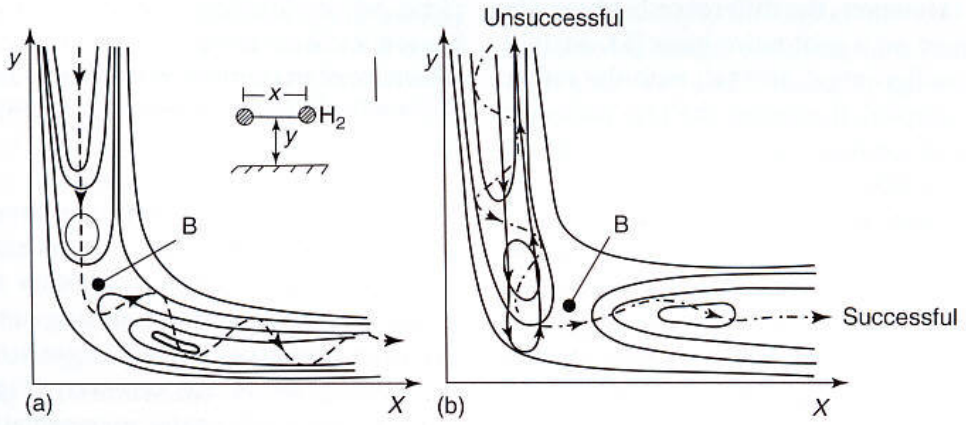

Fig. 8 Two-dimensional potential energy surfaces (schematic) for (a) early and (b) late barrier (B) of dissociation of H_2 on a transition metal surface.

excited), as indicated by the curved trajectory. In Fig. 8b the activation barrier is located more towards the exit channel. Here, a vibrationally excited molecule has a better chance to surmount the activation barrier, as indicated by the full trajectory. An unsuccessful attempt with a translationally excited molecule is shown for comparison. Once the vibrationally excited molecule has crossed the barrier, the hydrogen atoms formed will move across the surface with relatively high translational energy. The whole problem outlined so far can be mapped almost perfectly onto the so-called Polanyi rules [45], whereafter an exergonic reaction of type $A + BC \rightarrow AB + C$ with an early barrier request translational energy, whereas, if the reaction has a late barrier, it requires vibrational excitation of the reactants.

Molecular beam studies [46] have been undertaken in recent years to prepare selectively translationally or vibrationally excited molecules before they were scattered off the surface, and much has been learned about how the molecules stick to a metal surface, specifically for hydrogen transition metal systems [39–47]. In the case of hydrogen absorption on Cu, the barrier [48–51] is in an intermediate position, so that both translational as well as vibrational excitation helps to surmount the barrier. There remain many open questions as to which role rotational excitation plays [43], but even with a full understanding of the processes that occur on the potential energy surfaces shown in Figs. 8a and b, there are still some important ingredients missing. In particular, this concerns the fact that in the discussion so far the geometric and electronic structures of the surface have not been considered. It is known that chemisorption is structure-sensitive, and therefore these aspects must be considered. It should be pointed out that hydrogen adsorption on Cu surfaces may not be typical for interaction with transition metals in general [52]; in particular, it should be remembered that H_2 dissociates with almost no barrier on metals such as Ni, Pd, etc. [47]. It is clear that, in order to understand the barrier heights, electronic structure calculations must be resorted to [53, 54]. However, the difference between Cu and Ni may be argued on a qualitative basis [53, 54]. Cu has the electronic configuration $3d^{10}4s^1$, with the rather diffuse 4s orbitals occupied. If a closed-shell H_2 molecule approaches the Cu surface, it will be repelled by the diffuse 4s electrons so that it is difficult for the H_2 to come in close to dissociate. Ni has the electronic configuration $3d^9 4s^1$ in which the 4s orbital is occupied, which again leads to Pauli repulsion with the H_2 molecule. However, in Ni the 4s electron may be promoted into the hole within the d-shell, forming a $3d^{10}4s^0$ configuration – this reduces the repulsion dramatically and allows the H_2 molecule to come in close and dissociate. Therefore, the barrier for Ni is much lower than for Cu, where it is in the range of 1 eV [43, 55].

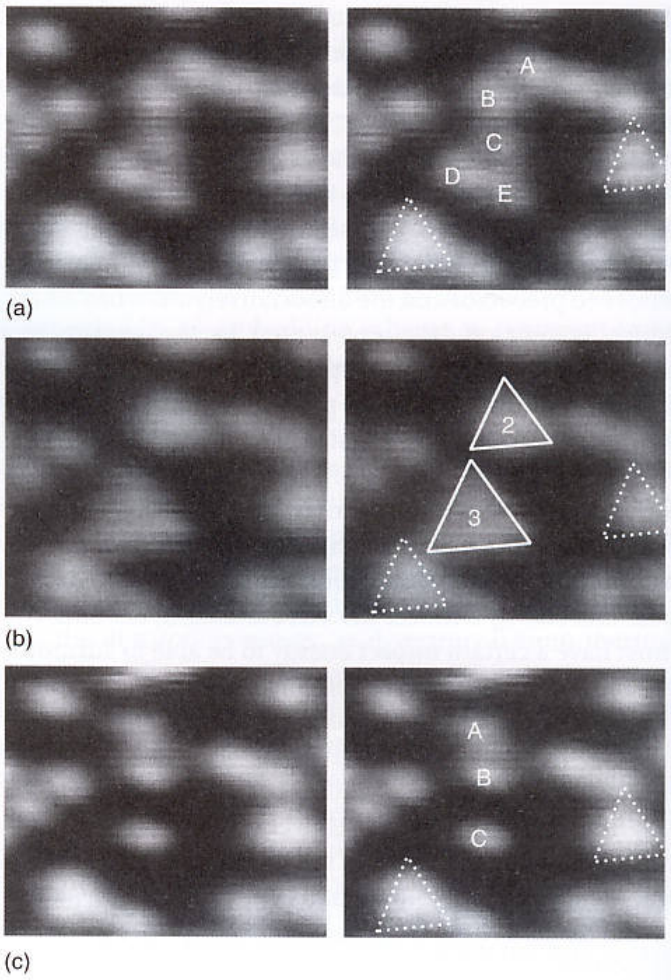

Fig. 9 Scanning tunneling microscopy (STM) images from a movie showing the formation, separation, and annihilation of H-vacancy clusters. The contrast is such that only the H vacancies are visible in the form of bright spots. The images on the left (3×2.5 nm) are repeated on the right with annotations. (a) Five vacancies near the center are labeled (A–E) and two triangular vacancy pairs (2V) are marked with dashed triangles for reference. In (b), vacancies A and B have formed a 2V cluster indicated by the triangle containing the number '2'. Vacancies C–E have formed a six-site, three-vacancy (3V) cluster, indicated by the larger triangle containing the number '3'. Rapid motion of the three H atoms inside the triangle explains the triangular appearance of these clusters. In (c), the 2V pair has separated into isolated vacancies A and B, while the 3V cluster has been annihilated by dissociative adsorption of an H_2 molecule, leaving a single remaining vacancy C. The other 2V clusters separated a few frames later.

In dissociative adsorption it is generally believed that two adjacent vacant sites are necessary and sufficient to allow for dissociative adsorption to occur. Recently, it was demonstrated via scanning tunneling microscopy (STM) studies that clearly a larger arrangement of three or more vacancies are necessary. Figure 9 shows STM images and a schematic representation of the surface indicating the formation and annihilation of a four-vacancy cluster. High hydrogen vacancies show a very

strong contrast (Fig. 9a–c), while the vacancy cluster (b) appears fussy due to the rapid diffusion of hydrogen atoms inside the vacancy cluster. In (c), the vacancy cluster has been annihilated by two hydrogen molecules, leaving two remaining vacancies. Such annihilation has never been observed for only two-vacancy clusters. This is a very interesting finding that may have implications for the minimal site of a metal atom ensemble that needs to be present for hydrogen dissociation to occur. In the case of dissociative oxygen adsorption, there is evidence that while one constituent molecule is adsorbed the energy released is used to move the second oxygen atom over large distances across the surface, as though it was ejected in the process and indicating that the process does not happen on the ground-state potential energy surfaces. The issue remains the subject of much debate, with conflicting evidence. However, it is useful to note that such phenomena must be taken into account when considering the dynamics of adsorption [56, 57].

Another aspect that is important in connection with the discussion of adsorbate thermodynamics and energetics, so far neglected, is the aspect of interaction between adsorbed species. In Langmuir's picture of adsorption [2, 3], the adsorbed particles occupy the lattice points of a 2-D substrate with equal probability and with hard wall potentials between them, preventing double or multiple occupancy of any particular site, and with well-defined adsorption energies typical of the site. (Note that at this point structure sensitivity comes into the picture; however, this aspect is deferred until later.) As a result of this view of adsorption, saturation would be characterized by complete coverage and the formation of a true 1×1 adsorbate layer. Obviously, the formation of ordered layers with coverages far below complete coverage are more the rule than the exception, and are a direct consequence of the existence of interaction potentials. Such an interaction potential is shown in Fig. 10 for the system CO/Pd(100) reported by Tracy and Palmberg in 1969, compared with a CO–CO interaction potential in the gas phase [58]. Interaction potentials may be either attractive or repulsive, and may be classified into direct and indirect interactions [59–62]. Direct interactions involve dipole–dipole (multipole–multipole) and orbital–overlap interactions, and are often repulsive. On the other hand, indirect interactions mediated through the metal surface may be either attractive or repulsive depending on distance and surface sites – that is, the type of charge modification of the electronic structure of the substrate by the adsorbate. The interplay of the interaction potential and the adsorption energy of the isolated particle with the clean surface finally determines the observed properties of the adsorbed layer. In other words, the structure of the adsorbed layer depends on the heat of adsorption as well as on the coverage [5].

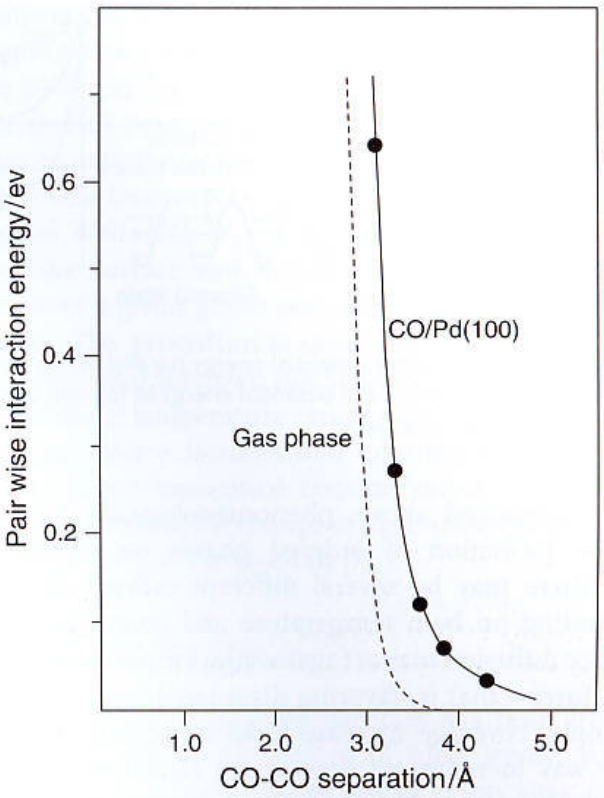

Fig. 10 Intermolecular potential for CO in the gas phase and CO adsorbed on a transition metal surface.

The situation again may be depicted in the form of a potential energy diagram; however, we must include the existence of different surface sites [63]. Figure 11a [7] shows a 1-D potential energy diagram where the spatial coordinate extends parallel to the surface. It has been assumed that every surface site provides identical binding conditions. All identical adsorption sites are separated by a small activation energy if compared with the activation energy for desorption, which gives rise to a sinusoidal energy dependence across the surface. At a low enough temperature the adsorbed particles will reside within the potential wells because their thermal energy is too small to overcome the activation barrier for diffusion. Correspondingly, for higher thermal energies, particles will site-exchange, resulting in a mobile adsorbed layer with short residence times in the individual wells (this situation will be discussed in more detail below). The potential energy diagram parallel to the surface changes significantly if the interaction between adsorbed particles is taken into account. This is depicted schematically in Fig. 11b, where we have added an attractive as well as a repulsive potential to the 1-D diagram of Fig. 11a. The consequences are energetic heterogeneities, weakening the adsorbate surface bond in the case of the repulsive interaction, and strengthening the adsorbate surface interaction in the case of attractive interaction potentials.

References see page 1410

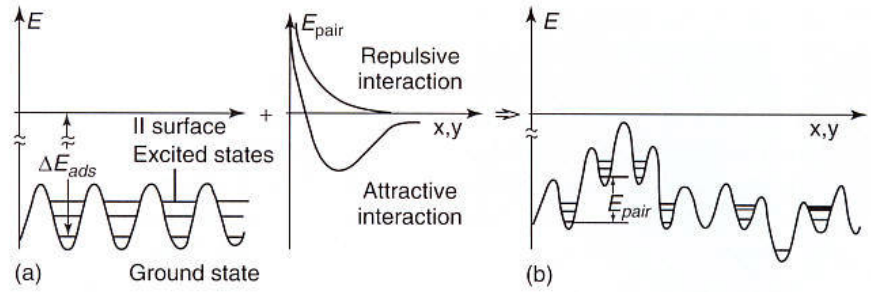

Fig. 11 One-dimensional potential energy parallel to the surface. (a) Empty surface with a single particle bound with adsorption energy E_{ads}; (b) superposition of the potential energy in (a) with a pairwise interaction potential of particles on the surface (E_{pair}), which may be either attractive or repulsive.

As mentioned above, phenomenologically this leads to the formation of ordered phases on surfaces. In fact, there may be several different ordered structures depending on both temperature and coverage, because surface diffusion may act against the formation of ordered structures – that is, favoring disordered layers while, for example, coverage increase locks in certain structures. One way to represent the various structures is to plot a so-called phase diagram [64]; an example is shown in Fig. 12. For the system CO/Cu(100), two ordered phases are found in the given temperature range [65]. These are denoted by I and II_+, and they occur at coverages 1/2 and 4/7. Phase I is a $c(2 \times 2)$ structure, while phase II_+ consists of stripes of the $c(2 \times 2)$ structure of width $n = 3$ separated by domain walls. The main part of the phase diagram is filled by a disordered phase. A very interesting and frequently studied aspect of such phase diagrams are the 2-D phase transitions. In two dimensions, similar to three dimensions, phase transitions may be classified as discontinuous first-order, and continuous higher-order. In general, phase transitions may be evaluated according to the temperature dependence of the thermodynamic functions. This subject is considered in greater detail elsewhere [66–70].

More important with regard to the heat of adsorption are the particle–particle interactions. As stated above, according to the Langmuir picture of adsorption [2, 3], we would expect constant adsorption energy until saturation of the surface is reached. In reality, this is never the case [64]. Rather, the adsorption energy generally decreases at medium and high coverages due to interactions between the adsorbed particles. It is possible to estimate the interactions from the coverage dependence of the isosteric heat of adsorption. In Fig. 13 [7] are several examples [71–73] where the work function has been used as a measure for the coverage (which may be sometimes dangerous). It is clear from Fig. 13 that, in all cases, the adsorption energy decreases sharply as saturation is approached. At low coverage, however, the isosteric heat turns out to be either constant, decreasing, or increasing

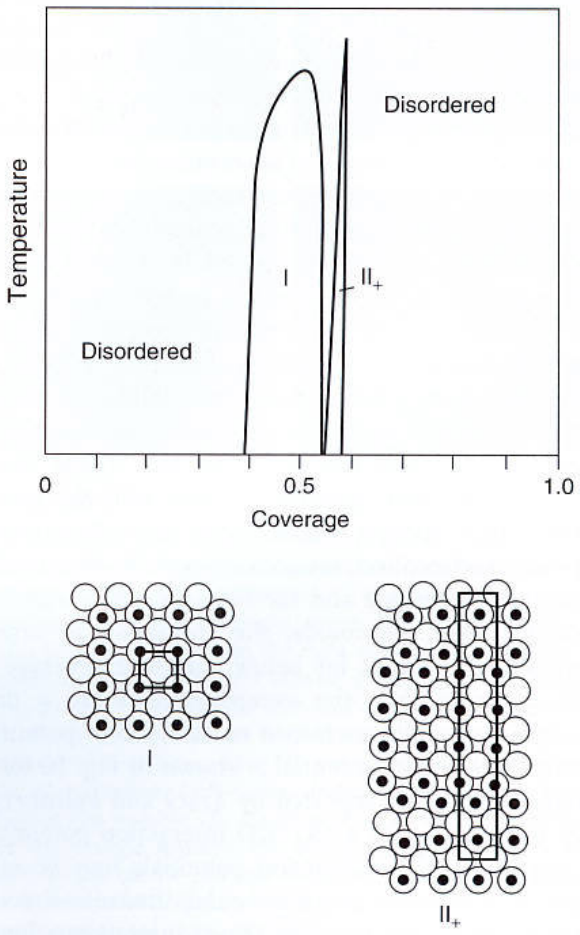

Fig. 12 Phase diagram for the system CO/Cu(100), also showing the ordered structures [65].

with coverage. The observed changes are a consequence of the particle–particle interactions on the surface, in the sense that increase means attractive interactions, as for example in the case of hydrogen on Ni(110) for low coverage [73], decrease repulsive interaction, as in the case of CO on Ni(111) [71]. The step-like decrease of the heat of adsorption close to saturation for CO/Pd(100) [72] is due to the population of additional weakly bound species

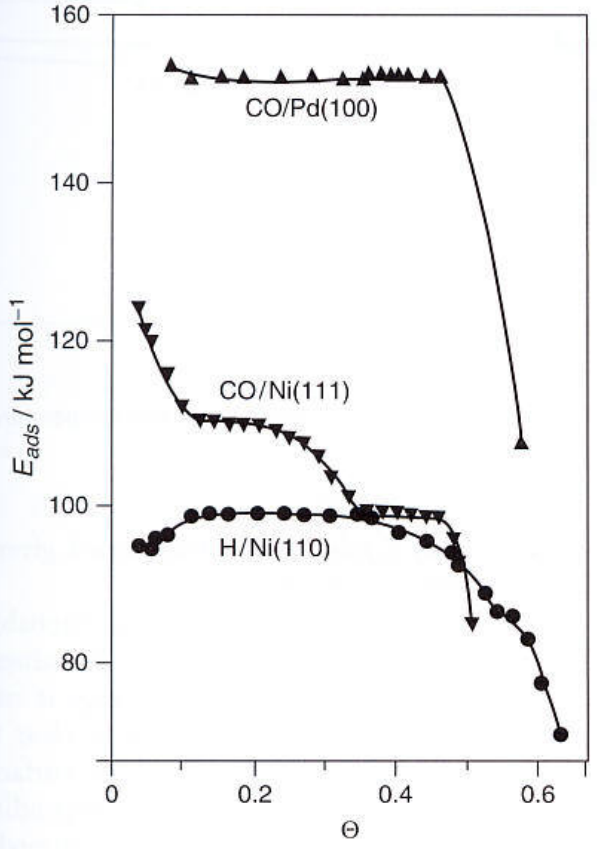

Fig. 13 Adsorption energy (E_{ads} as a function of surface coverage Θ [7]: (▲) CO/Pd(100) [72]; (▼) CO/Ni(111) [71]; (●) H/Ni(110) [73].

on the surface [74, 75]. These weakly bound species may be rather reactive. Owing to their small heat of adsorption they may react rather easily with coadsorbed, neighboring functional groups. At high reactant pressures and not too-elevated substrate temperatures, this type of scenario may play a significant role.

5.1.1.3 Sticking

In this section we consider the traditional description of the process where a molecule approaches a solid surface and eventually is trapped by the potential. A convenient way to gain access to this problem is through the consideration of the rate of adsorption. In the most simple case, the rate of adsorption is proportional to the number of molecules impinging per unit time on the surface (the so-called "particle flux") and to the (dimensionless) efficiency with which an impinging particle actually sticks to the surface, that is, the so-called "sticking probability". The initial sticking coefficient s_o is the ratio of the number of adsorbed particles σ_s, and the number of impinging particles for the uncovered surface. Therefore,

$$0 < s_o < 1 \tag{17}$$

In principle, determination of this quantity is straightforward. In an adsorption experiment, a clean surface held at temperature T is exposed to a well-defined pressure P for a given time t [exposure is measured in Langmuir (L): 1 L = 10^{-6} torr for 1 s], and the amount of gas taken up by the surface (by a suitable surface science technique) is compared with the total amount of gas that has struck the surface. One frequently used method is that proposed by King and Wells [76, 77]. In this case, a molecular beam strikes the surface and the change in the background pressure of a given gas is measured using a mass spectrometer. The procedure is calibrated with respect to a gold sample that is known not to adsorb any molecules in the considered temperature range.

Knowing how s is measured experimentally, we can turn to further conceptual considerations. The rate of adsorption – that is, the change of the number of adsorbed particles with time – is given by [7]

$$r_{ad} = \frac{d\sigma_s}{dt} = \frac{P}{\sqrt{2\pi mkT}} s_o f(\sigma_s) \tag{18}$$

where the flux of impinging particles has been treated according to the kinetic theory of ideal gases, and a function $f(\sigma_s)$ accounts for the loss of empty sites as the adsorption process proceeds. The term s_o may be written in terms of a preexponential ${}^{o}s$ and an activation energy ${}^{ads}E_{act}$ as

$$s_o = {}^{o}s \exp\left(-\frac{{}^{ads}E_{act}}{kT}\right)$$

There is a different adsorption probability depending on whether the adsorption site is occupied, or not. From what has been said before, the sticking coefficient must also depend on the population of internal and external degrees of freedom of the impinging molecule. This can be done in a closed form by assuming the sticking probability s to be composed of terms for the vibrational states involved, each weighted by a Boltzmann factor (F_B) representing the population of the corresponding vibrational state [43]:

$$s(v, E_e, T) = \sum_v F_B(v, T) s_a(v, E_e) \tag{19}$$

where v represents the vibrational quantum state under consideration, which is populated according to the Boltzmann factor depending on the temperature T of the gas (effectively, the nozzle temperature in a molecular beam experiment). The effective translation energy E_e is given by [48]

$$E_e = E_i \cos^n(\vartheta_i) \tag{20}$$

in which E_i is the translation energy of the incident particle, and ϑ_i is the angle of incidence with respect to

References see page 1410

the surface normal. If $n = 2$, then the effective translation energy shows a typical "normal energy scaling" – in other words, an exclusive dependence of the sticking probability on the normal component of the energy of the incident particle, which has been found rather frequently [78–83], and in particular for hydrogen adsorption on transition metals.

With this in mind we can return to Eq. (18) and analyze the rate of adsorption further. First, we write the rate in terms of coverage and not in terms of the absolute number of particles:

$$r_{ad}(\Theta) = \frac{d\Theta}{dt} = \frac{P}{\sqrt{2\pi mkT}} s_o f(\Theta) \tag{21}$$

In the case of the most simple treatment according to Langmuir [2, 3], where it is assumed that each adsorbed particle occupies only one surface site, the adsorbed species does not interact with other adsorbed particles present on the surface. It is further assumed that the adsorption energy is completely exhausted as soon as one monolayer (ML) has been formed; the function $f(\Theta)$ reduces to $(1 - \Theta)$. If the particle dissociates upon adsorption – it occupies two sites – the function $f(\Theta)$ becomes $(1 - \Theta)^2$. Remembering that, under equilibrium conditions, the rate of adsorption must equal the rate of desorption

$$r_{ad} = r_{des} \tag{22}$$

we arrive at the following condition for the coverage:

$$(\Theta) = \frac{b(T)P}{1 + b(T)P} \tag{23}$$

which is the famous Langmuir adsorption isotherm [2]. In its derivation we have employed Eq. (14) for the desorption rate, assuming a first-order process, and consecutively just solved for Θ. In addition, we have used an abbreviation for a constant $b(T)$ which only depends explicitly on temperature once the adsorbate parameters are known. $b(T)$ is given by

$$b(T) = \frac{{}^{o}s}{\upsilon\sqrt{2\pi mkT}} \exp\left(-\frac{{}^{ads}E_{act} - {}^{des}E_{act}}{kT}\right) \tag{24}$$

In this case, the preexponential factor ${}^{o}s$ should not depend on coverage because it has been assumed for the derivation that there is no intermolecular interaction.

Many different adsorption isotherms may be derived where all or some of the basic assumptions going into the derivation have been released or relaxed [84–88]. It should be stated, however, that the general form of the Langmuir isotherm, which is shown for two temperatures in Fig. 14, may be used for a phenomenological description of many processes. It is clear, from the adsorption isotherm, the sticking probability s_o may also be determined, given that all other parameters are known [1, 7].

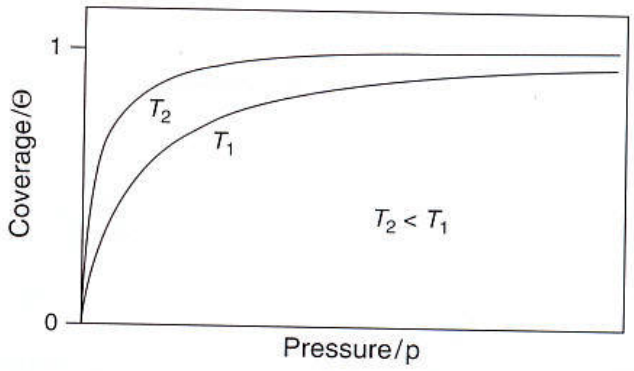

Fig. 14 Plot of the Langmuir isotherm for two temperatures (T_1 and T_2).

In Table 3 is listed a set of sticking probabilities determined for various adsorbate systems. The values vary between unity and 10^{-8}, although the range is usually between 0.15 and 1. Obviously, there is a clear trend that sticking is higher for atomically rough surfaces as compared with atomically smooth surfaces, depending on the nature of the gas. It seems that energy accommodation is particularly easy on the rough surfaces as compared to the smooth ones. Carbon monoxide and nitric oxide stick quite effectively on many transition metal surfaces, regardless of their crystallographic orientation. On open surfaces they even tend to dissociate. The tendency to dissociate increases when going from the right to the left in the Periodic Table, with Co approximately on the border line.

It should be noted at this point that, in addition to the surface crystallography, surface defects (point defects as well as steps) are important to accommodate chemically active species [89–91]. Initial sticking probabilities are interesting, but for real systems it is important to consider the coverage dependence of the sticking coefficient. Of course, a model-free discussion of this aspect is very difficult, and it is therefore common practice to assume a set of possible kinetic processes which are important in connection with sticking to a surface. A possible scenario is shown in Fig. 15 separately for adsorption and desorption [7].

Here, we introduce precursor states which may be classified as either intrinsic or extrinsic precursor states [92, 93]. The former exist at empty surface sites, and the latter at sites already occupied. While trapped into such a precursor state, the particle is only weakly held to the surface; thus, it can diffuse across the surface and be eventually trapped into an empty surface site. Given a precursor lifetime of 10^{-6} s, the molecule probes the surface for a sufficiently long time to find an empty site, if the precoverage is not too large. In order to set up a scheme

Tab. 3 Initial sticking coefficients

Adsorbate	Substrate	Sticking coefficient	Remarks	References
H	Ni(100)	0.06		[307, 308]
	Ni(111)	≥0.01		[309]
	Ni(110)	≈1		[310]
		0.96		[311]
	Pt(111)	0.1		[312]
		≤0.0001		[89, 313]
	Rh(110)	≈1		[301]
	Ru(1010)	≈1		[302]
	Co(1010)	0.75 (±20%)		[303]
	W(100)	1		[314]
O	Cu(100)	0.03	300 K	[315]
	Ni(100)	1		[316]
	Pt(111)	0.2		[317]
CO	Ni(111)	1		[71, 318]
	Ni(110)	0.89		[208]
	Pd(100)	0.6		[72]
	Pd(111)	0.96		[95]
	Ru(1010)	1		[295]
	Pt(111)	1		[319]
N	W(100)	0.2–0.6		[77]
	W(110)	$1-5 \times 10^{-3}$	β-N_2	[320, 321]
		0.22	γ-N_2	[322]
	W(111)	0.08		[76]
N_2	Fe(100)	$10^{-6}-10^{-7}$		[323]
	Fe(111)	$10^{-6}-10^{-7}$		[219]
	Fe(111) > (100) > (110)	$10^{-6}-10^{-8}$		[219]

we have to define probabilities (p_i) with which the various states at the surface are populated. On the basis of this (Fig. 15), it is possible to arrive at equations for the rate of adsorption and desorption. However, in the present case (which is different from the situation discussed above for direct sticking) the sticking probability $s(\Theta)$ will be dependent on the surface coverage. Kisliuk, as one of the first, has proposed a coverage-dependent sticking coefficient based upon such considerations [93, 94]:

$$s(\Theta) = \frac{s_0}{1 + \frac{\Theta}{(1-\Theta)}K} \tag{25}$$

The constant K is connected with the probabilities to populate a chemisorptive state via the various precursor states or desorb from them, respectively (Fig. 15):

$$K = \frac{p_d^{\parallel}}{p_{ch}^{\downarrow} + p_d^{\downarrow}} \tag{26}$$

The Kisliuk model for a coverage-dependent sticking coefficient contains the linear Langmuir behavior as well as the coverage-independent sticking probability as limiting cases. Clearly, as $K = 0$, $s(\Theta) = s_o$. Also, as $K = 1$, $s(\Theta) = s_o(1 - \Theta)$; that is, the linear Langmuir behavior is retained. As K is always larger than zero, we must consider two cases, namely for $K > 1$, and for $0 < K < 1$. The result is a convex curve for the former, and a concave curve for the latter case (Fig. 16) [93, 94].

Which behavior is actually encountered is largely determined by the probability $p_d^{\parallel}$; that is, the probability for desorption out of the extrinsic precursor. This must become smaller than the sum of probabilities to desorb out of the intrinsic precursor and the probability to chemisorb out of the intrinsic precursor, in order to achieve $K < 1$. Under UHV conditions, the population of extrinsic precursors is only easy to realize at low substrate temperatures. Therefore, concave sticking probabilities are generally found, as demonstrated for some examples in Fig. 17 [73, 95–97]. However, at higher pressures, the population of weakly bound precursor states may be important, so that the population of the chemisorbed state through the precursor becomes rate-limiting. In such cases we may find a convex curve of the sticking probabilities. Of course, additional complications may arise if the structure of the surface changes upon changes of coverage [98, 99], when the dependences may become very different altogether. Oscillatory surface chemical reactions are connected with such behavior in some cases [100].

References see page 1410

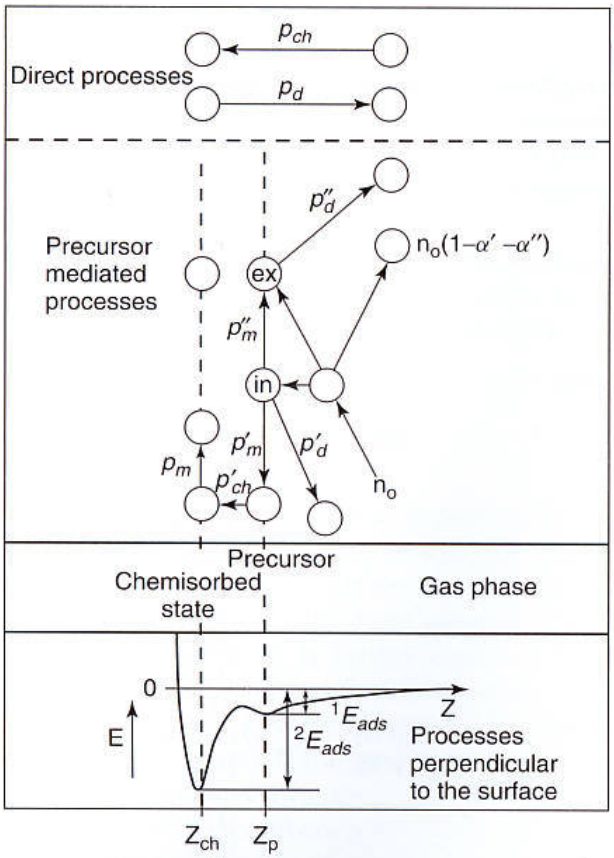

Fig. 15 Schematic representation of direct and precursor-mediated processes on a surface [92, 285]. Processes occurring along the surface normal are plotted along the abscissa. The processes are correlated with the potential energy diagram of Fig. 7b. (ex = extrinsic precursor, in = intrinsic precursor, n_o = number of impinging particles from the gas phase; α' and α'' are fractions of trapped molecules; p = probabilities; p''_m = migration probability along the surface.)

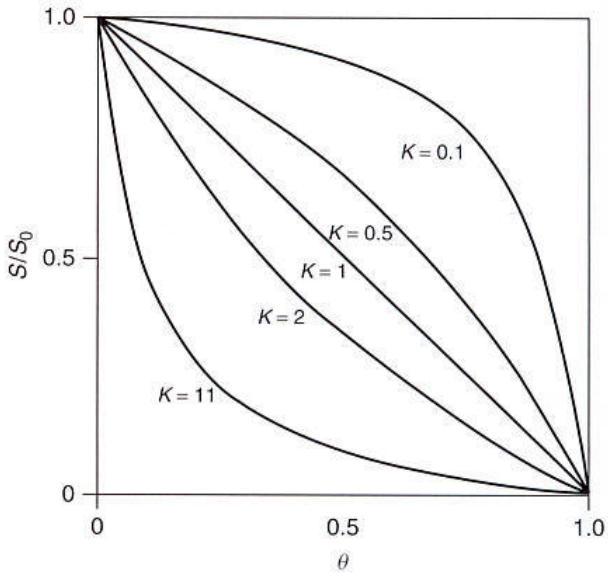

Fig. 16 Relative sticking probabilities as a function of surface coverage according to the Kisliuk model [93, 94]. For an explanation of K, see the text.

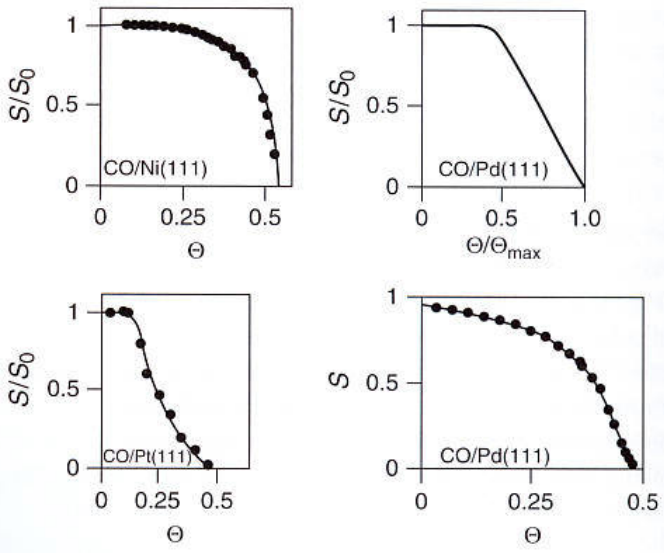

Fig. 17 Relative and absolute sticking probabilities for carbon monoxide as a function of surface coverage [73, 95–97].

To complete this section on sticking, we describe an interesting development that has recently become more visible, namely the experimental investigation of the dependence of sticking on the orientation of the particle, in particular a molecule, upon surface impact. Kleyn and coworkers [101, 102], as well as Heinzmann and colleagues [103–105], have shown that a molecule such as NO can be state-selected and focused by taking advantage of a hexapolar electric field, and subsequently oriented in a homogeneous electric field, as shown schematically in Fig. 18 [104], before colliding with the substrate. Depending on the polarity of the electric field in front of the surface, two different orientations can be achieved: preferential N-end and preferential O-end collisions. The rotational temperature of the colliding molecules determines the degree of orientation of the molecules. Therefore, seeded pulsed nozzle beams are used to cool the particles before collision. The integral number of molecules leaving the surface after scattering is detected from the NO partial pressure with a quadrupole mass spectrometer located behind the target and thus shielded from the direct beam [76].

Figure 19 shows a typical result in terms of partial pressures (right panel) for the scattering of NO from Pt(100) as a function of field strength and orientation of the NO molecule [106]. The observed asymmetry (left panel) is very high. Note that the degree of orientation, given as the averaged cosine ($\cos\vartheta$) of the angle between molecular axis and external electric field ϑ, is 30%. The result documents the strong preference for trapping in the chemisorptive potential if the molecules

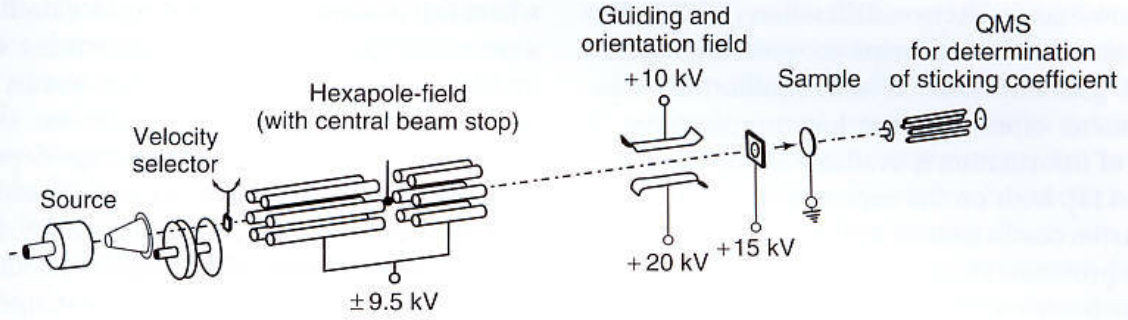

Fig. 18 Experimental set-up to study sticking probabilities of oriented NO molecules [103].

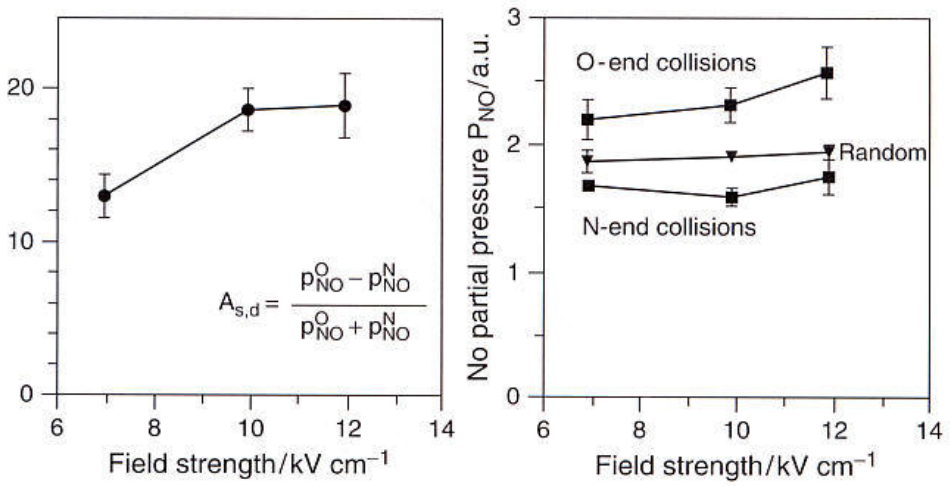

Fig. 19 Right: NO partial pressure after scattering from a Pt(100) surface as a function of field strength and NO orientation [105]. Left: corresponding orientation asymmetry of the partial pressure of NO [106].

approach the surface with the N-end. At higher surface temperatures the asymmetry decreases as expected, because the number of molecules that do not stick increases for both orientations. It seems that, for a detailed understanding of the temperature dependence, a kinetic model involving precursor states must be invoked. A fit to a Kisliuk model [93, 94] (see above) indicates that not only chemisorption is favored for N-end oriented molecules but also trapping into a precursor state. If we change the adsorbate system from a chemisorptive system such as NO on Pt(100) to a more weakly interacting system such as NO/Ag(111) [101], we realize that the observed symmetries are actually much smaller even at low temperature, and indeed, slightly favor trapping of NO molecules with the O-end approaching the surface even at lower coverage.

5.1.1.4 Surface Diffusion

The motion of adsorbed particles clearly plays an important role for adsorbates and for surfaces in general, because this process enables the system to achieve its equilibrium structure. Particularly, at elevated temperatures the atoms of the substrate material can move, lowering the free energy content of the surface. The process of diffusion of substrate atoms has been investigated frequently in the past. Applying various methods such as scattering methods, field emission and contact potential measurements Bonzel and coworkers [107–109], Butz and Wagner [110, 111], Ehrlich [112], and Hölzl and coworkers [113, 114] have contributed to this area. Due to the rather high activation energies required for the substrate atom displacements, temperatures up to 1000 K must be employed in order to obtain reasonable rates of diffusion of substrates atoms. In connection with the discussion of chemisorption, however, we are more concerned with a different type of surface diffusion, namely when diffusion occurs within the adsorbate phase. Such processes may be separated from the motion of substrate atoms because much lower temperatures are needed to induce diffusion. Typical diffusion coefficients can be found in Refs. [115] and [116].

Diffusion within the adsorbed layer is instrumental to establish long-range order and to obtain optimal experimental conditions to perform diffraction experiments, for

References see page 1410

example, via low-energy electron diffraction (LEED). Furthermore, surface diffusion helps to overcome lateral concentration gradients due to non-equilibrium clustering phenomena often found at low temperatures. A large amount of information is available on surface diffusion [92, 112, 113], both on the experimental methods to measure diffusion coefficients as well as on the theoretical aspects of the problem. Hence, at this point only a brief, non-exhaustive overview of the situation is provided [7].

Conceptually, the process is thought to occur as a random walk where adparticles hop between adjacent sites – that is, from an occupied to an adjacent empty site. The hopping frequency depends then exponentially on the temperature of the system which leads to the following form of the diffusion coefficient:

$$D = D_0 \exp\left(-\frac{\Delta E_{\text{diff}}}{RT}\right) \tag{27}$$

with the preexponential factor D_0 and the activation energy for diffusion ΔE_{diff}. It is correlated with the height of the energy barrier in Fig. 11 parallel to the surface. An expression for D_0 may be derived from transition state theory, and depends on the activation entropy of the process. The important quantity for surface diffusion is the activation energy, the magnitude of which is about one-tenth of the adsorption energy for a typical chemisorbate such as CO/Pd (i.e., it amounts to approximately 15–20 kJ mol^{-1}). For physisorbates, it is probably considerably lower.

The diffusion coefficient may be measured using several experimental techniques. At present, the most prominent are the direct observation of a diffusion boundary in either a field electron microscope [117, 118] or a photoelectron emission microscope [119], or via laser desorption experiments [120, 121]. In the latter case, a short laser pulse is used to heat the surface to momentarily desorb the adsorbate from a well-defined region of the crystal. Subsequent laser pulses with well-defined time delays with respect to the first pulse, and measurement of the number of particles leaving the surface, allow one to determine the rate of diffusion into the depleted zone. Other methods used to determine surface diffusion include spectroscopic measurements which cover the proper time window, for example magnetic resonance-based methods [122, 123]. In favorable cases these methods may even be applied to single-crystal surfaces [124].

As mentioned above, the diffusion process is thought to be a random walk across the surface. Then, the mean-square displacement of the adparticles is related to the diffusion coefficient via the relationship:

$$\langle x^2 \rangle = 4Dt \tag{28}$$

where is it understood that the surface itself only contains a very low concentration of adparticles which do not interfere with each other. In other words, the model so far is coverage-independent. However, we know from previous considerations that coverage dependence must be considered. For example, if a particle wishes to move to an empty site, the probability to hop clearly depends on the number of empty sites in the neighborhood, or even on the concerted motion of adparticles. Coverage dependences may be introduced by using the general transport equations, or specifically Fick's law [125]. The solution of Fick's law again yields an exponential dependence of the diffusion coefficient, as in Eq. (27):

$$D(\Theta) = D_o \exp\left(-\frac{\Delta E_{\text{diff}}(\Theta)}{RT}\right) \tag{29}$$

where the coverage dependence of the process enters through a coverage dependence of the activation energy:

$$E_{\text{diff}}(\Theta) = E_{\text{diff}}(\Theta - 0) + \frac{ZE_{\text{pair}}}{2}\left[\frac{1-2\Theta}{\sqrt{1-4\Theta(1-\Theta)B}}\right] \tag{30}$$

where B is the short-range order parameter, $B = 1 - \exp(E_{\text{pair}}/RT)$, Z is the number of nearest neighbor sites, and E_{pair} is the nearest neighbor interaction energy. Using this approach, Fick's equation may be solved numerically.

The tables in Refs. [115] and [116] have been determined experimentally for a variety of adsorbate systems. The values may vary considerably, which is of course due to the specific bonding of the adsorbate to the surface under consideration. Surface diffusion plays a vital role in surface chemical reactions because it is one factor that determines the rates of the reactions. Those reactions with diffusion as the rate-determining step are known as "diffusion-limited" reactions. The above-mentioned photoelectron emission microscope is an interesting tool with which to study (very effectively) diffusion processes under reaction conditions [119]. In the world of real catalysts, diffusion may be vital because the porous structure of the catalyst particle may impose stringent conditions on molecular diffusivities, which in turn leads to massive consequences for reaction yields.

5.1.1.5 Structure Sensitivity

So far, we have neglected the fact that the substrate has a particular geometric structure which influences the adsorption behavior in a very pronounced way. Furthermore, in practical cases the macroscopic geometric structure is rather complex. Consider, for example, a real catalyst used in heterogeneous reactions. This may consist of bimetallic precipitates, or of thin films supported on alumina, silica,

or titania, or highly dispersed metals such as platinum black. However, even these materials possess a regular geometric structure on the microscopic scale. Often, microscopically analyzed, these materials expose regular crystallographic planes, which may be characterized via scattering methods or real-space imaging. In catalysis, the correlation between surface geometric and electronic structure, the geometric shape and electronic structure of a molecule, and the observed macroscopic reactivity represents a very important and long-discussed (but not yet solved) problem. One distinguishes between structure-sensitive and structure-insensitive reactions. Special site requirements have been discussed in terms of the so-called ensemble effect [126–129] whereafter a molecule can only adsorb if a certain group of adjacent surface atoms is available. Studies on bimetallic alloy surfaces have often been used as examples for such ensemble effects [126–128].

The present section enters into a discussion of the electronic and geometric structure by considering first an example where we can vary the strength of interaction between a given adsorbate and various metal and metal-oxide surfaces. We have chosen carbon monoxide as the adsorbate because it offers the largest available data set, including structure determination. Photoelectron spectroscopy (PES) is a very sensitive tool with which to monitor the change in the electronic structure, which is why it is the method of choice to shed light on this question [130]. Figure 20 shows a set of photoelectron spectra of CO adsorbates on four different hexagonally close packed metal surfaces [131], as well as on two transition metal-oxide surfaces [132, 133]. For comparison, we show the spectrum of gaseous [134] and condensed CO [135]. The binding energy ($E_b = E_{kin} - h\nu$) refers to the vacuum level, which allows us to place adsorbates on metals, on insulators, and molecular solids on the same energy scale. (Often the binding energy is referenced to the Fermi level (E_F) of the system. The binding energy with respect to the vacuum level and the binding energy with respect to the Fermi level are connected via the work function Φ of the system.) The region where we expect photoelectron emission from the three outer valence levels of CO (i.e., the 5σ, 1π and 4σ levels) is shown, and most of the following discussion will concentrate on these levels. From the bottom to the top, the heat of adsorption increases from 19 kJ mol^{-1} to 142 kJ mol^{-1} for the metal surfaces. This is accompanied by clearly recognizable changes in the photoelectron spectra. There are several interesting differences in binding energies, line intensities and line shapes between gas phase [134], condensed phase [135] and adsorbate phases [132, 133, 136–139], which we shall comment on in the following. We shall start with the adsorbates on the metal surfaces [136–139], and later turn to the oxide surfaces [132, 133] because bonding considerations are rather different for these systems.

In order systematically to approach an understanding of molecule–metal bonding, and to relate the conceptual considerations to experiment, we briefly refer to Fig. 21 [131]. Here, the molecule–metal as well as the molecule–molecule interaction effects are illustrated on the basis of a one-electron level diagram for the valence electrons. It shows on the right-hand side a diagram for an isolated CO molecule correlated with a one-electron level diagram for a CO molecule interacting with a single metal atom. On the left-hand side the band structure of an

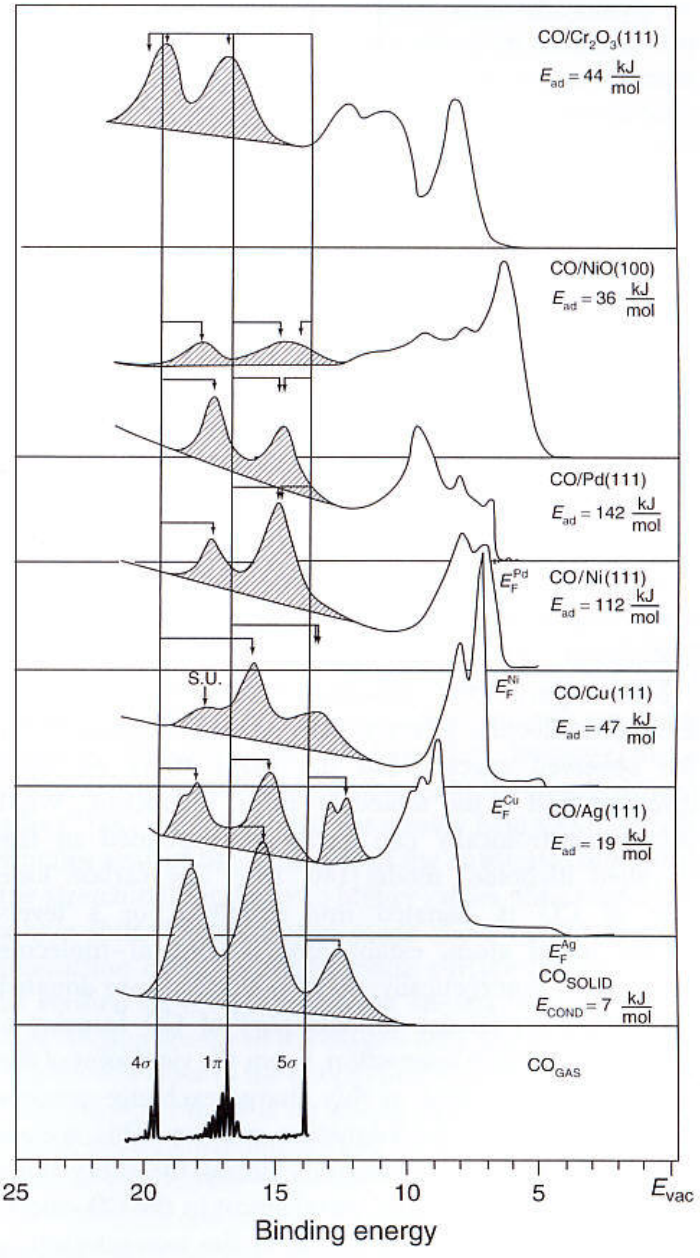

Fig. 20 Photoelectron spectra of CO adsorbed on metal and metal oxide surfaces in comparison with gaseous and condensed CO. The spectra are taken in normal electron emission.

References see page 1410

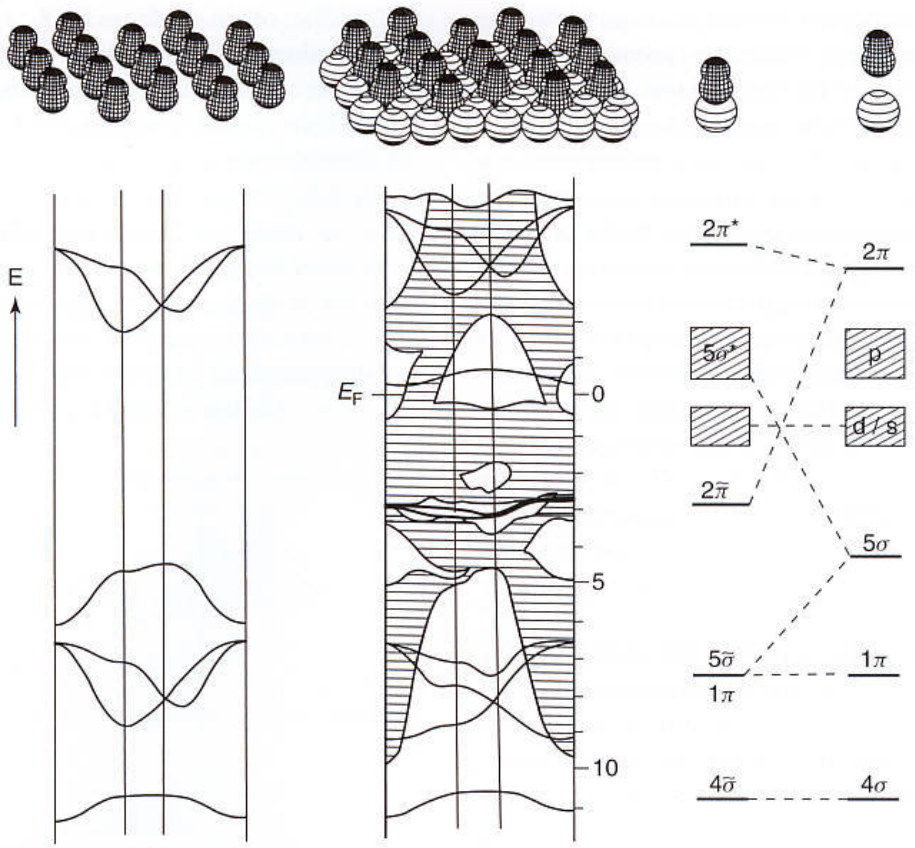

Fig. 21 Schematic diagram for the bonding of an isolated CO molecule to a metal atom (right-hand side) and a free 2-D array of CO molecules (left-hand side) to a metal surface (middle).

isolated CO overlayer is displayed, and compared in the middle with the full band structure of the CO adsorbate interacting with the compact metal substrate with (111) orientation.

Both aspects – the molecule substrate as well as the intermolecular interactions – have consequences for the observed spectra, but the main effect we shall dwell on first is the molecule–metal interaction. What occurs electronically can easily be explained in the so-called Blyholder model [140, 141]. The carbon lone pair of CO is donated into empty d or s levels of the metal atom, establishing a σ-metal–molecule interaction; synergetically, metal d electrons are donated into empty molecular orbitals (2π) of CO forming a π-metal–molecule interaction. From the viewpoint of the molecule we can look at this charge exchange process as a σ-donation–π-backdonation process. This means that the distribution of electrons among the subsystems (i.e., the CO molecule and metal atom) in the CO–metal cluster is considerably different to the non-interacting subsystems. For example, the electron configuration of the metal atom in the cluster may be different from the isolated metal atom, or the electron distribution within the CO molecule bonded towards the metal atom may resemble the electron distribution of an "excited" CO molecule rather than the ground state CO molecule [142]. This scheme has been used to explain the well-known changes in the vibrational properties of adsorbed CO as compared with the gas phase. In addition to the loss of the rotational fine structure upon adsorption, the CO stretching frequency often shifts by more than 100 cm^{-1} to lower values [143–146]. It is the filling of the CO antibonding 2π orbital via the backdonation contribution which weakens the CO bond in the adsorbate and concomitantly shifts the stretching frequency to lower values [147]. Certain electronic levels of the subsystems are also strongly influenced as a consequence of this interaction. Naturally, the distortions of the molecular, as well as the metal levels, are reflected by changes in the ionization energies, their ionization probabilities, and the line shapes of the ionization bands. In CO/Ag(111) [136] at $T = 20\ K$ CO is physisorbed as documented by the small adsorption energy of 19 kJ mol^{-1}. This explains why a spectrum so similar to condensed CO is observed for this adsorbate. The splittings in the 4σ and 5σ ionizations are connected with the formation of a 2-D layer, and will not be discussed at this point [148]. If compared with the gas phase, however, rather dramatic changes are found. The bands are shifted by about 1 eV to lower binding energy and the line widths increase, which also destroys to a large

extent the vibrational fine structure observed in the gas phase. Theories have been developed that allow one to understand these processes on the basis of hole hopping and relaxation (i.e., effects in the ionized state) within the quasi-2-D solid, but for the present we refer to the literature for details [149–154]. If the heat of adsorption increases to about 47 kJ mol^{-1} [155], as for example in the case of CO on Cu(111) [137], the features in the spectrum shift and the intensities are altered. Three lines are still found, but their assignment is very different as compared with the physisorbate [137].

We only briefly state here that many-particle effects in the ionized state of the adsorbate due to the presence of the highly polarizable metal electrons dominate the spectrum, and this alters the assignment considerably [137]. If we later turn to the oxide surfaces where such effects do not occur as strongly but the bond strength is comparable, we shall see that the interaction may be directly deduced from the spectrum. We note in passing that the assignment of the bands to states of different symmetry has been made on the basis of experimental investigations using angle-resolved photoelectron spectroscopy (ARUPS) [131], several reviews on which have been published [131, 156, 157]. The next step is the study of the strongly chemisorbed systems with adsorption energies larger than 100 kJ mol^{-1}. Among a wealth of experimental data [158–176], we have shown here only two systems, namely CO/Ni(111) and CO/Pd(111). In these cases the spectra show two bands, the binding energies of which are almost independent of the particular system under consideration as long as intermolecular interaction does not play an important role. The bands are shifted by more than 2 eV with respect to the gas phase. Using ARUPS [130], it has been shown that the two bands actually contain three components (as indicated in the figure) as well as expected from the simple bonding considerations made above [158]. The carbon lone pair is shifted close to the 1π ionization due to the strong charge exchange, and is actually located at a higher binding energy. The overall shift of the bands to a lower binding energy is a consequence, again, of the relaxation in the ionized state of the adsorbate due to the presence of the highly mobile metal electrons. Therefore, the experimental observations are in line with our simple charge-exchange model for CO–metal bonding, although care must be taken during the interpretation not to forget the effects of the probe, in the case of PES the creation of a hole in the system [130].

We now come to comparisons of the electronic structure of the adsorbates on the metal surfaces with those on oxide surfaces [177, 178]. Recently, detailed electronic structure calculations [179–190] have shown that the interaction of molecules with oxide surfaces differs considerably from that with metal surfaces in the sense that, in the latter case, the interaction – at least on the regular surfaces – is much weaker. However, it is not necessarily a physisorptive interaction. Briefly, on the (100) surface of the strongly ionic NiO the interaction of a CO molecule is not governed by short-range charge-exchanges processes (as in the case of the metal surface) but rather by electrostatic interaction between the multipolar moment of the molecular electron density and the multipolar moment of the ionic surface. The reason for this behavior is that, due to the presence of the closed shell oxygen ions in the (100) surface, the molecule cannot approach the Ni site close enough to exchange charge. Pauli repulsion sets in at rather large distances from the surface and repels the molecule. The balance between the electrostatic attractive forces and the Pauli repulsion results in a rather weak chemisorptive bond of CO on a typical oxide surface. In addition, due to the rather weak interaction there is no longer a strong preference for one given orientation of the molecule with respect to the surface. For example, the molecular axis may be either perpendicular or tilted, or there may be interaction either with the carbon end or the oxygen end of the molecule with the surface. In other words, from an experimental point of view, we must check in each case individually which situation is adopted by the system [132].

To a certain extent, the vibrational spectra [191–193] again provide a clue towards a verification of the general statement made above. On oxide surfaces, in general, the observed shifts of the stretching frequencies are considerably smaller as compared to adsorbates on metals [144–146]. The vibrations may be either red- or blue-shifted, depending on the interaction. The small red shift observed in some cases may be interpreted by a limited charge transfer from the oxide to the adsorbed molecule, in the same sense as for adsorbates on metal surfaces. The often-observed blue shift, however, has a different origin, and can be explained by the so-called "wall effect" [181–184] in which the weakly held CO molecule vibrates against the hard wall of the substrate; this shifts the stretching frequency to higher values, thus leading to a blue shift. The statement made above concerning the interaction of CO with the oxide surface can now also be verified via the photoelectron spectra in Fig. 20 [132]. The binding energy of the oxygen lone pair is found to be located very close to the energy in the condensed CO film, indicating that there is no strong intermingling between the oxygen lone-pair density and the surface electrons. The same is true for the CO π-bond electrons. However, we see a pronounced shift of the carbon lone-pair electrons originating from the strong Pauli repulsion with the surface electronic charge. The relaxation shift found for the metal-oxide systems is also rather small, because the response of the oxide surface towards the creation

References see page 1410

of holes on the molecule in the ionization process is less pronounced than with the metal surface. Comparing the spectrum for the CO/NiO(100) system with the last example, (i.e., $CO/Cr_2O_3(111)$ [194]) indicates a similar situation as far as the overall position of the adsorbate induced features are concerned. However, a detailed analysis of this $\sqrt{3} \times \sqrt{3}$)-ordered adsorbate system shows that the individual ionizations are considerably shifted with respect to the CO/NiO(100) system. The reason is simple, and it can be proved (by ARUP or X-ray absorption measurements) that the orientation of the molecule with respect to the surface has changed. CO is no longer vertically oriented on the surface but rather is strongly inclined. A schematic model of the local bonding situation is shown in Fig. 22. The analysis of the chromium oxide system underlines the need to determine individually the orientation of the molecular axis before discussing details of the electronic structure of a system, in particular on an oxide surface.

The next step in the discussion of structure sensitivity of chemisorption is to consider the site of adsorption on a given surface, and to answer the question as to whether and how the site changes as the coverage of the adsorbate is increased. Figure 23 shows the famous dependence of the CO stretching frequency on coverage for the system CO/Ni(111) [145]. This dependence has been interpreted as being due to two effects, namely a change of adsorbate site upon increase of coverage, and additionally a shift caused by the coupling of the dynamic dipoles which depends on intermolecular distance [144–146]. Figure 23 indicates the adsorbate geometry deduced for the various coverage ranges based on the stretching frequency data. In recent years, however, it has become increasingly clear that a structural assignment based on vibrational data must be viewed with caution. At low coverage, a CO stretching vibration at 1816 cm^{-1} is identified, and this is replaced by a band at 1831 cm^{-1} if the coverage increases and eventually shifts to 1905 cm^{-1} at $\Theta = 0.5$,

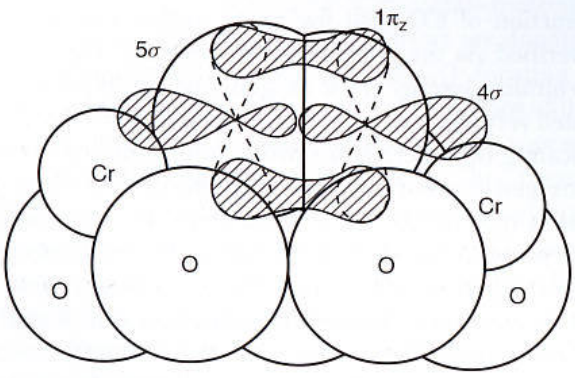

Fig. 22 Schematic proposed arrangement of CO on a Cr_2O_3 surface [133].

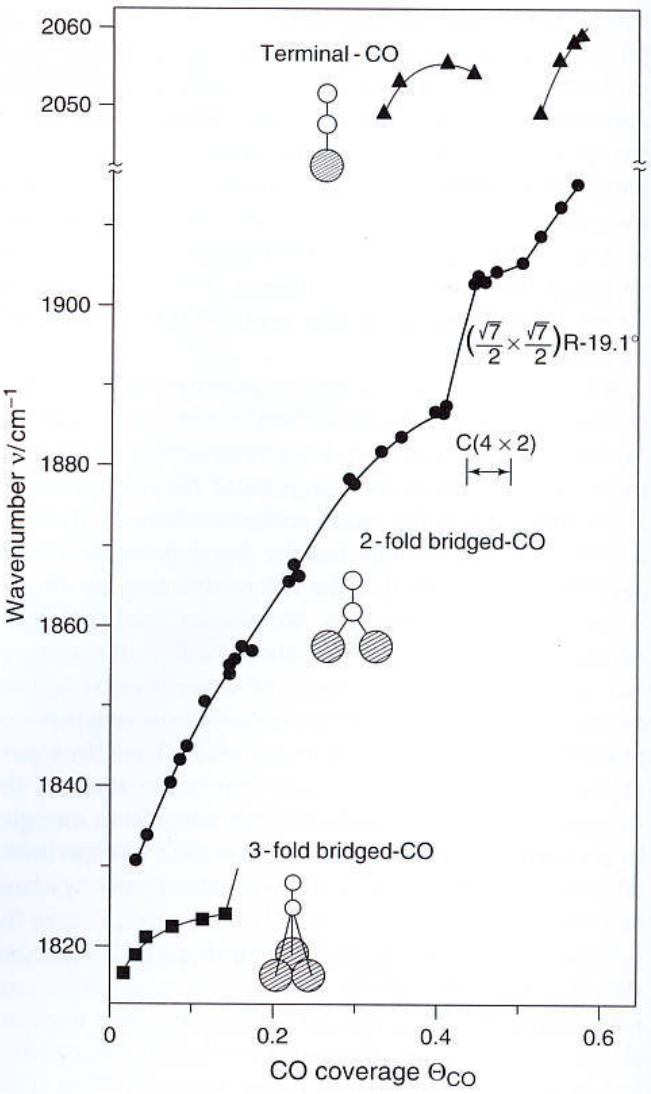

Fig. 23 Stretching frequency of CO adsorbed on Ni(111) as a function of CO coverage. The surface was dosed at 90 K and subsequently annealed to 240 K [145].

corresponding to a $c(4 \times 2)$ structure. On the basis of suggestions made by Eischens and Pliskin [143], the band at 1816 cm^{-1} has been interpreted to be due to adsorption in a threefold hollow site at low coverage, and the band shifting in the range 1831–1905 cm^{-1} to a CO bridge site.

In a very convincing study based on the analysis of X-ray photoelectron diffraction data, Bradshaw and coworkers [195–197] have shown that the adsorbate site over the whole coverage regime remains the same, and is a threefold hollow site, as indicated in Fig. 24. The observed shift in the stretching frequency is then purely due to intermolecular dynamic dipole coupling. Note that both the inequivalent threefold hollow sites (fcc and hcp) are occupied in this structure [196]. Another important factor in chemisorption becomes clear by examining the structures in Fig. 24, namely the

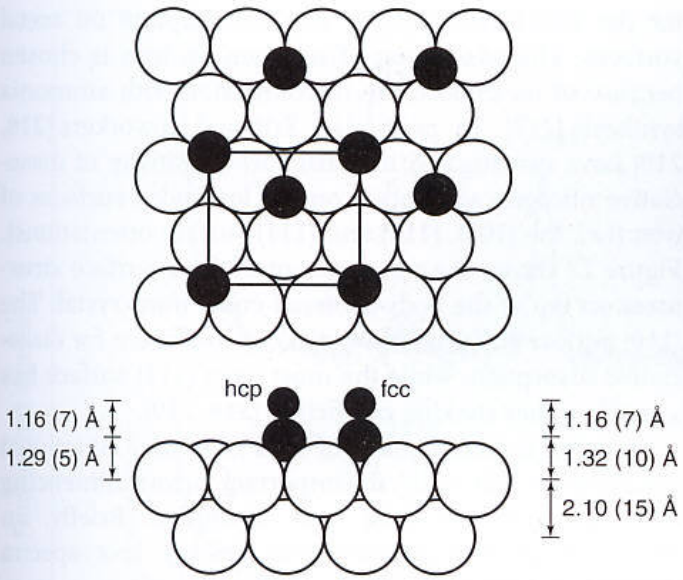

Fig. 24 Schematic diagram of the geometric arrangement CO on Ni(111) in the $c(4 \times 2)$ superstructure. Values are distances as determined by XPD [196].

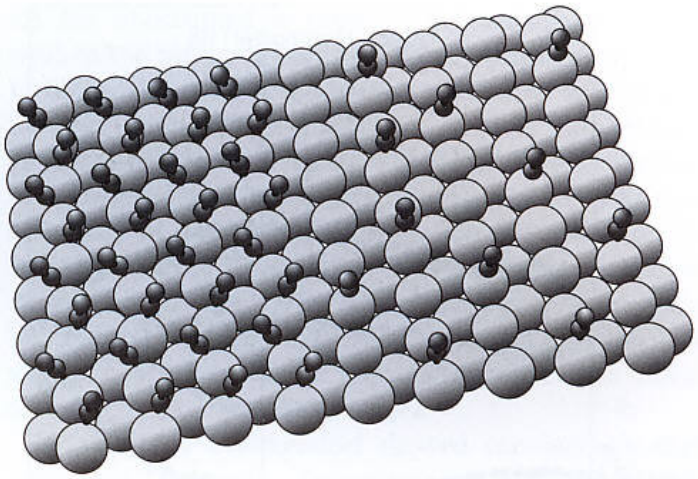

Fig. 25 Geometric arrangement of CO molecules on a Ni(110) surface at low coverage (right) and high coverage (left).

cooperativity of the process. There is a 3% expansion (+0.07 Å) of the outermost Ni–Ni lattice spacing. This is meant here to stress the finding that, although the surface provides a particular site for adsorption, the final geometry is determined via the interaction with the adsorbate and therefore depends on its chemical identity. This phenomenon is important in connection with the well-known adsorbate-induced reconstructions of surfaces [98, 99]. If the reactivity of the surface towards another adsorbate changes through the reconstruction, then cooperative phenomena are essential for the overall chemical reactivity in the system. In general, adsorbate structure determination with high accuracy remains a matter of active research, and Woodruff and associates have published a series of impressive studies using photoelectron diffraction [195, 198–202].

Whereas in the above example the local structure remains the same for increasing coverage, there are other cases where intermolecular interaction changes the geometry of the adsorbate. In the case of CO on Ni(110), at low coverage CO molecules adsorb in two different adsorption sites, namely on atop and on bridge sites with vertically oriented axis, as shown in Fig. 25 [203–206]. The molecule–substrate bond in this case is so strong that the system can tolerate even large lateral intermolecular stress. At a coverage of $\Theta = 1$, the intermolecular distance would be 2.5 Å if the molecular axis remained perpendicular.

Therefore, the molecular axis tilts from the normal orientation in order to enlarge the average distance between molecules [207–210]. The equilibrium structure assumed is shown in Fig. 25, on the left. This system has been studied in some detail in order to understand the electronic structure of the system [160, 211–213]. In line with Fig. 21, where the schematic band structure of an adsorbate system is shown, the present system has been studied with ARUP and the band structure experimentally determined [148]. Figure 26 shows the complete experimental band structure in the occupied region; that is. of the 5σ, 1π, and 4σ levels [160, 212, 213]. Included is the band structure in the unoccupied region as determined by inverse photoemission. The 5σ, 1π, and 4σ levels lead to twice the number of bands due to the nonsymmorphic space group symmetry of the system with two molecules per unit cell [207]. Following the bands through the Brillouin zone shows that the energetically close 5σ and 1π bands hybridize. Also, one can clearly identify the CO(2π)–Ni(3d) backbonding states below the Fermi edge. The unoccupied 2π-derived levels are located above the Fermi edge. It is interesting to note the different magnitudes of the band dispersions for the different levels. This is clearly due to the variations in interaction strength for the different molecular orbitals, depending on directionality and spatial extent. The largest dispersions are exhibited by the π orbitals; in fact, the 2π orbital shows the largest effects because they are most diffuse and show a large electron density off the molecular axis. To summarize, the strong intermolecular interaction is reflected in the adsorbate band structure and mainly due to $\pi - \pi$ interaction.

We now turn to the question of how the adsorption properties of a given molecule changes when we change the geometric structure of the surface but keep its chemical constitution constant. Many such examples have been published, and again CO adsorption could be chosen [214]. Yet, hydrogen chemisorption [47] or oxygen

References see page 1410

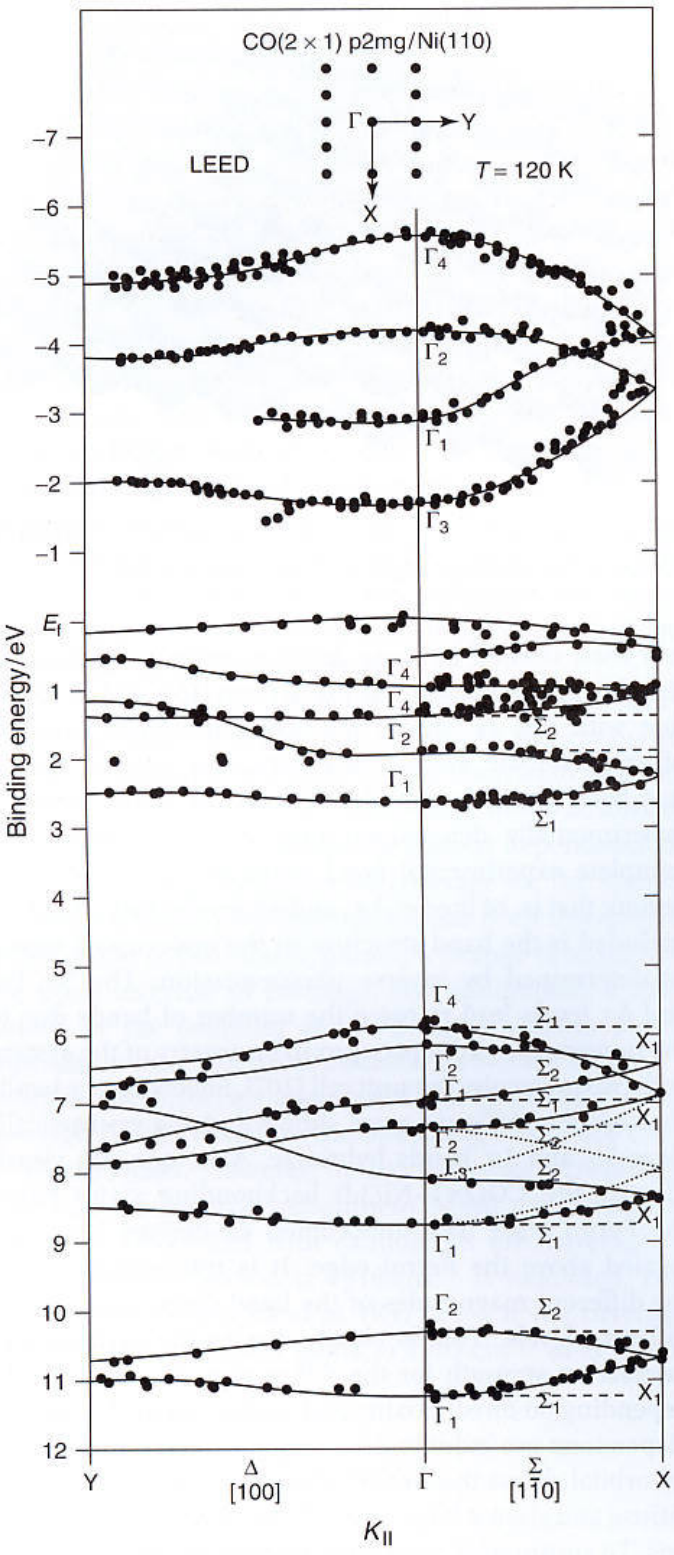

Fig. 26 Measured band structure in the range of occupied and unoccupied levels for CO(2 × 1)p2mg/Ni(110). The wave vector K is determined along the two orthogonal directions in the surface Brillouin zone, as shown at the top, and its energy dependence according to $K_{||} = (2m_e\hbar^{-2}E_{kin})^{1/2} \sin\vartheta$.

chemisorption [215, 216], which has been studied and reviewed in detail by Christmann [47], Wandelt [215], Brundle [216] and others are also prominent examples for the structure-sensitivity of chemisorption on metal surfaces. The adsorption of nitrogen on iron is chosen because of its importance in connection with ammonia synthesis [217]. In particular, Ertl and coworkers [218, 219] have investigated the structure-sensitivity of dissociative nitrogen adsorption on the low-index surfaces of iron (i.e., the (100), (110) and (111) surface orientations). Figure 27 shows the arrangement of these surface structures on top of the body-centered cubic iron crystal. The (110) surface has a very low sticking coefficient for dissociative adsorption, while the most open (111) surface has a much higher sticking coefficient [218, 219].

By using a combination of PES [220] and vibrational spectroscopy [221–223], the important factors influencing this face specificity have been identified. Briefly, on Fe(111) high-resolution electron energy loss spectra (HREELS) [223] are observed as a function of temperature (Fig. 28), while at about liquid nitrogen temperature, a dominant feature with a stretching frequency at 2100 cm^{-1} is found. With ARUP [220], it has been shown that this species is oriented perpendicular to the surface, being most likely bound to an atop site. The same species is found on all low-index iron surfaces [217], where it

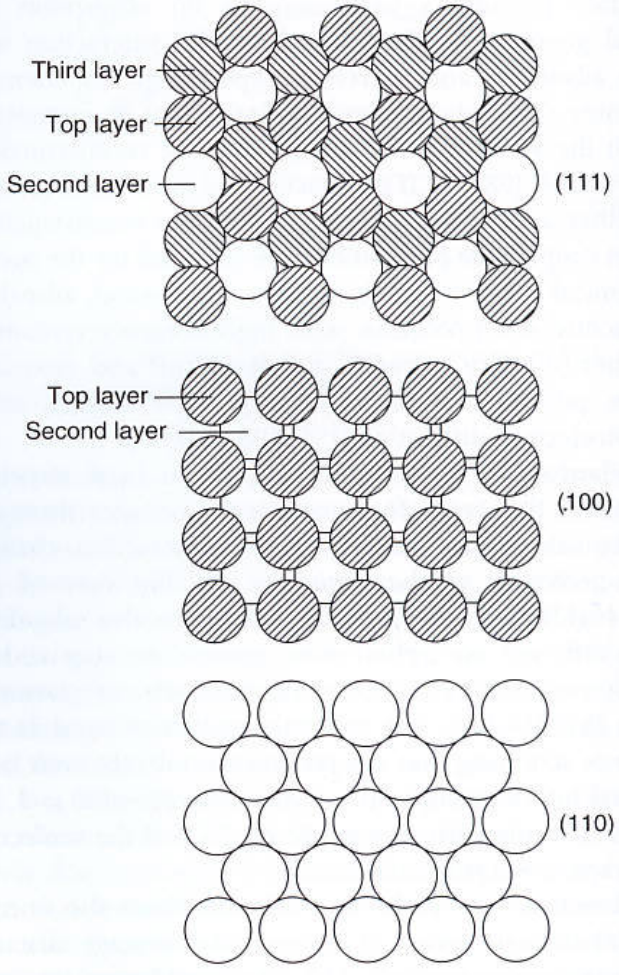

Fig. 27 Structure of the close-packed surfaces of iron (bcc).

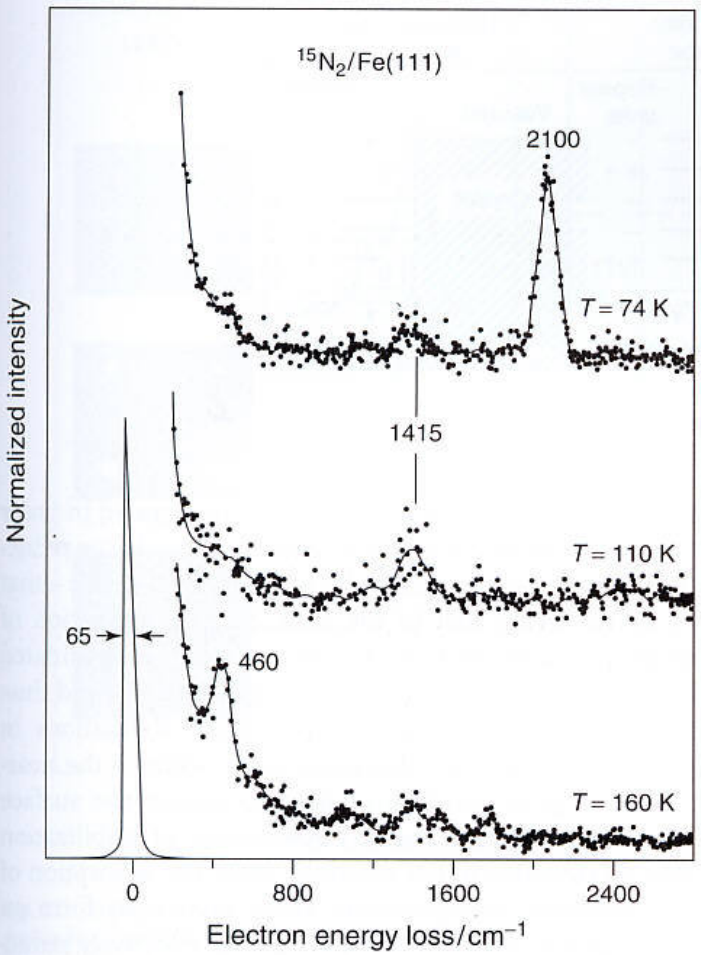

Fig. 28 Electron energy loss spectra of $^{15}N_2$ on Fe(111) as a function of surface temperature [223].

is weakly held by the surface. Upon heating the system slightly above 100 K, a second molecular nitrogen species shows up in the vibrational spectra of N_2/Fe(111) at a lower stretching frequency (1415 cm^{-1}).

Again, PES has been used to show that this species is bound in a strongly tilted geometry, in line with the low stretching frequency typical for side-on bonded dinitrogen complexes. This species only exists on the surface within a limited temperature range. Above 160 K, the stretching frequency typical for molecular nitrogen species disappears and only atomic nitrogen (460 cm^{-1}) is present on the surface. This scenario is typical for the (111) surface, while the existence of the intermediate species cannot be detected on the other low-index planes [i.e., (110) and (100)] [217]. It is now generally accepted that the intermediate with the low stretching frequency is a precursor to nitrogen dissociation, and it is thought that the (111) surface provides the sites, necessary to assume the strongly tilted geometry [217]. Figure 29 shows the bonding geometry for the intermediate species [220]. The nitrogen molecule can donate both its lone pair as well as the 1π electrons into empty metal orbitals, and at the same time establish a back-donative bond via the unoccupied π orbital. The back-donation will weaken the nitrogen–nitrogen bond, which finally leads to dissociation. Since both nitrogen atoms are already in close contact with the metal surface, this picture appears to provide a natural pathway to dissociation. It is believed also to explain the observed strong face specificity of dissociative nitrogen chemisorption on Fe surfaces. Figure 30 shows a semi-empirical potential energy diagram for N_2/Fe(111), where the pathway from the molecular precursor to the dissociative adsorption is shown [224]. The value for the activation barrier is based on experimental data [225].

Nørskov and Chorkendorf showed convincingly that steps are extremely important in the dissociative chemisorption of N_2 in the case of Ru surfaces. A number of calculations showing how steps are more reactive for a number of metals and v reactant molecules have been

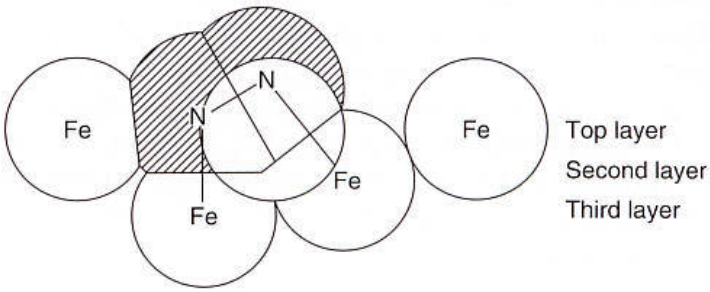

Fig. 29 Proposed arrangement of N_2 on Fe(111) [220].

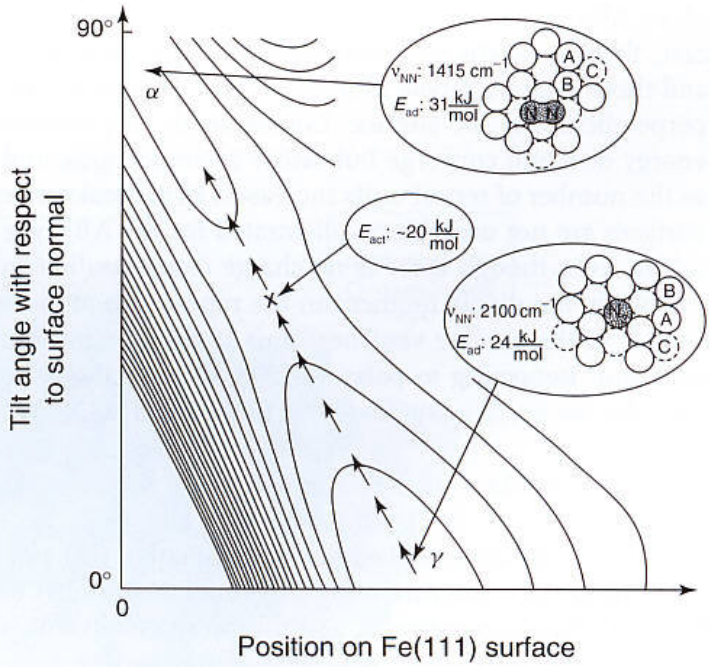

Fig. 30 Two-dimensional potential energy diagram for the conversion of γ-N_2 (vertically adsorbed) to α-N_2 (side-on bonded) [221–223] on the Fe(111) surface [224].

References see page 1410

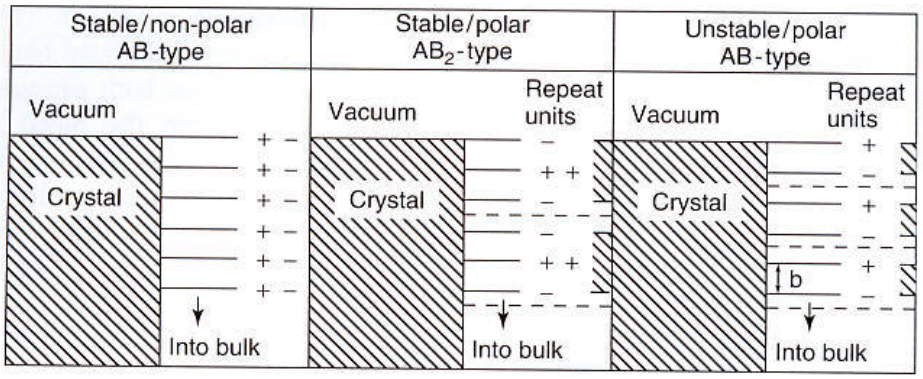

Fig. 31 Stable and unstable surfaces of AB-type and AB_2-type ionic crystals [232, 233].

published which focus on both geometric and electronic effects [226–228].

Finally, we should briefly examine the structure-sensitivity of transition metal oxide surfaces [177]. For such systems [229, 230] it is necessary to resort to some basic considerations about the electrostatics of ionic or partly ionic systems with respect to surface stabilities. Figure 31 shows schematically the arrangements of planes in a crystal of rock salt (AB) structure for the termination of (100) type on the left and of (111) type on the right [231]. The (100) surface of an AB-type solid is the typical case for a non-polar surface with vanishing dipole moments between the planes and full charge compensation within the planes.

This arrangement leads to a converged, finite electrostatic surface energy. Upon going to the (111) surface of an AB-type lattice, we create a polar surface. In this case, there is no charge compensation within each layer, and there is also a dipole moment within the repeat unit perpendicular to the surface. Consequently, the surface energy does not converge but rather increases unbound as the number of repeat units increases. In general, polar surfaces are not unstable, as illustrated for the AB_2-type solids. Even though there is no charge compensation in the plane, the dipole moment in the repeat unit perpendicular to the surface vanishes, thus leading to a stable situation. Returning to polar surfaces of the AB-type to consider the surface potential V in more detail [232, 233],

$$V = \frac{2\pi}{S}[Nb(2\sigma - 1) + (1 - \sigma)b] \qquad (31)$$

where S is the area of the unit cell. Equation (31) provides the surface potential as a function of the number of layers N, their separation b, and the parameter σ which describes the difference in charge of the surface layer with respect to the bulk layer. It is quite clear that the reduction of the surface charge such that $\sigma = 1/2$ leads to the disappearance of the first term in Eq. (31), and thus to a converging surface potential independent of the number of layers. While this is only a qualitative argument, it shows possible routes for the system to respond in order to stabilize polar AB-type surfaces. Surface-charge reduction may be accomplished by reconstructing [231] – that is, by removing half of the ions, or by the creation of steps. The latter leads to the coexistence of A-terminated and B-terminated patches on the same surface, and thus to a microscopic charge compensation. Relaxations in the layer distance are also expected to occur in the near-surface region, which may help to reduce the surface potential. In certain cases, other causes of stabilization may be considered. For example, upon the adsorption of H^+, provided by exposure to water, OH^- may form on an oxygen-terminated surface, thereby effectively reducing the surface charge [230]. Hence, one would predict a strong structure-sensitivity of water adsorption on oxide surfaces, and this has indeed been observed [231, 234] and is exemplified in Fig. 32, where the O(1s) XPS spectra are shown for three different samples [234].

The lower trace shows the spectrum of a cleaved NiO(100) surface with very low defect concentration (sharp LEED pattern). The feature is symmetric after cleavage, and it remains symmetric even after exposure to water at room temperature [235]. At low temperature an ice layer forms which can be removed without residue by heating to room temperature. This indicates that a NiO(100) surface does not dissociatively chemisorb water. The situation is different for a NiO(100) surface containing defects, as indicated by the much broader LEED spots as compared with the cleaved surface [230, 234]. Here, a small feature is found at 2.2 eV higher binding energy. This becomes particularly pronounced in the spectra if they are recorded at grazing electron excidence in order to amplify the surface-sensitivity of the method. Electron energy loss spectroscopy (EELS) investigations have shown that the feature is due to hydroxyl groups on the surface. These groups may be removed from a NiO(100) surface by thermal treatment. Exposure of the cleaned surface to water leads to the reappearance of hydroxyl, indicating that water dissociatively chemisorbs on defect sites of a NiO(100) surface. Dissociative chemisorption becomes

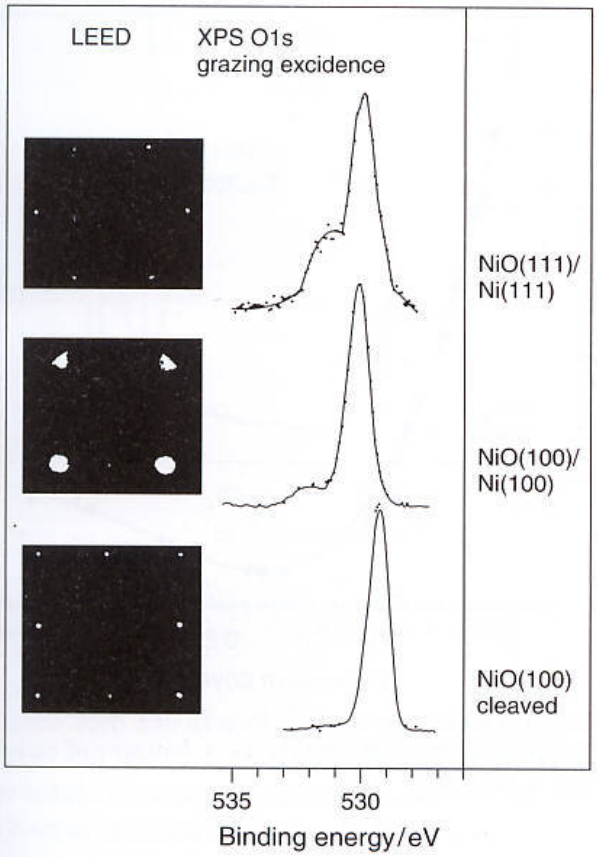

Fig. 32 O(1s) XP spectra of a cleaved NiO(100) crystal (lower); a grown NiO(100) film (middle); and a grown NiO(111) film (upper). The corresponding LEED patterns are shown [231, 234].

even more pronounced on the NiO(111) surface. The upper trace in Fig. 32 indicates a rather high concentration of hydroxyl groups at the surface. When (111) polar surfaces are prepared, they often become OH-stabilized, due to the electrostatic instability discussed above. In favorable cases such as NiO(111), the hydroxyl groups can be removed from the NiO(111) surface as water by thermal treatment. As a consequence, the OH-free unstable surface reconstructs. The most stable reconstruction of a polar surface of an ionic crystal is, according to Lacman [236] and to Wolf [237], the so-called octopolar arrangement, shown in Fig. 33 in comparison to the ideal (1 × 1) surface. The octopolar reconstruction leads to a p(2 × 2) unit cell on the surface, and is characterized by the removal of three out of four oxygen ions in the first layer (in the case of an oxygen-terminated surface), and one out of four nickel ions within the second layer [231, 238]. The third layer contains then again a complete hexagonally close-packed oxygen layer. A p(2 × 2) reconstruction has been observed for iron oxide and nickel oxide, but only in the latter case are there clear indications that an octopolar reconstruction has actually taken place [234].

Readsorption of water leads to a lifting of the reconstruction and the reoccurrence of the (1 × 1) structure [231]. Note for completeness that the reconstructed surface exhibits a considerably higher chemical activity (e.g., in the DeNO$_x$ reaction) than the hydroxyl-covered surface, which is basically inactive towards further chemisorption [235]. In other words, water desorption and readsorption leads to a strong change in the chemical activity of certain crystallographic planes of oxide surfaces, and this may be relevant with respect to the catalytic activity of powders of real samples.

References see page 1410

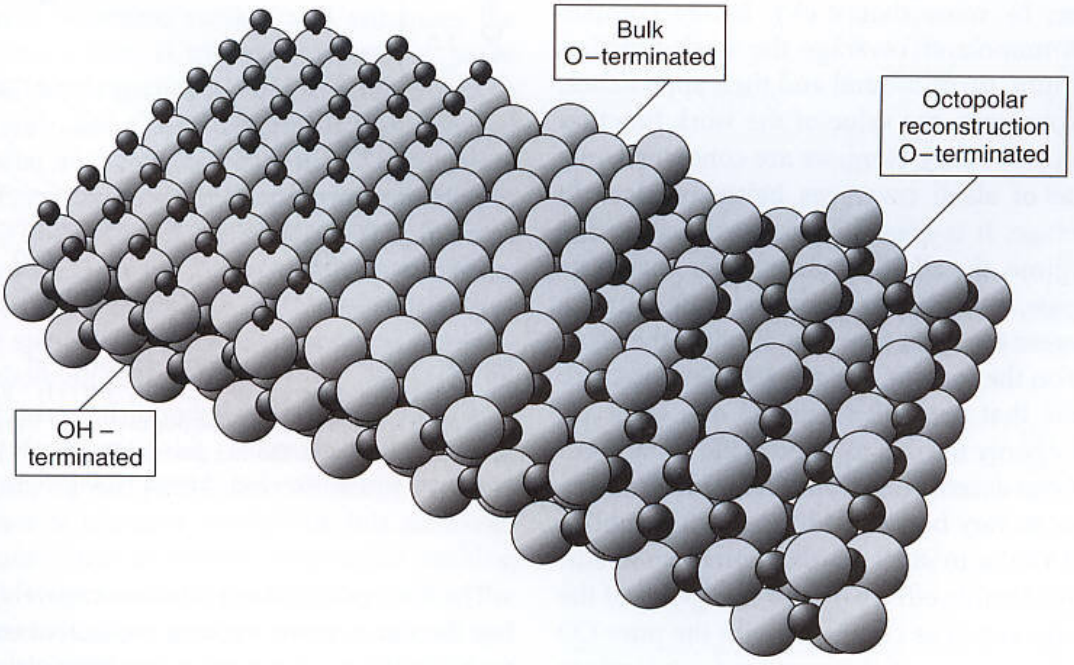

Fig. 33 Schematic diagram of OH-terminated (left), bulk-terminated (middle), and octopolar reconstructed (right) NiO(111) surfaces.

Previous sections have discussed the interaction between adsorbed species in connection with the coverage dependence of adsorbate properties and, especially, energetics. Coadsorption of different chemical species is the general case in connection with the discussion of intermolecular interaction, although the latter serves as the basis for understanding chemical reactions between adsorbed species. There is such a vast literature on the subject [239] that a comprehensive and exhaustive review of the field cannot be provided here. Nevertheless, we can briefly address two coadsorbate systems where a broad knowledge has been accumulated over the years. To represent the limiting cases, we resort again to CO as one component and study its coadsorption with both electropositive and electronegative additives. Needless to say, all aspects discussed above for chemisorbate systems in general are important, even at a more complex level, for coadsorbate systems. In the latter case, it is necessary to consider the different chemical identities of the adsorbed species, and more importantly their influence on the electronic structure of the substrate, and on each other. In other words, the aspect of cooperativity that adsorbates and substrate interfere and determine each others properties becomes particularly noteworthy.

The most prominent and most frequently studied electropositive additives are alkali metals. Several comprehensive reviews have been published on the subject which provide more detailed information [239–241]. Characteristically, the adsorption of alkali leads to dramatic changes in the work function of the system [239–241]. An example, K on Pt(111), is shown in Fig. 34 [242]. In general, small alkali coverages already lower the work function considerably before monolayer coverage is reached (in the present case, by more than 4 eV). Before completion of the first monolayer coverage the work function reaches a minimum, turns around and then approaches, for increasing coverages, the value of the work function of the bulk alkali [239–241]. Here, we are concerned only with the regime of alkali coverages below or close to monolayer coverage. It is generally accepted that, in the low-coverage regime, the alkali atoms transfer charge towards the substrate, setting up a strong adsorbate–surface dipole which lowers the work function, hinders the alkali atoms to cluster on the surface, and allows them to adsorb as isolated atoms that are well separated one from another [243]. The energy needed to remove the alkali from the surface has been determined from TDS and calorimetric investigations to vary between 130 and 250 kJ mol^{-1}. Coadsorption of CO onto such an alkali-precovered surface leads to considerable effects on the energetics of the CO–substrate interaction as compared with the pure CO adsorbate. The TD spectra of the pure and coadsorbate systems are shown in Fig. 35 [244].

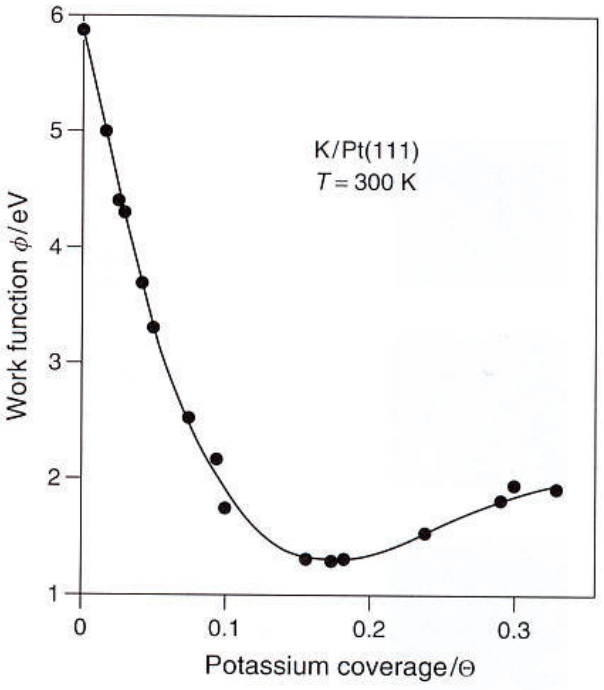

Fig. 34 Work function of Pt(111) as a function of potassium coverage at 300 K [242].

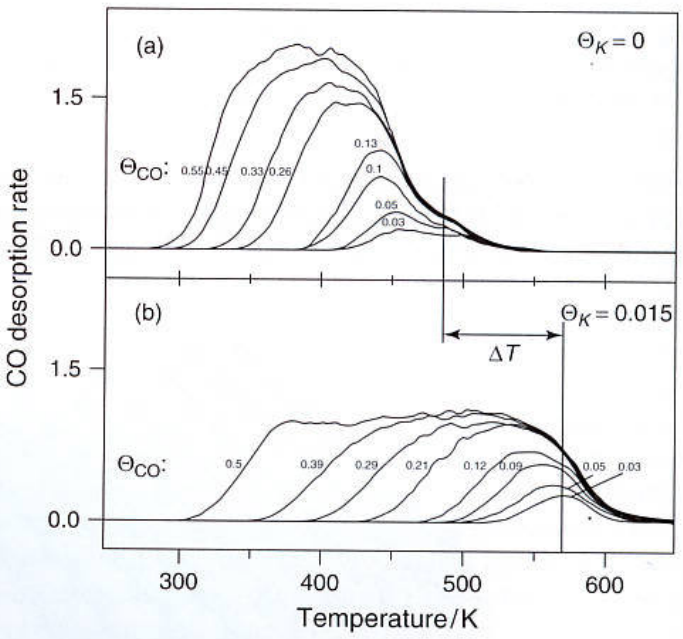

Fig. 35 Thermal desorption spectra of (a) clean and (b) potassium-covered ($\theta = 0.015$) Pt(111). Various CO coverages are plotted indicating the population of sites close to the alkali at low CO coverage. On the unmodified Pt(111) surface at higher coverages similar sites are observed [244].

The molecule still adsorbs associatively on the surface, but the dissociative sticking coefficient increases considerably in the coadsorbate, as has been observed for several CO–alkali coadsorbates [239]. The adsorption enthalpy

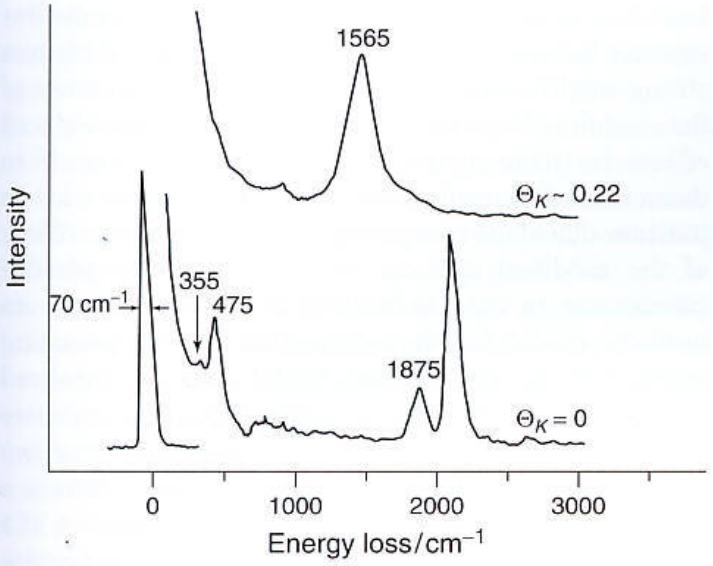

Fig. 36 Electron energy loss spectra of CO on clean (lower trace) and K-modified (upper trace, $\theta_K = 0.02$) Pt(111) [246].

increases from 130 kJ mol^{-1} for a typical CO–metal system to 197 kJ mol^{-1} for the alkali-adsorbed system [245]. There are also coverage dependences, but we shall concentrate here on a single coverage. To learn more about how the observed energetic changes come about, consider the vibrational spectra of the system shown in Fig. 36 [246]. As compared with the pure CO adsorbate, the CO stretching frequency in the coadsorbate is lowered by several hundred wavenumbers, indicating a weaker C–O bond in the coadsorbate. The explanation is straightforward: electrons from the electropositive additive are transferred either directly or via the substrate surface into the unoccupied CO antibonding orbitals, thus weakening the CO bond [240]. Simultaneously, this stabilizes the CO–alkali interaction on the substrate surface and enhances the CO–substrate interaction. It turns out, however, to be rather difficult to exactly partition the interaction strength between CO–alkali and CO–substrate. It was believed for some time that in the coadsorbate the CO–substrate interaction changes dramatically, leading to a change in the CO bonding geometry on the surface – that is, from a vertically bound CO in the pure adsorbate to a side-on-bonded CO in the coadsorbate [247]. Near-edge X-ray absorption fine structure (NEXAFS) has again been instrumental in showing that this is not the case [248]. In fact, CO remains vertically bonded on the surface and possibly interacts side-on with the coadsorbed alkali atom. The side-on geometry was particularly attractive because, similar to the case of nitrogen adsorption, this geometry could easily explain the increased dissociative sticking coefficient [239]. However, as it stands today, either the molecules transiently pass through such a side-on geometry before dissociation, and the concentration is so low that it cannot be identified, or dissociation can also start from vertically oriented, but electronically strongly modified CO. The described interaction between alkali and CO in a coadsorbate may be considered as special case of alkali promotor action, which is well established in catalysis [239].

A completely different situation is encountered when we coadsorb CO with an electronegative species. Table 4 [239] lists desorption energies for CO absorbed on transition metals modified by electronegative additives. In general, and opposite to the effect observed for the electropositive modifier, coadsorption with electronegative modifiers leads to a decrease in the desorption energy. This may occur for different reasons: it may be due to repulsive modifier–CO interaction, or due to the fact that the modifier blocks those sites of the surface leading to the strong CO–substrate interaction for the clean surface [239]. As judged from the vibrational data, the influence of an electronegative additive onto the CO stretching frequency is much less pronounced if compared to the electropositive additives [249]. Often, instead of a strong red shift (as observed for electropositive coadsorbates), a weak blue shift is observed which, in certain cases, may even lead to stretching frequencies higher than in the gas phase [249]. In this case it is even

Tab. 4 Desorption energies for some transition metal surfaces modified by electronegative additives

Adsorbate	*Surface*	*Modifier*	E_d^0/kJ mol^{-1}	*Reference*
CO	Ni(100)	–	140	[250]
		P(2 × 2)S	90	
			110	
		C(2 × 2)S	≈30	
		P(2 × 2)O	120	
		P(2 × 2)N	≈90	[324]
		(2 × 2)p4gC	93	[204]
	Ni(111)	–	140	[325]
		P(2 × 2)S	91	[325]
		P(2 × 2)O	105	[326]
	Pd(100)	–	160	[327]
		P(2 × 2)S	86	
			60	
	Pt(111)	–	154	[328]
		P(2 × 2)S	106	[328]
		P(2 × 2)Se	110	[329]
	Ru(0001)	–	170	[330]
		P(2 × 2)S	105	[330]
H	Ni(100)	–	102 ± 5	[331]
		P(2 × 2)S	84 ± 10	
		C(2 × 2)S	48 ± 16	
	Fe(100)	–	87 ± 50	[318]
		P(1 × 1)O	60 + 10	[318]
	Pd(100)	–	85	[332]
		O.15S	49	[332]

References see page 1410

more difficult to disentangle the various contributions (i.e., direct and substrate-mediated interactions). The wealth of data presently available suggest that an electronegative additive mainly influences the substrate locally – that is, in its direct vicinity, in the sense that: (i) the adsorption sites which involve substrate atoms directly coordinated to the modifier are blocked; and (ii) the adsorption sites sharing some substrate atoms with the modifier are substantially perturbed. This means that, as shown schematically in Fig. 37 [239], for a fcc(100) plane and a modifier residing in a fourfold site, four atop sites and four bridge sites are blocked, and eight bridge sites, four close and four remote fourfold sites are perturbed.

With increasing modifier coverage, the number of affected sites per modifier atom decreases, because of the overlap of effects. Following this simple model, clearly the most tightly bound states of the coadsorbate associated with the unaffected surface should be rapidly removed with increasing modifier coverage. In the case of Ni(100), where CO favors the atop site on the clean surface, one S atom, for example, is found to remove four atop CO molecules [250]. In addition, as evidenced by EELS data and TD spectra [250], CO is pushed to occupy the close bridge sites and the close fourfold hollow sites, in which the coupling with the substrate is reduced. In generalizing this observation, it can be stated that coadsorption of electronegative additives often leads to a situation where a coadsorbate accesses the less strongly bound surface sites, and this in turn leads to a strong modification of the reactivity in the presence of the modifier [239]. In catalysis, such coadsorbate-induced effects are summarized as "poisoning", particularly in connection with sulfur. However, as we have tried to indicate, due to the complexity arising from the specificity of the modified systems and the variety of possible interactions in the coadsorbed layer, there is still no uniform model for the mechanism of the poisoning action, even for the idealized model systems considered in this section [239]. The situation becomes even more complex if the additive induces surface reconstruction, or even surface compound formation. Also, if there is a lack of a tendency towards ordering and occupation of a definite adsorption site, coadsorption phenomena become increasingly complicated. In the case of modifying the surface with C, N, or O as opposed to S, P, etc., either transition metal surfaces may reconstruct or carbides, nitrides, and oxides are formed [239]. Then, of course, the activity of the surface is determined by the properties of the new types of compound formed. Often, island formation is encountered in these systems, and this leads to a considerable reduction in the relative number of modified surface sites because the effect is restricted to the neighbors of the modifier island boundary. In summarizing, for such systems the problem of cooperativity – that is, the phenomenon that the adsorbate and coadsorbate create their own active sites which are not present on the clean surface – becomes particularly important. The future study of these effects in chemisorption is essential, even under ambient conditions, in order to identify which are the key effects that operate during catalysis at a microscopic level.

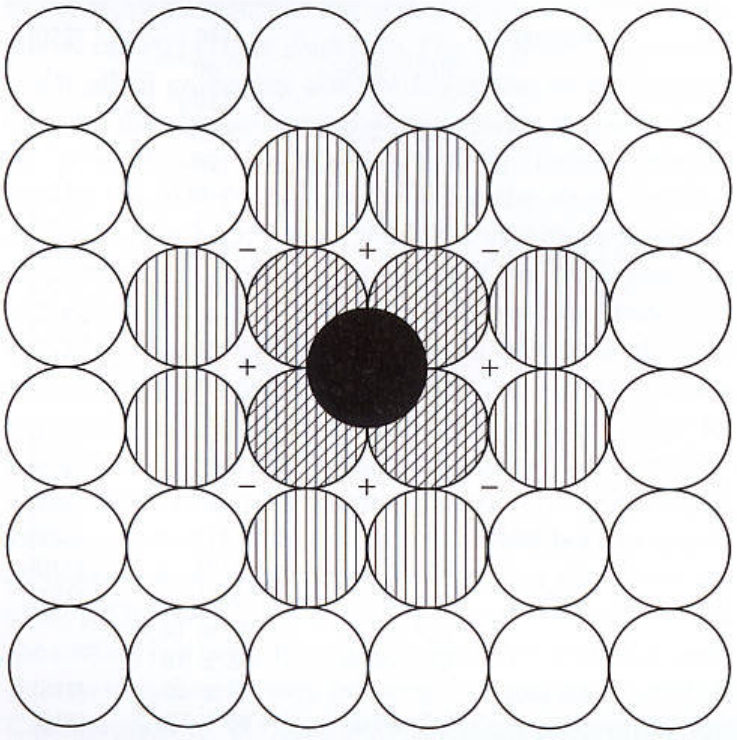

Fig. 37 Schematic representation of the influence of an adsorbed electronegative modifier in a fourfold hollow site (black circle) on the neighboring sites. Neighboring fourfold hollow sites which are strongly (+) or less strongly (−) influenced are indicated [239].

It is important to study chemisorption not only under UHV conditions but also under ambient or higher-pressure conditions. Here, we discuss the case of CO adsorption on Pd(111) and present a comparison between UHV and ambient conditions. CO on Pd(111) has been repeatedly studied with IR reflection absorption spectroscopy (IRAS), LEED, and TPD, for example, by the groups of Bradshaw [144, 251], Hoffmann [252], Ertl [253, 254], Somorjai [255], Goodman [256] and others [257]. As shown by Doyen and Ertl [258], the close-packed (111) surface is energetically "smooth" for CO adsorption and the low surface diffusion barriers facilitate ordering of the adsorbate layer. Accordingly, a variety of ordered CO structures has been determined with a $(\sqrt{3} \times \sqrt{3})$ R30° at 0.33 ML, a $c(4 \times 2)$ at 0.5 ML, a $(4\sqrt{3} \times 8)$ react at 0.63 ML, and a (2×2) at 0.75 ML as the most prominent structures (1 ML equals the density of Pd atoms in the (111) plane; $1.53 \times 1015\ cm^{-2}$). The vibrational spectrum of CO on Pd(111) strongly depends on coverage, and is more complex than that of CO on Pt(111) [259].

According to an IRAS study conducted by Tüshaus et al. [251], CO initially adsorbs in threefold hollow sites with stretching frequencies from 1830 to 1900 cm^{-1}. At half-ML coverage, a peak at 1920 cm^{-1} was reported and originally attributed to bridge-bonded CO. However, recent photoemission and photoelectron diffraction studies [260, 261] and stretching frequency calculations [262] have shown that CO occupies fcc and hcp threefold hollow sites at $\theta = 0.5$. At about $\theta = 0.6$–0.7, CO is preferentially bridge-bonded (~1960 cm^{-1}) with a smaller amount of linear (on-top) CO (~2090 cm^{-1}). If the coverage is further increased, the bridge-site intensity decreases, and finally, at saturation coverage ($2 \times 2, \theta = 0.75$), two intense bands at 1895 and 2110 cm^{-1} (hollow and on-top CO) are observed.

Figure 38 shows a series of sum frequency generation (SFG) spectra of Pd(111) exposed to 10^{-4} Pa (10^{-6} mbar) CO acquired at decreasing temperature from 450 to 115 K. CO coverages as determined by TPD (and by comparison with previous LEED/TPD studies [251, 253, 256, 263–265]) are also indicated. Adding CO at high temperature and then cooling generally produced better-ordered structures and avoided less-ordered non-equilibrium adsorption configurations [256, 266–268]. Some selected LEED images are presented in Fig. 39 [263]. The series in Fig. 38 is comparable to an isothermal exposure series in UHV, except that here the coverage is increased by decreasing the substrate temperature. At 400 to 350 K, a small SFG signal at 1910–1920 cm^{-1} was observed that had previously been attributed to bridge- or hollow-bonded CO at half-ML coverage. With decreasing temperature (i.e., increasing coverage), the peak shifted to a higher wavenumber and a second peak characteristic of the stretching vibration of terminal (on-top) CO evolved.

At 190 K, the spectrum consisted of two distinct peaks at 1955 cm^{-1} (bridge-bonded CO) and 2087 cm^{-1} (on-top CO) at a coverage of 0.63 ML (in good agreement with an SFG study by Bourguignon et al. [266]). This structure exhibits the characteristic "flower" LEED pattern shown in Fig. 39b,c. When the temperature was further decreased, the bridge peak shifted back to a lower wavenumber and disappeared, while the on-top peak grew and shifted to a higher frequency. At 115 K, saturation (0.75 ML) was obtained and the LEED image of Fig. 39d was observed. The corresponding SFG spectrum exhibits two peaks characteristic of hollow CO (1895 cm^{-1}) and of on-top CO (2107 cm^{-1}) [251, 256]. Structural models by Bradshaw, Hoffmann, and others [144, 252, 263], based on LEED and IRAS data, are also shown in Fig. 40 (for refined models, see Refs. [251] and [261]).

The SFG spectra in Fig. 38 qualitatively reproduce IRAS data obtained under UHV conditions. However, differences can be recognized that are most likely due to the different selection rules of SFG and IRAS. A

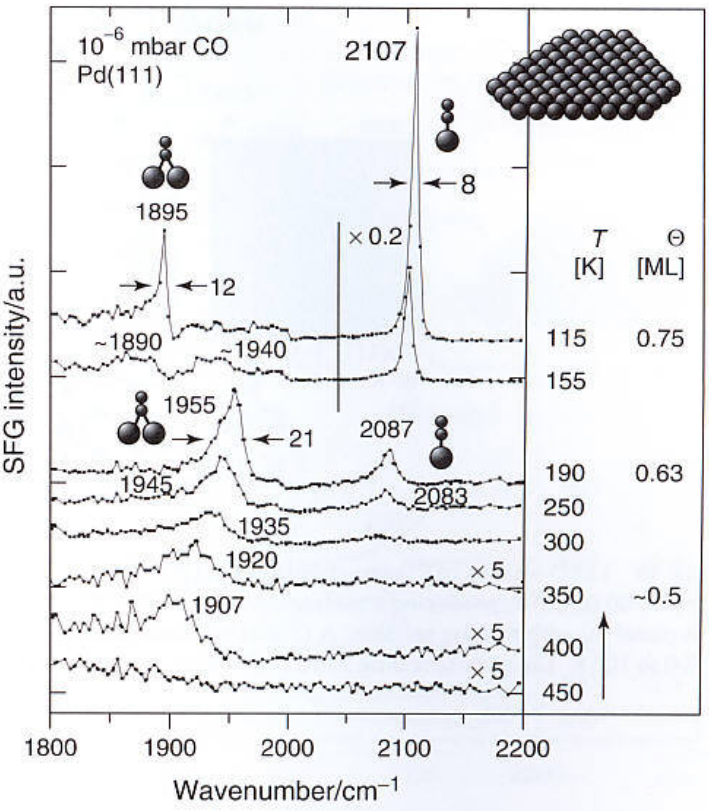

Fig. 38 SFG spectra of 10^{-6} mbar CO on Pd(111) from 450 to 115 K. The spectra were recorded from high to low temperature. Coverages as determined from TPD are also indicated [268].

comparison of Figs. 38 and 40 shows that the high-pressure adsorbate structures of CO up to 10^5 Pa at 190 K are very similar to the high-coverage structures observed under UHV conditions by SFG or IRAS. There is no evidence for the formation of high-pressure species that are different from those under UHV. While high CO pressures have been reported to disrupt Rh nanoparticles [269] and restructure Pt single crystals [270], under our experimental conditions such an effect was absent for Pd(111). The spectra were fully reversible with pressure, and the 10^{-4} Pa spectrum could be reproduced with great accuracy even after several hours of gas exposure (Fig. 41; compare also the 1 mbar spectrum in Fig. 40). Small differences may be due to carbon deposition, which is probably unavoidable in light of the time scale of the experiment (one spectrum takes about 15 min to record). LEED images obtained after pumping out CO were identical to Fig. 39b, and after heating to 700 K and cooling to 90 K, a (1×1) LEED pattern was observed. In summary, no evidence for major surface rearrangements has been found. The high-pressure CO spectra on Pd(111) were comparable to the high-coverage structures observed under UHV conditions. No evidence for high-pressure species or major surface restructuring

References see page 1410

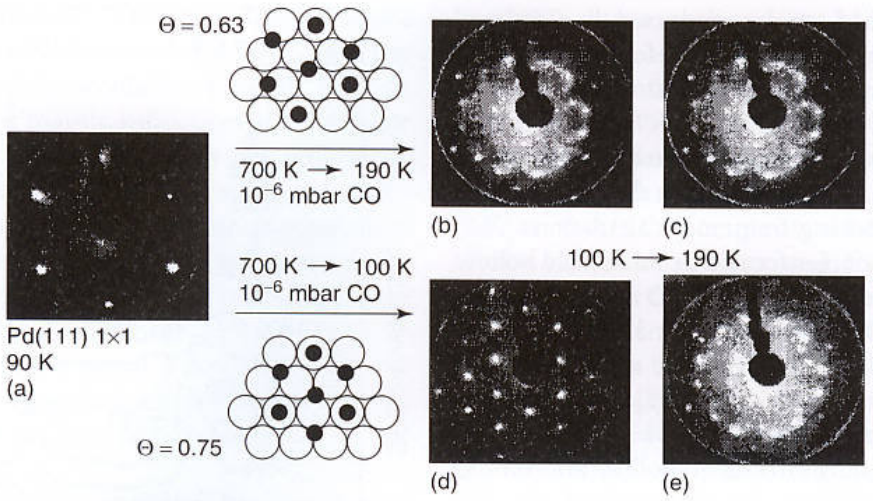

Fig. 39 LEED images of CO structures on Pd(111). (a) The clean (1 × 1) Pd(111) surface; (b) after cooling the surface in 10^{-6} mbar CO from 700 to 190 K, producing a surface coverage of 0.63 ML. This structure is sensitive to the electron beam, and converts to the structure in panel (c) within a few seconds. A (2 × 2) structure with 0.75 ML coverage is obtained after cooling the surface in 10^{-6} mbar CO from 700 to 100 K. The corresponding structural models (adapted from Tüshaus et al. [251]) are also shown (small circles, CO; large circles, Pd).

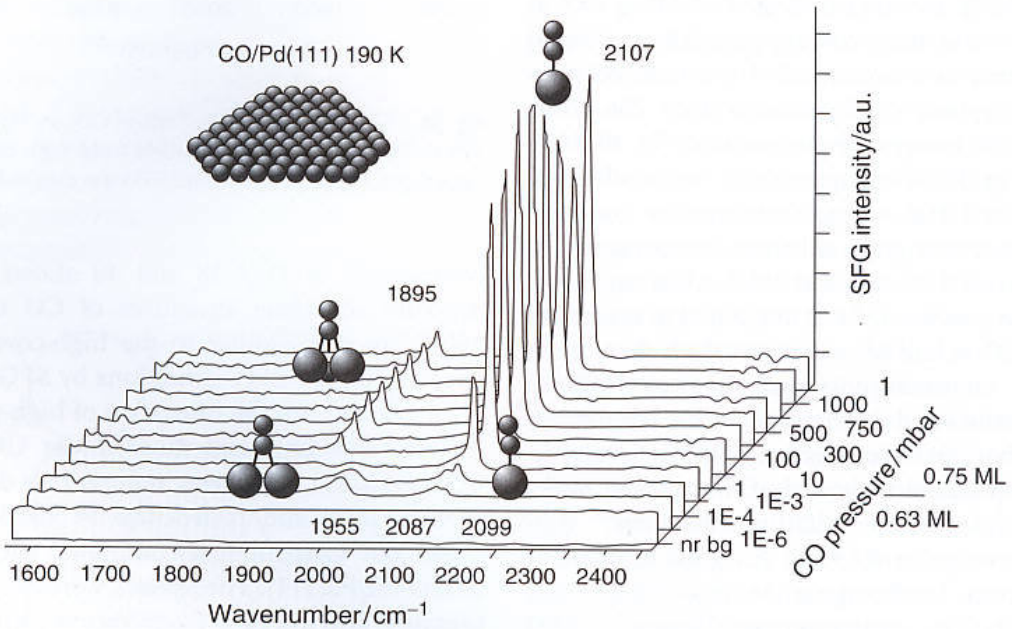

Fig. 40 SFG spectra of CO adsorption on Pd(111) at 190 K from 10 to 1000 mbar. The final spectrum at 1 mbar demonstrates the reversibility of the adsorbate structure.

was observed. In Ref. [259], it was stressed that great care must be taken to control the CO cleanliness during high-pressure experiments. For Pt(111), it was observed that coadsorbed water induces a red shift of the on-top CO frequency. When long-term experiments are carried out below the desorption temperature of water (~160 K for Pt and ~175 K for Pd), water traces from the residual gas cannot be fully excluded.

In the following, the results on Pd(111) will be briefly compared to SFG spectra of CO adsorbed on "rough" Pd(111) and alumina-supported Pd nanoparticles.

The SFG spectra in Fig. 42 were taken from a "defect-rich" Pd(111) surface. Auger electron spectroscopy (AES) indicated that the crystal was clean, but LEED showed a (1 × 1) pattern with broad spots. The crystal surface can be considered as being composed of (111) terraces and all sorts of "defects" that may include steps and kinks; the steps may also be regarded as (110) or (113) microfacets (or more precisely nanofacets). The temperature series in Fig. 42 is very similar to the corresponding spectra of the well-ordered (111) surface (Fig. 38), except that on the imperfect surface an additional peak is observed at

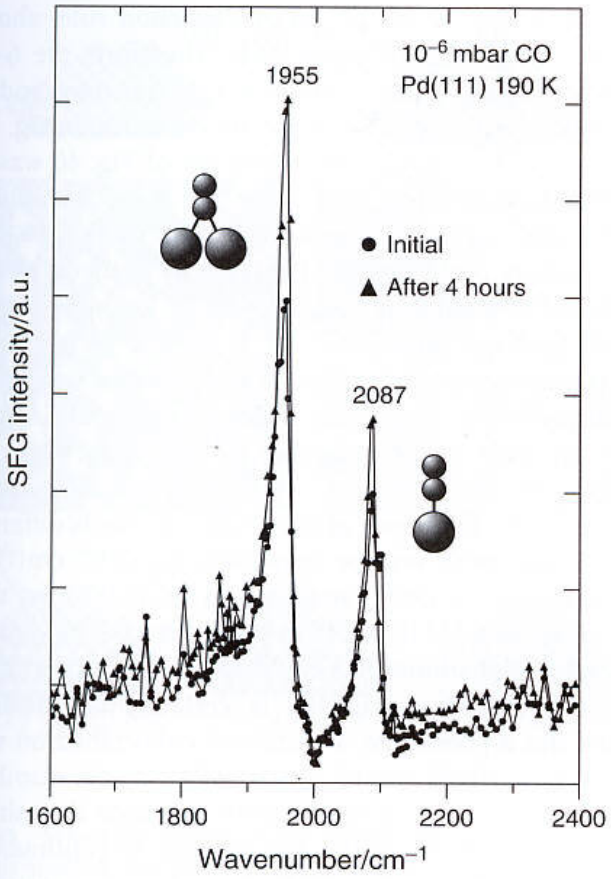

Fig. 41 SFG spectra of 10^{-6} mbar CO on Pd(111) at 190 K: ●, initial spectrum; ▲, after 4 h of high-pressure exposure.

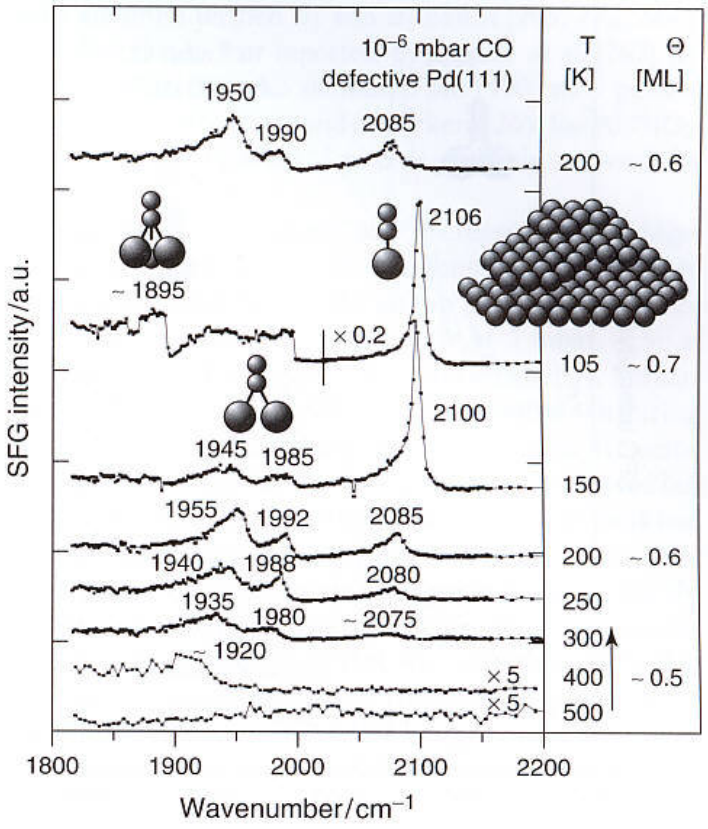

Fig. 42 SFG spectra of 10^{-6} mbar CO on "defect-rich" Pd(111) from 500 to 105 K. The spectra were recorded from high to low temperature. Approximate coverages are also indicated [286]. When compared to the perfect (111) surface, an additional peak at 1980–1990 cm^{-1} appeared.

1980–1990 cm^{-1}. It is therefore apparent that this species is related to CO adsorbed on step (low coordination) sites. The frequency range (1980–1990 cm^{-1}) suggests that it is a defect-related, bridge-bonded species, for example, bridged CO on a step edge. Bridge-bonded species around 1985 cm^{-1} have also been assigned to CO on Pd(100) [72, 144, 271], Pd(110) [267, 272, 273], Pd(210) [144, 252], and rough Pd thin films [252, 274].

The physical origin of the species at 1980–1990 cm^{-1} may be explained in several ways. It may originate from a specific binding site at a step edge (or nanofacet), but it may also arise from coupling between CO molecules on a step and neighboring CO molecules on a (111) terrace. In order deliberately to introduce defects on a smooth Pd(111) surface, we sputtered the surface at low temperature (700 eV Ar^+ at 100 K) without subsequent annealing. Figure 43 shows a sequence of spectra acquired on such a sputtered surface. At 10^{-4} Pa (10^{-6} mbar) CO and 200 K (Fig. 43a), a bridge peak and a broad band in the on-top region were observed, but the bridge peak had a resonance frequency characteristic for the defect/step sites (1990 cm^{-1}) described above. When the surface was heated to 300 K in the gas and then cooled to 200 K, the bridge species increased in intensity (Fig. 43b). This ordering effect is also known from the regular (111) surface. When CO is exposed at higher temperature and the crystal is cooled, the higher mobility of CO allows it to obtain better-ordered structures. However, when the sample was annealed to 600 K and cooled, the regular bridge species at 1954 cm^{-1} and a sharp on-top peak were observed (Fig. 43c). Obviously, on Pd(111), annealing to 600 K is sufficient to heal defects produced by sputtering.

We will now compare the results described above to the SFG spectra of CO on alumina-supported Pd nanoparticles [275]. Two aspects will be considered: (i) the relative ratio of on-top/ bridge adsorption; and (ii) the resonance frequencies. Figure 44a shows SFG spectra of CO on Pd particles of 6-nm mean size (ca. 4000 atoms per particle) taken at 190 K between 10^{-5} and 2×10^4 Pa CO background pressure (at higher pressure, the signal became very small because of IR absorption). The Pd particles were grown at 300 K and mainly exhibited (111) and (100) surface facets, as shown in Fig. 45c,e [276–279]. The (111) top facet dominates the particle morphology because the contribution of (111) and (100) side facets is rather small. In addition, CO adsorbed on the side facets is tilted with respect to the underlying metal substrate

References see page 1410

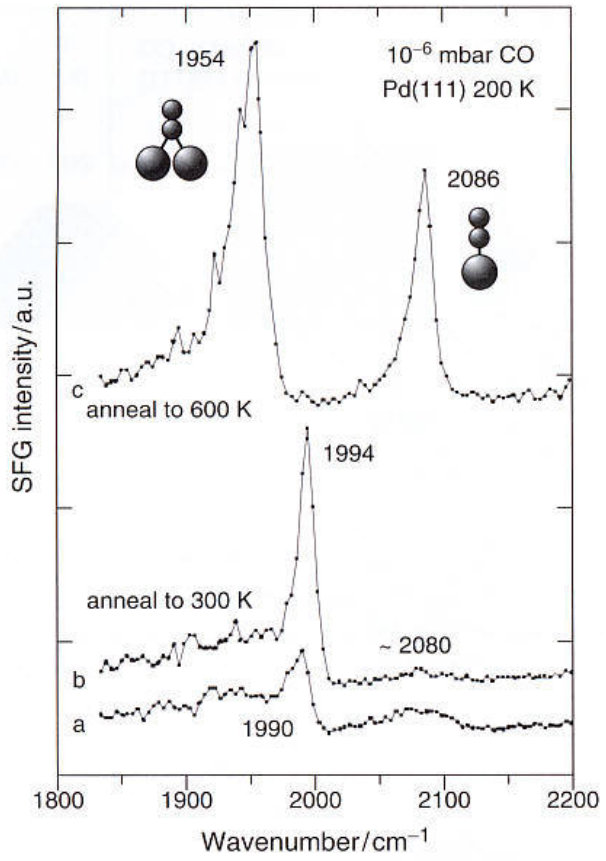

Fig. 43 Effect of sputtering on the SFG spectra of CO on Pd(111) at 200 K. (a) 10^{-6} mbar CO on a strongly sputtered surface; (b) after annealing to 300 K. The observed peak is characteristic of a defect-related bridge site. After annealing to 600 K (c), a vibrational spectrum typical of perfect Pd(111) is obtained. All spectra were recorded at 200 K.

and, according to the IR surface-selection rule, should produce only a small signal [252]. Therefore, the 6-nm particles should behave similarly to a (111) surface, and the corresponding single-crystal spectra are shown in Fig. 44b (for ease of comparison the spectrum of Fig. 40 was replotted in a different way). The 10^{-5} Pa CO spectrum on the Pd particles is indeed similar to the 10^{-4} Pa (10^{-6} mbar) spectrum on Pd(111). In both cases, CO preferred to bond as a bridging species and only a small on-top peak was observed.

It was mentioned previously that a quantitative analysis is difficult, but if we take the integrated SFG signal intensity as a rough estimate, the on-top/bridge ratio is ~0.2 on Pd(111) and <0.1 on the nanoparticles. However, the frequency of the bridge species is different. The bridge peak on the nanoparticles (1977 cm^{-1}) is characteristic for defective (stepped) Pd(111) rather than CO bridge bonded to a perfect (111) terrace (1955 cm^{-1}). Several explanations may account for this observation. The ball model in Fig. 45e is certainly an idealized model (for a given size, a truncated cuboctahedron with complete surfaces would consist of a "magic number" of atoms). During particle growth by vapor deposition, the number of Pd atoms per particle is continuously increased, and consequently some surface steps must be present even on well-faceted nanoparticles. The particle will have monatomic steps, and such steps have been actually imaged by high-resolution transmission electron microscopy (HRTEM) [280, 281] and STM (see Fig. 41 (top) in Ref. [278]). This is equivalent to the presence of

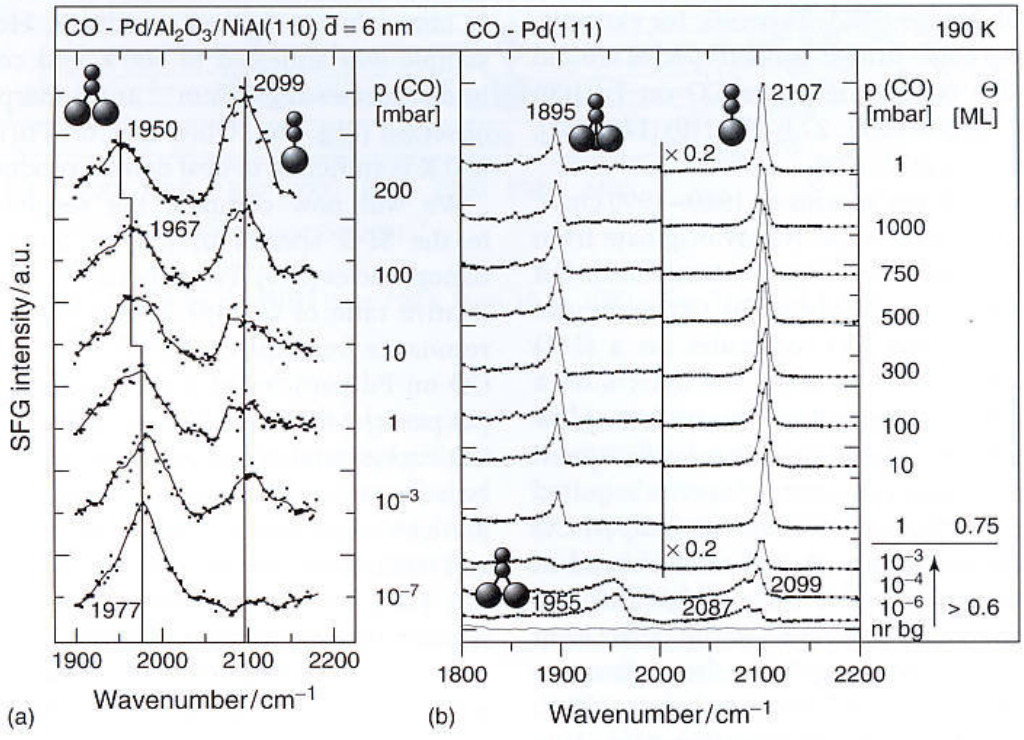

Fig. 44 Comparison of CO adsorption on Al_2O_3-supported Pd nanoparticles (mean size 6 nm) and on Pd(111) at 190 K (see text).

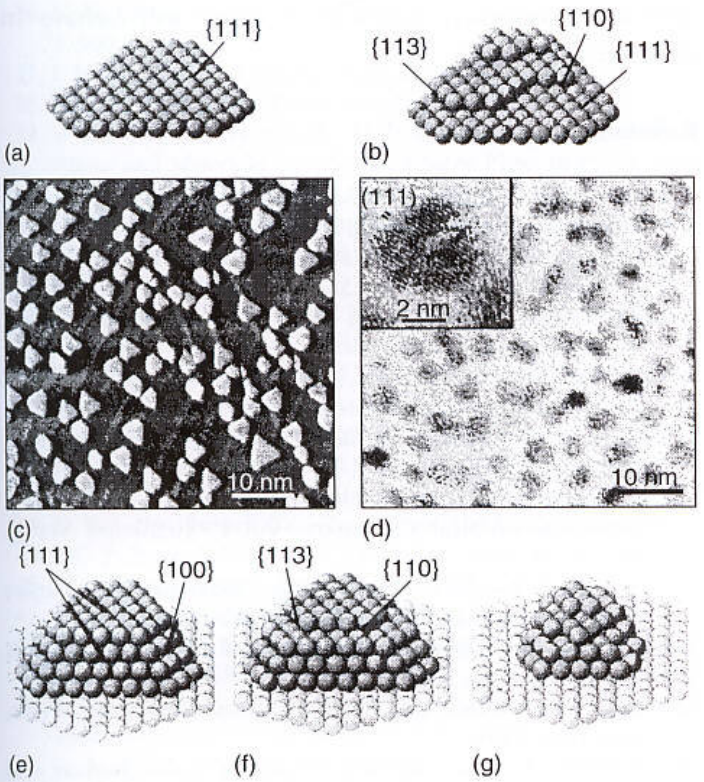

Fig. 45 Schematic models of the different Pd surfaces employed in this study. A well-ordered Pd(111) and a "defect rich" Pd(111) including various defects are shown in panels (a) and (b). An STM image (CCT, 100 nm ×100 nm; adapted from Refs. [278] and [279]) of Pd nanoparticles grown on Al_2O_3/NiAl(110) and a transmission electron micrograph are displayed in panels (c) and (d); see text for details. Depending on the growth conditions, the Pd particles may have different morphologies and surface structures; for example, a well-faceted truncated cuboctahedron (e), with surface steps (f), and highly defective (g).

{110} and {113} nanofacets. It is therefore not surprising that the resonance frequency of bridge-bonded CO is different on nanoparticles and on Pd(111). The observed frequency is not necessarily characteristic for a specific binding site, but may represent the whole ensemble. The coupling of CO molecules bound to steps and particle edges to those on the terraces may give rise to a peak that cannot be observed on the perfect Pd(111) surface. Density functional studies of CO adsorption on cuboctahedral Pd nanoparticles by Neyman and Rösch [282] have indeed shown that the vibrational frequency of bridge-bonded CO on the particle edges is different from that of bridge-bonded CO on the terraces.

IRAS spectra of $Pd/Al_2O_3/NiAl(110)$ by Wolter et al. [283], which provide higher spectral resolution, have identified two bridge-bonded species on large well-faceted Pd particles at saturation coverage of CO. The dominant species was defect (edge or step)-related, bridge-bonded CO (ca. 1990 cm^{-1}), but a smaller peak due to CO bridge bonded to "perfect" (111) terraces at −1950 cm^{-1} (i.e., at the (111) single-crystal value) was also evident (these peaks are often termed B_1 and B_2 bands [265, 272, 284]). A similar result was reported by Rainer et al. [267] for $Pd/Al_2O_3/Ta(110)$, who attributed the 1990 cm^{-1} peak to (100) facets, and by Yates and coworkers [265] for Pd/SiO_2. In any case, the 1950 cm^{-1} peak is probably too weak for our SFG set-up.

When the CO pressure was increased, the bridge-bonded CO peak decreased in intensity and shifted to lower wavenumber, while the on-top peak increased (on-top/bridge ratio at 10^{-3} mbar, 0.5; at 1 mbar, 0.5; at 10 mbar, 0.7; at 100 mbar, 1.2; at 200 mbar, 1.7). Similar spectral changes can be seen on Pd(111) in Fig. 44b during the bridge/on-top to hollow/on-top transition. It seems that the CO coverage on the nanoparticles is increased but the 0.75 ML structure is not reached – the bridge peak had not even disappeared at 200 mbar. Gelin and Yates [265] and Rainer et al. [267] report a similar behavior for Pd particles on silica and alumina. This effect is probably related to the heterogeneity of the particle surface that prevents the phase transition from (fully) occurring. If this argument-based on surface roughness is true, then one would expect a different SFG spectrum on defect-rich "rough" Pd particles.

Figure 46 shows the corresponding SFG spectra of CO adsorbed on 3.5-nm Pd particles (ca. 850 atoms per particle) grown at 90 K. These particles exhibited "rough" surfaces with many defects, and distinct facets were absent [276] (Fig. 45g). The bridge frequency was again found at 1978 cm^{-1}, indicating a defect-related bridge species. Whilst on Pd(111) and on the 6-nm particles the on-top peak was rather small, a pronounced on-top peak was observed on the 3.5-nm nanoparticles (on-top/bridge ratio of −1.1), in good agreement with impregnated samples [284]. The higher abundance of on-top CO is a clear indication of the highly defective surface of the nanoparticles. On rough particles, many defect sites (e.g., protruding Pd atoms) are available and lateral CO interactions are much reduced; this presumably favors a higher fraction of on-top CO.

If the SFG spectra of the 6- and 3.5-nm Pd particles at 10^{-7} mbar are compared, it is evident that the adsorption site occupancy is different. If this were to be extrapolated directly to the high-pressure regime, one might be tempted to explain any difference in the catalytic activity of the 6- and 3.5-nm Pd particles by the different adsorption site distribution. However, as discussed below, this assumption is incorrect.

Upon increasing the CO pressure on the 3.5-nm Pd particles (Fig. 46), similar changes as for the 6-nm particles were observed (frequency shift and intensity decrease of bridgebonded CO, intensity increase of on-top CO; on-top/bridge ratio at 10^{-7} mbar of 1.1; at 10^{-3} mbar

References see page 1410

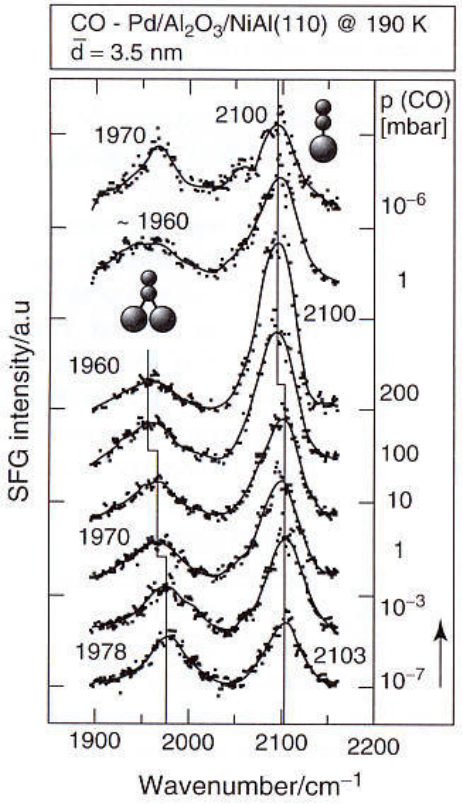

Fig. 46 SFG spectra of CO adsorption on Al_2O_3-supported Pd nanoparticles at 190 K and between 10^{-7} and 200 mbar. The Pd particles had a mean size of 3.5 nm, and were expected to have rough surfaces due to their growth at 90 K. At low pressure, a higher fraction of on-top CO is observed on the "rough" Pd particles when compared to well-faceted nanocrystals (cf. Fig. 45a).

of 1.6; at 1 mbar of 2.2; at 10 mbar of 2.2; at 100 mbar of 2.5; at 200 mbar of 4.4; at 1 mbar of 1.9; at 10^{-6} mbar of 1.4). At high pressure (e.g., 200 mbar), an adsorption site occupancy was achieved that is very similar for both particle sizes. The pressure series in Fig. 46 again shows the tendency toward a bridge/on-top to hollow/on-top transition, but this process is still incomplete at 200 mbar because of the heterogeneity of the surface. In contrast, on smooth Pd(111), even a pressure of 1 mbar was enough for the disappearance of bridge-bonded CO (see Fig. 45b). The defect concentration on defect-rich Pd(111) was probably not high enough to prevent the phase transition (cf. Fig. 43). When the pressure was decreased, the initial spectra could be reproduced, indicating the absence of structural changes.

Of course this may be different for other transition metals, but in the present case there are no changes in structure detected, and the differences in spectra can be fully accounted for by the morphological differences. The example, however, serves to show that studies on chemisorption under UHV can be extended to ambient conditions, while the knowledge gained under UHV conditions can be used to explain observations at high pressure. Certainly, different systems will behave in different ways.

References

1. G. Wedler, *Adsorption, Chemische Taschenbücher*, Vol. 9, Verlag Chemie, Weinheim, 1970.
2. I. Langmuir, *J. Am. Chem. Soc.* **1916**, *38*, 2221.
3. I. Langmuir, *J. Am. Chem. Soc.* **1918**, *40*, 1361.
4. W. Friedrich, P. Knipping, M. v. Laue, *Sitzungsber. Bayer. Akad. Wiss.*, **1912**, 303/367.
5. T. N. Rhodin, G. Ertl (Eds.), *The Nature of the Surface Chemical Bond*, North Holland, Amsterdam, 1979.
6. A. Zangwill, *Physics at Surfaces*, Cambridge University Press, Cambridge, 1988.
7. K. Christmann, *Introduction to Surface Physical Chemistry*, Topics in Physical Chemistry, Vol. 1, Steinkopff Verlag, Darmstadt, 1991.
8. G. Ertl, J. Küppers, *Low Energy Electrons and Surface Chemistry*, 2nd edn. Verlag Chemie, Weinheim, 1985.
9. A. Clark, *The Theory of Adsorption and Catalysis*, Academic Press, New York, 1970.
10. J. G. Dash, *Films on Solid Surfaces*, Academic Press, New York, 1975.
11. S. Cerny, in *The Chemical Physics of Solid Surfaces and Heterogeneous Catalysis*, D. A. King, D. P. Woodruff (Eds.), Vol. 2, Elsevier, Amsterdam, 1983, pp. 1–57.
12. W. A. Steele, *The Interaction of Gases with Solid Surfaces*, Pergamon Press, Oxford, 1974.
13. K. Christmann, J. E. Demuth, *Surf. Sci.* **1982**, *120*, 291.
14. O. Beeck, W. A. Cole, A. Wheeler, *Faraday Disc.* **1950**, 314.
15. J. Bagg, F. C. Tompkins, *Trans. Faraday Soc.* **1955**, *51*, 1071.
16. D. Brennan, D. O. Hayward, B. M. W. Trapnell, *Proc. R. Soc. London, Ser. A* **1960**, *256*, 81.
17. G. Wedler, *Z. Phys. Chem. (Frankfurt/M.)* **1960**, *24*, 73.
18. F. J. Brocker, G. Wedler, *Faraday Disc.* **1966**, 87.
19. G. Wedler, H. Strothenk, *Ber. Bunsenges. Phys. Chem.* **1966**, *70*, 214.
20. G. Wedler, I. Ganzmann, D. Borgmann, *Ber. Bunsen-Ges. Phys. Chem.* **1993**, *97*, 293.
21. C. Pluntke, G. Wedler, G. Rau, *Surf. Sci.* **1983**, *134*, 145.
22. D. A. King, *Phys. Scr.* **1993**, *T49*, 560.
23. N. Al-Sarraf, J. T. Stuckless, C. E. Wartnaby, D. A. King, *Surf. Sci.* **1993**, *283*, 427.
24. C. E. Borronibird, N. Alsarraf, S. Andersson, D. A. King, *Chem. Phys. Lett.* **1991**, *183*, 516.
25. C. E. Borronibird, D. A. King, *Rev. Sci. Inst.* **1991**, *62*, 2177.
26. S. J. Dixonwarren, M. Kovar, C. E. Wartnaby, D. A. King, *Surf. Sci.* **1994**, *16*, 307.
27. J. T. Stuckless, N. A. Frei, C. T. Campbell, *Rev. Sci. Inst.* **1998**, *69*, 2427.
28. S. F. Diaz, J. F. Zhu, N. Shamir, C. T. Campbell, *Sens. Actuators, B* **2005**, *107*, 454.
29. G. Ehrlich, *Adv. Catal.* **1963**, *14*, 255.
30. P. A. Redhead, *Vacuum* **1962**, *12*, 203.
31. D. A. King, *Surf. Sci.* **1975**, *47*, 384.
32. D. Menzel, in *Interactions on Metal Surfaces*, R. Gomer (Ed.), Topics in Applied Physic Vol. 4, Springer, Heidelberg, 1975, p. 102.
33. L. A. Petermann, *Prog. Surf. Sci.* **1972**, *3*, 1.
34. H. Niemantsverdriet, *Spectroscopy in Catalysis: An Introduction*, Verlag Chemie, Weinheim, 1993.
35. M. Polanyi, *Trans. Faraday Soc.* **1932**, *28*, 314.

36. C. M. Chan, R. Aris, W. H. Weinberg, *Appl. Surf. Sci.* **1978**, *1*, 360.
37. J. L. Falconer, R. J. Madix, *Surf. Sci.* **1975**, *48*, 393.
38. J. E. Lennard-Jones, *Trans. Faraday Soc.* **1932**, *28*, 333.
39. V. Bortolani, N. H. March, M. P. Tosi (Eds.), *Interactions of Atoms and Molecules with Solid Surfaces*, Plenum Press, New York, 1990.
40. M.-C. Derjonquéres, D. Spanjaard (Eds.), *Concepts in Surfaces Physics*, Springer Series in Surfaces Science Vol. 30, Springer, Heidelberg, 1993.
41. K. Horn, M. Scheffler (Eds.), *Electronic Structure*, Handbook of Surface Science Vol. 2, Elsevier, Amsterdam, 2000.
42. P. S. Bagus, G. Pacchioni, *J. Elect. Spect. Rel. Phenom.* **1994**, *69*, R7.
43. H. A. Michelsen, C. T. Rettner, D. J. Auerbach, in *Surface Reactions*, R. J. Madix (Ed.), Springer Series in Surface Science, Vol. 34, Springer, Heidelberg, 1994, 185.
44. G. Ertl, *Ber. Bunsen-Ges. Phys. Chem.* **1982**, *86*, 425.
45. J. C. Polanyi, *Science* **1987**, *236*, 680.
46. G. Comsa, R. David, *Surf. Sci. Rep.* **1985**, *5*, 145.
47. K. Christmann, *Surf. Sci. Rep.* **1988**, *9*, 1.
48. M. Balooch, M. J. Cardillo, D. R. Miller, R. E. Stickney, *Surf. Sci.* **1974**, *46*, 358.
49. G. D. Kubiak, G. O. Sitz, R. N. Zare, *J. Chem. Phys.* **1985**, *83*, 2538.
50. G. Anger, A. Winkler, K. D. Rendulic, *Surf. Sci.* **1989**, *220*, 1.
51. H. F. Berger, M. Leisch, A. Winkler, K. D. Rendulic, *Chem. Phys. Lett.* **1990**, *175*, 425.
52. J. K. Norskov, P. Stoltze, *Surf. Sci.* **1987**, *189*, 91.
53. J. Harris, S. Andersson, *Phys. Rev. Lett.* **1985**, *55*, 1583.
54. J. Harris, *Appl. Phys. A* **1988**, *47*, 63.
55. T. Mitsui, M. K. Rose, E. Fomin, D. F. Ogletree, M. Salmeron, *Nature* **2003**, *422*, 705
56. H. Brune, J. Wintterlin, R. J. Behm, G. Ertl, *Phys. Rev. Lett.*, *68*, 624.
57. M. Schmid, G. Leonardelli, R. Tscheließnig, A. Biedermann, P. Varga, *Surf. Sci.* **2001**, *478*, L355.
58. J. C. Tracy, P. W. Palmberg, *J. Chem. Phys.* **1969**, *51*, 4852.
59. J. Koutecky, *Trans. Faraday Soc.* **1958**, *54*, 1038.
60. T. B. Grimley, *Adv. Catal.* **1960**, *12*, 1.
61. T. B. Grimley, *Ber. Bunsenges. Phys. Chem.* **1971**, *75*, 1003.
62. T. L. Einstein, J. R. Schrieffer, *Phys. Rev. B* **1973**, *7*, 3629.
63. G. Ertl, in *The Nature of Surface Chemical Bond*, T. N. Rhodin, G. Ertl (Eds.), North-Holland, Amsterdam, 1979.
64. R. L. Park, T. L. Einstein, A. R. Kortan, L. D. Roelofs, in *Ordering in Two Dimensions*, S. K. Sinha (Ed.), North Holland, Amsterdam, 1980, pp. 17–24.
65. B. N. J. Persson, *Surf. Sci.* **1991**, *258*, 451.
66. T. L. Hill, *An Introduction to Statistical Thermodynamics*, Addison Wesley, Reading, 1962.
67. W. Gebhardt, U. Krey, *Phasenübergänge und kritische Phänomene*, Vieweg, Braunschweig, 1980.
68. G. Kortüm, *Einführung in die chemische Thermodynamik*, 6th edn., Vandenhoeck und Ruprecht, Göttingen, 1972.
69. G. Ertl, in *Chemistry and Physics of Solid Surfaces VIII*, R. Vanselow, R. Howe (Eds.), Springer Series in Surface Science, Vol. 22, Springer, Heidelberg, 1990, 1.
70. E. Bauer, in *Structure and Dynamics of Surfaces II*, W. Schommers, P. von Blankenhagen (Eds.), Springer, Berlin, 1987, 115–779.
71. K. Christmann, O. Schober, G. Ertl, *J. Chem. Phys.* **1974**, *60*, 4719.
72. R. J. Behm, K. Christmann, G. Ertl, M. A. van Hove, *J. Chem. Phys.* **1980**, *73*, 2984.
73. K. Christmann, O. Schober, G. Ertl, M. Neumann, *J. Chem. Phys.* **1974**, *60*, 4528.
74. J. P. Biberian, M. A. van Hove, *Surf. Sci.* **1982**, *118*, 443.
75. J. Pritchard, *Surf. Sci.* **1979**, *79*, 231.
76. D. A. King, M. G. Wells, *Surf. Sci.* **1972**, *29*, 454.
77. D. A. King, M. G. Wells, *Proc. R. Soc. London, Ser. A* **1974**, *339*, 245.
78. K. D. Rendulic, G. Anger, A. Winkler, *Surf. Sci.* **1989**, *208*, 404.
79. C. T. Rettner, H. E. Pfnur, D. J. Auerbach, *Phys. Rev. Lett.* **1985**, *54*, 2716.
80. C. T. Rettner, L. A. DeLouise, D. J. Auerbach, *J. Chem. Phys.* **1986**, *85*, 1131.
81. M. B. Lee, Q. Y. Yang, S. T. Ceyer, *J. Chem. Phys.* **1987**, *87*, 2724.
82. A. V. Hamza, H. P. Steinruck, R. J. Madix, *J. Chem. Phys.* **1987**, *86*, 6506.
83. A. C. Luntz, D. S. Bethune, *J. Chem. Phys.* **1989**, *90*, 1274.
84. M. J. Temkin, V. Pyshev, *Acta Physicochim.* **1940**, *12*, 327.
85. S. Brunauer, P. H. Emmett, E. Teller, *J. Am. Chem. Soc.* **1938**, *60*, 309.
86. H. Freundlich, *Colloid and Capillary Chemistry*, Methew, London, 1926.
87. J. Zeldowitsch, *Acta Physicochim.* **1934**, *1*, 961.
88. D. M. Young, A. D. Crowell, *Physical Adsorption of Gases*, Butterworth, London, 1962.
89. B. Poelsema, L. K. Verheij, G. Comsa, *Surf. Sci.* **1985**, *152*, 496.
90. K. D. Rendulic, *Appl. Phys. A* **1988**, *47*, 55.
91. J. N. Russell, I. Chorkendorff, A. M. Lanzillotto, M. D. Alvey, J. T. Yates, *J. Chem. Phys.* **1986**, *85*, 6186.
92. M. A. Morris, M. Bowker, D. A. King, in *Simple Processes at the Gas Solid Interface*, C. H. Bamford, C. F. H. Tipper, R. G. Compton (Eds.), Elsevier, Amsterdam, 1984, p. 1179.
93. P. J. Kisliuk, *J. Phys. Chem. Solids* **1957**, *3*, 95.
94. P. J. Kisliuk, *J. Phys. Chem. Solids* **1958**, *5*, 78.
95. T. Engel, *J. Chem. Phys.* **1978**, *69*, 373.
96. G. Ertl, J. Koch, *Z. Naturforsch. A* **1970**, *A25*, 1906.
97. C. T. Campbell, G. Ertl, H. Kuipers, J. Segner, *Surf. Sci.* **1981**, *107*, 207.
98. K. Heinz, *Prog. Surf. Sci.* **1988**, *27*, 239.
99. K. Heinz, *Vacuum* **1990**, *41*, 328.
100. G. Ertl, *Science* **1991**, *254*, 1750.
101. M. G. Tenner, E. W. Kuipers, A. W. Kleyn, S. Stolte, *J. Chem. Phys.* **1988**, *89*, 6552.
102. E. W. Kuipers, M. G. Tenner, A. W. Kleyn, S. Stolte, *Nature* **1988**, *334*, 420.
103. G. H. Fecher, N. Bowering, M. Volkmer, B. Pawlitzky, U. Heinzmann, *Surf. Sci.* **1990**, *230*, L169.
104. G. H. Fecher, M. Volkmer, B. Pawlitzky, N. Bowering, U. Heinzmann, *Vacuum* **1990**, *41*, 265.
105. H. Muller, B. Dierks, F. Hamza, G. Zagatta, G. H. Fecher, N. Bowering, U. Heinzmann, *Surf. Sci.* **1992**, *270*, 207.
106. H. Muller, G. Zagatta, N. Bowering, U. Heinzmann, *Chem. Phys. Lett.* **1994**, *223*, 197.
107. H. P. Bonzel, *Surf. Sci.* **1971**, *27*, 387.
108. H. P. Bonzel, R. Ku, *J. Chem. Phys.* **1973**, *59*, 1641.
109. H. P. Bonzel, E. E. Latta, *Surf. Sci.* **1978**, *76*, 275.
110. R. Butz, H. Wagner, *Surf. Sci.* **1979**, *87*, 85.
111. R. Butz, H. Wagner, *Surf. Sci.* **1979**, *87*, 69.
112. G. Ehrlich, in *Surface Science: Recent Progress and Perspectives*, T. S. Jayadenaah, R. Vanselow (Eds.), CRC Press, Cleveland, Ohio, 1974.
113. J. Holzl, G. Porsch, *Thin Solid Films* **1975**, *28*, 93.

114. P. Schrammen, J. Holzl, *Surf. Sci.* **1983**, *130*, 203.
115. G. L. Kellogg, *Surf. Sci. Rep.* **1994**, *21*, 1.
116. E. G. Seebauer, C. E. Allen, *Prog. Surf. Sci.* **1995**, *49*, 265.
117. J. R. Chen, R. Gomer, *Surf. Sci.* **1979**, *79*, 413.
118. S. C. Wang, R. Gomer, *J. Chem. Phys.* **1985**, *83*, 4193.
119. H. H. Rotermund, S. Nettesheim, A. von Oertzen, G. Ertl, *Surf. Sci.* **1992**, *275*, L645.
120. A. A. Deckert, J. L. Brand, M. V. Arena, S. M. George, *Surf. Sci.* **1989**, *208*, 441.
121. Z. Rosenzweig, I. Farbman, M. Asscher, *J. Chem. Phys.* **1993**, *98*, 8277.
122. B. Boddenberg, V. Grundke, G. Auer, *Ber. Bunsen-Ges. Phys. Chem.* **1990**, *94*, 348.
123. L. Kevan, M. K. Bowman, *Modern Pulsed and Continuous Wave Electron Spin Resonance*, Wiley, New York, 1990.
124. H. Schlienz, M. Beckendorf, U. J. Katter, T. Risse, H.-J. Freund, *Phys. Rev. Lett.* **1995**, *74*, 761.
125. L. Boltzmann, *Wien. Ann.* **1904**, *53*, 53.
126. W. M. Sachtler, *Le Vide* **1973**, *28*, 67.
127. P. van der Plank, W. M. Sachtler, *J. Catal.* **1967**, *7*, 300.
128. P. van der Plank, W. M. Sachtler, *J. Catal.* **1968**, *12*, 35.
129. A. A. Balandin, *Adv. Catal.* **1958**, *10*, 96.
130. S. D. Kevan (Ed.) *Angle Resolved Photoemission: Theory and Current Applications*, Studies in Surface Science and Catalysis, Vol. 74, Elsevier, Amsterdam, 1982.
131. H.-J. Freund, M. Neumann, *Appl. Phys. A* **1988**, *47*, 3.
132. D. Cappus, J. Klinkmann, H. Kuhlenbeck, H.-J. Freund, *Surf. Sci.* **1995**, *325*, L421.
133. C. Xu, B. Dillmann, H. Kuhlenbeck, H.-J. Freund, *Phys. Rev. Lett.* **1991**, *67*, 3551.
134. D. W. Turner, C. Baker, A. D. Baker, C. R. Brundle, *Molecular Photoelectronic Spectroscopy*, Wiley, New York, 1970.
135. W. Eberhardt, H.-J. Freund, *J. Chem. Phys.* **1983**, *78*, 700.
136. D. Schmeisser, F. Greuter, E. W. Plummer, H. J. Freund, *Phys. Rev. Lett.* **1985**, *54*, 2095.
137. H. J. Freund, W. Eberhardt, D. Heskett, E. W. Plummer, *Phys. Rev. Lett.* **1983**, *50*, 768.
138. C. L. Allyn, Thesis, University of Pennsylvania, 1978.
139. G. Odörfer, Diploma Thesis, Universität Erlangen-Nürnberg, 1987.
140. G. Blyholder, *J. Phys. Chem.* **1964**, *68*, 2772.
141. G. Blyholder, *J. Vac. Sci. Technol.* **1974**, *11*, 865.
142. C. M. Kao, R. P. Messmer, *Phys. Rev. B* **1985**, *31*, 4835.
143. R. P. Eischens, W. A. Pliskin, *Adv. Catal.* **1958**, *10*, 1.
144. A. M. Bradshaw, F. M. Hoffmann, *Surf. Sci.* **1978**, *72*, 513.
145. L. Surnev, Z. Xu, J. T. Yates, *Surf. Sci.* **1988**, *201*, 1.
146. J. G. Chen, W. Erley, H. Ibach, *Surf. Sci.* **1989**, *223*, L891.
147. G. McElhiney, H. Papp, J. Pritchard, *Surf. Sci.* **1976**, *54*, 617.
148. H.-J. Freund, H. Kuhlenbeck, in *Applications of Synchrotron Radiation*, W. Eberhardt (Ed.), Springer Series in Surface Sciences, Vol. 35, Springer Verlag, Heidelberg, 1995, pp. 9–63.
149. T.-C. Chiang, G. Kaindl, D. E. Eastman, *Solid State Commun.* **1980**, *36*, 25.
150. C. B. Duke, *Surf. Sci.* **1978**, *70*, 674.
151. C. B. Duke, W. R. Salaneck, T. J. Fabish, J. J. Ritsko, H. R. Thomas, A. Paton, *Phys. Rev. B* **1978**, *18*, 5717.
152. J. W. Gadzuk, S. Holloway, C. Mariani, K. Horn, *Phys. Rev. Lett.* **1982**, *48*, 1288.
153. U. Hoefer, M. J. Breitschafter, E. Umbach, *Phys. Rev. Lett.* **1990**, *64*, 3050.
154. M. Bertolo, W. Hansen, K. Jacobi, *Phys. Rev. Lett.* **1991**, *67*, 1898.
155. J. Kessler, F. Thieme, *Surf. Sci.* **1977**, *67*, 405.
156. N. V. Richardson, A. M. Bradshaw, in *Electron Spectroscopy*, C. R. Brundle, A. D. Baker (Eds.), Vol. 4, Academic Press, New York, 1982.
157. E. W. Plummer, W. Eberhardt, *Adv. Chem. Phys.* **1982**, *49*, 533.
158. C. L. Allyn, T. Gustafsson, E. W. Plummer, *Chem. Phys. Lett.* **1977**, *47*, 127.
159. K. Horn, A. M. Bradshaw, K. Jacobi, *Surf. Sci.* **1978**, *72*, 719.
160. H. Kuhlenbeck, M. Neumann, H. J. Freund, *Surf. Sci.* **1986**, *173*, 194.
161. F. Greuter, D. Heskett, E. W. Plummer, H. J. Freund, *Phys. Rev. B* **1983**, *27*, 7117.
162. E. S. Jensen, T. N. Rhodin, *Phys. Rev. B* **1983**, *27*, 3338.
163. N. D. Shinn, *J. Vac. Sci. Technol. A* **1986**, *4*, 1351.
164. R. Miranda, K. Wandelt, D. Rieger, R. D. Schnell, *Surf. Sci.* **1984**, *139*, 430.
165. K. Horn, A. M. Bradshaw, K. Hermann, I. P. Batra, *Solid State Commun.* **1979**, *31*, 257.
166. G. Borstel, M. Neumann, G. Seitz, W. Braun, *Proceedings 4th International Conference on Solid Surfaces*, Cannes, 1980.
167. P. Hofmann, J. Gossler, A. Zartner, M. Glanz, D. Menzel, *Surf. Sci.* **1985**, *161*, 303.
168. D. Heskett, E. W. Plummer, R. A. Depaola, W. Eberhardt, F. M. Hoffmann, H. R. Moser, *Surf. Sci.* **1985**, *164*, 490.
169. M. Steinkilberg, Thesis, Technische Universität München, 1977.
170. W. Braun, G. Meyer-Ehmsen, M. Neumann, E. Schwarz, *Surf. Sci.* **1979**, *89*, 354.
171. H. Kuhlenbeck, Diploma Thesis, Universität Osnabrück, 1984.
172. C. W. Seabury, T. N. Rhodin, M. M. Traum, R. Benbow, Z. Hurych, *Surf. Sci.* **1980**, *97*, 363.
173. D. Rieger, R. D. Schnell, W. Steinmann, *Surf. Sci.* **1984**, *143*, 157.
174. P. Hofmann, S. R. Bare, D. A. King, *Surf. Sci.* **1982**, *117*, 245.
175. G. Apai, P. S. Wehner, R. S. Williams, J. Stohr, D. A. Shirley, *Phys. Rev. Lett.* **1976**, *37*, 1497.
176. R. J. Smith, J. Anderson, G. J. Lapeyre, *Phys. Rev. Lett.* **1976**, *37*, 1081.
177. H.-J. Freund, E. Umbach (Eds.), *Adsorption on Ordered Surfaces of Ionic Solids and Thin Films*, Springer Series in Surface Sciences, Vol. 33, Springer, Heidelberg, 1993.
178. V. E. Henrich, P. A. Cox, *The Surface Science of Metal Oxides*, Cambridge University Press, Cambridge, 1994.
179. M. Poehlchen, V. Staemmler, *J: Chem. Phys.* **1992**, *97*, 2583.
180. V. Staemmler, in *Adsorption on Ordered Surfaces of Ionic Solids and Thin Films*, H.-J. Freund, E. Umbach (Eds.), Springer Series in Surface Science, Vol. 33, Springer Verlag, Berlin, 1993, p. 169.
181. G. Pacchioni, G. Cogliandro, P. S. Bagus, *Surf. Sci.* **1991**, *255*, 344.
182. G. Pacchioni, T. Minerva, *Surf. Sci.* **1992**, *275*, 450.
183. G. Pacchioni, *Surf. Sci.* **1993**, *281*, 207.
184. G. Pacchioni, P. S. Bagus, in *Adsorption on Ordered Surfaces of Ionic Solids and Thin Films*, H.-J. Freund, E. Umbach (Eds.), Springer Series in Surface Science, Vol. 33, Springer Verlag, Berlin, 1993, p. 180.
185. G. Pacchioni, K. M. Neyman, N. Roesch, *J. Elect. Spect. Rel. Phenom.* **1994**, *69*, 13.
186. K. M. Neyman, N. Roesch, *Chem. Phys.* **1992**, *168*, 267.
187. K. M. Neyman, N. Rosch, *Surf. Sci.* **1993**, *297*, 223.
188. K. M. Neyman, N. Roesch, *Chem. Phys.* **1993**, *177*, 561.
189. C. Pisani, R. Dovesi, R. Nada, S. Tamiro, *Surf. Sci.* **1989**, *216*, 489.

190. M. A. Nygren, L. G. M. Pettersson, *J. Elect. Spect. Rel. Phenom.* **1994**, *69*, 43.
191. S. M. Vesecky, X. P. Xu, D. W. Goodman, *J. Vac. Sci. Technol. A* **1994**, *12*, 2114.
192. M. C. Wu, C. M. Truong, D. W. Goodman, *J. Phys. Chem.* **1993**, *97*, 4182.
193. C. M. Truong, M. C. Wu, D. W. Goodman, *J. Am. Chem. Soc.* **1993**, *115*, 3647.
194. C. Xu, B. Dillmann, H. Kuhlenbeck, H. J. Freund, *Phys. Rev. Lett.* **1991**, *67*, 3551.
195. D. P. Woodruff, A. M. Bradshaw, *Rep. Prog. Phys.* **1994**, *57*, 1029.
196. K. M. Schindler, P. Hofmann, V. Fritzsche, S. Bao, S. Kulkarni, A. M. Bradshaw, D. P. Woodruff, *Phys. Rev. Lett.* **1993**, *71*, 2054.
197. A. M. Bradshaw, D. P. Woodruff, in *Applications of Synchrotron Radiation*, W. Eberhardt (Ed.), Springer Series in Surface Sciences, Vol. 35, Springer, Heidelberg, 1995, p. 127.
198. D. P. Woodruff, *Appl. Surf. Sci.* **2004**, *237*, 13.
199. J. H. Kang, R. L. Toomes, M. Polcik, M. Kittel, J. T. Hoeft, V. Efstathiou, D. P. Woodruff, A. M. Bradshaw, *J. Chem. Phys.* **2003**, *118*, 6059.
200. M. Kittel, D. I. Sayago, J. T. Hoeft, M. Polcik, M. Pascal, C. L. A. Lamont, R. L. Toomes, D. P. Woodruff, *Surf. Sci.* **2002**, *516*, 237.
201. M. Pascal, C. L. A. Lamont, M. Kittel, J. T. Hoeft, L. Constant, M. Polcik, A. M. Bradshaw, R. L. Toomes, D. P. Woodruff, *Surf. Sci.* **2002**, *512*, 173.
202. M. Kittel, J. T. Hoeft, S. Bao, M. Polcik, R. L. Toomes, J. H. Kang, D. P. Woodruff, M. Pascal, C. L. A. Lamont, *Surf. Sci.* **2002**, *499*, 1.
203. B. A. Gurney, W. Ho, *J. Vac. Sci. Technol. A* **1985**, *3*, 1541.
204. J. C. Bertolini, B. Tardy, *Surf. Sci.* **1981**, *102*, 131.
205. M. Nishijima, S. Masuda, Y. Sakisaka, M. Onchi, *Surf. Sci.* **1981**, *107*, 31.
206. P. R. Mahaffy, M. J. Dignam, *Surf. Sci.* **1980**, *97*, 377.
207. R. M. Lambert, *Surf. Sci.* **1975**, *49*, 325.
208. R. J. Behm, G. Ertl, V. Penka, *Surf. Sci.* **1985**, *160*, 387.
209. D. A. Wesner, F. P. Coenen, H. P. Bonzel, *Phys. Rev. B* **1989**, *39*, 10770.
210. D. A. Wesner, F. P. Coenen, H. P. Bonzel, *Phys. Rev. Lett.* **1988**, *60*, 1045.
211. H. Kuhlenbeck, H. B. Saalfeld, U. Buskotte, M. Neumann, H. J. Freund, E. W. Plummer, *Phys. Rev. B* **1989**, *39*, 3475.
212. N. Memmel, G. Rangelov, E. Bertel, V. Dose, K. Kometer, N. Roesch, *Phys. Rev. Lett.* **1989**, *63*, 1884.
213. G. Rangelov, N. Memmel, E. Bertel, V. Dose, *Surf. Sci.* **1991**, *251–252*, 965.
214. D. A. King, D. P. Woodruff (Eds.), *The Chemical Physics of Solid Surfaces and Heterogeneous Catalysis*, Vol. 3, Elsevier, Amsterdam, 1990.
215. K. Wandelt, *Surf. Sci. Reports* **1982**, *2*, 1.
216. C. R. Brundle, J. Q. Broughton, in *The Chemical Physics of Solid Surfaces and Heterogeneous Catalysis*, D. A. King, D. P. Woodruff (Eds.), Vol. 3, Elsevier, Amsterdam, 1990, p. 131.
217. R. Reval, M. A. Harrison, D. A. King, in *The Chemical Physics of Solid Surfaces and Heterogeneous Catalysis*, D. A. King, D. P. Woodruff (Eds.), Vol. 3, Elsevier, Amsterdam, 1990, p. 39.
218. F. Bozso, G. Ertl, M. Grunze, M. Weiss, *J. Catal.* **1977**, *49*, 18.
219. G. Ertl, *J. Vac. Sci. Technol. A* **1983**, *1*, 1247.
220. H. J. Freund, B. Bartos, R. P. Messmer, M. Grunze, H. Kuhlenbeck, M. Neumann, *Surf. Sci.* **1987**, *185*, 187.
221. M. Grunze, M. Golze, W. Hirschwald, H. J. Freund, H. Pulm, U. Seip, M. C. Tsai, G. Ertl, J. Kuppers, *Phys. Rev. Lett.* **1984**, *53*, 850.
222. M. C. Tsai, U. Seip, I. C. Bassignana, J. Kuppers, G. Ertl, *Surf. Sci.* **1985**, *155*, 387.
223. L. J. Whitman, C. E. Bartosch, W. Ho, G. Strasser, M. Grunze, *Phys. Rev. Lett.* **1986**, *56*, 1984.
224. D. Tomanek, K. H. Bennemann, *Phys. Rev. B* **1985**, *31*, 2488.
225. M. Grunze, M. Golze, J. Fuhler, M. Neumann, E. Schwarz, Berlin, in *Proceedings of the 8th Intern. Congr. on Catalysis* 1984, p. 233.
226. J. K. Norskov, T. Bligaard, A. Logadottir, S. Bahn, L. B. Hansen, M. Bollinger, H. Bengaard, B. Hammer, Z. Sljivancanin, M. Mavrikakis, Y. Xu, S. Dahl, C. J. H. Jacobsen, *J. Catal.* **2002**, *209*, 275.
227. S. Dahl, A. Logadottir, R. C. Egeberg, J. H. Larsen, I. Chorkendorff, E. Tornqvist, J. K. Norskov, *Phys. Rev. Lett.* **1999**, *83*, 1814.
228. B. Hammer, O. H. Nielsen, J. K. Norskov, *Catal. Lett.* **1997**, *46*, 31.
229. F. Winkelmann, S. Wohlrab, J. Libuda, M. Baumer, D. Cappus, M. Menges, K. Al-Shamery, H. Kuhlenbeck, H.-J. Freund, *Surf. Sci.* **1994**, *307–309*, 1148.
230. D. Cappus, C. Xu, D. Ehrlich, B. Dillmann, J. Ventrice, C. A. K. Al Shamery, H. Kuhlenbeck, H.-J. Freund, *Chem. Phys.* **1993**, *177*, 533.
231. F. Rohr, K. Wirth, J. Libuda, D. Cappus, M. Bäumer, H.-J. Freund, *Surf. Sci.* **1994**, *315*, L977.
232. P. W. Tasker, *Philos. Mag. A* **1979**, *39*, 119.
233. P. W. Tasker, *J. Phys. C: Solid State Phys.* **1978**, *12*, 4977.
234. D. Cappus, M. Haßel, E. Neuhaus, M. Heber, F. Rohr, H.-J. Freund, *Surf. Sci.* **1995**, *337*, 268.
235. G. Illing, Thesis, Ruhr-Universität Bochum, 1990.
236. R. Lacman, *Colloq. Int. CNRS* **1965**, *152*, 195.
237. D. Wolf, *Phys. Rev. Lett.* **1992**, *68*, 3315.
238. C. A. Ventrice Jr., T. Bertrams, H. Hannemann, A. Brodde, H. Neddermeyer, *Phys. Rev.* **1994**, *B49*, 5773.
239. M. Kiskinova, in *Poisoning and Promotion in Catalysis Based on Surface Science Concepts and Experiments*, Studies in Surface Science and Catalysis, Vol. 70, Elsevier, Amsterdam, 1992.
240. H. P. Bonzel, *Surf. Sci. Rep.* **1987**, *8*, 43.
241. H. P. Bonzel, A. M. Bradshaw, G. Ertl (Eds.), *Physics and Chemistry of Alkali Metal Adsorption*, Material Science Monographs Vol. 57, Elsevier, Amsterdam, 1989.
242. M. Kiskinova, G. Pirug, H. P. Bonzel, *Surf. Sci.* **1983**, *133*, 321.
243. M. Scheffler, C. Droste, A. Fleszar, F. Maca, G. Wachutka, G. Barzel, *Physica B* **1991**, *172*, 143.
244. L. J. Whitman, W. Ho, *J. Chem. Phys.* **1989**, *90*, 6018.
245. H. Pfnür, P. Feulner, D. Menzel, *J. Chem. Phys.* **1983**, *79*, 4613.
246. J. E. Crowell, E. L. Garfunkel, G. A. Somorjai, *Surf. Sci.* **1982**, *121*, 303.
247. T. E. Madey, C. Benndorf, *Surf. Sci.* **1985**, *164*, 602.
248. F. Sette, J. Stohr, E. B. Kollin, D. J. Dwyer, J. L. Gland, J. L. Robbins, A. L. Johnson, *Phys. Rev. Lett.* **1985**, *54*, 935.
249. J. G. Chen, W. Erley, H. Ibach, *Surf. Sci.* **1989**, *224*, 215.
250. J. L. Gland, R. J. Madix, R. W. McCabe, C. Demaggio, *Surf. Sci.* **1984**, *143*, 46.
251. T. Tüshaus, W. Berndt, H. Conrad, A. M. Bradshaw, B. Persson, *Appl. Phys. A* **1990**, *51*, 91.
252. F. M. Hoffmann, *Surf. Sci. Rep.* **1983**, *3*, 107.
253. H. Conrad, G. Ertl, J. Koch, E. E. Latta, *Surf. Sci.* **1974**, *43*, 462.

254. H. Conrad, G. Ertl, J. Küppers, E. E. Latta, *Surf. Sci.* **1977**, *65*, 235.
255. H. Ohtani, M. A. Van Hove, G. A. Somorjai, *Surf. Sci.* **1987**, *187*, 372.
256. W. K. Kuhn, J. Szanyi, D. W. Goodman, *Surf. Sci. Lett.* **1992**, *274*, L611.
257. X. Guo, J. T. Yates, Jr., *J. Chem. Phys.* **1989**, *90*, 6761.
258. G. Doyen, G. Ertl, *Surf. Sci.* **1974**, *43*, 197.
259. G. Rupprechter, T. Dellwig, H. Unterhalt, H.-J. Freund, *J. Phys. Chem. B* **2001**, *105*, 3797.
260. S. Surnev, M. Sock, M. G. Ramsey, F. P. Netzer, M. Wiklund, M. Borg, J. N. Andersen, *Surf. Sci.* **2000**, *470*, 171.
261. T. Giessel, O. Schaff, C. J. Hirschmugl, V. Fernandez, K. M. Schindler, A. Theobald, S. Bao, R. Lindsay, W. Berndt, A. M. Bradshaw, C. Baddeley, A. F. Lee, R. M. Lambert, D. P. Woodruff, *Surf. Sci.* **1998**, *406*, 90.
262. D. Loffreda, D. Simon, P. Sautet, *Surf. Sci.* **1999**, *425*, 68.
263. H. Conrad, G. Ertl, J. Küppers, *Surf. Sci.* **1978**, *76*, 323.
264. X. Guo, A. Hoffman, J. T. Yates, Jr., *J. Chem. Phys.* **1989**, *90*, 5787.
265. P. Gelin, A. Siedle, J. T. Yates, *J. Phys. Chem.* **1984**, *88*, 2978.
266. B. Bourguignon, S. Carrez, B. Dragnea, H. Dubost, *Surf. Sci.* **1998**, *418*, 171.
267. D. R. Rainer, M. C. Wu, D. I. Mahon, D. W. Goodman, *J. Vac. Sci. Technol. A* **1996**, *14*, 1184.
268. H. Unterhalt, P. Galletto, M. Morkel, G. Rupprechter, H. J. Freund, *Phys. Stat. Sol. A* **2001**, *188*, 1495.
269. A. Berko, G. Menesi, F. Solymosi, *J. Phys. Chem.* **1996**, *100*, 17732.
270. B. J. McIntyre, M. Salmeron, G. A. Somorjai, *J. Vac. Sci. Technol. A* **1993**, *11*, 1964.
271. A. Ortega, F. M. Hoffmann, A. M. Bradshaw, *Surf. Sci.* **1982**, *119*, 79.
272. J. Evans, B. E. Hayden, G. Lu, *Surf. Sci.* **1996**, *360*, 61.
273. R. Raval, S. Haq, M. A. Harrison, G. Blyholder, D. A. King, *Chem. Phys. Lett.* **1990**, *167*, 391.
274. A. M. Bradshaw, F. M. Hoffmann, *Surf. Sci.* **1975**, *52*, 449.
275. T. Dellwig, G. Rupprechter, H. Unterhalt, H.-J. Freund, *Phys. Rev. Lett.* **2000**, *85*, 776.
276. M. Bäumer, H.-J. Freund, *Prog. Surf. Sci.* **1999**, *61*, 127.
277. K. H. Hansen, T. Worren, S. Stempel, E. Lægsgaard, M. Bäumer, H.-J. Freund, F. Besenbacher, I. Stensgaard, *Phys. Rev. Lett.* **1999**, *83*, 4120.
278. M. Frank, M. Bäumer, *Phys. Chem. Chem. Phys.* **2000**, *2*, 3723.
279. S. K. Shaikhutdinov, M. Heemeier, M. Bäumer, T. Lear, D. Lennon, R. J. Oldman, S. D. Jackson, H.-J. Freund, *J. Catal.* **2001**, *200*, 330.
280. G. Rupprechter, H.-J. Freund, *Top. Catal.* **2000**, *14*, 3.
281. G. Rupprechter, J. J. Calvino, C. López-Cartes, M. Fuchs, J. M. Gatica, J. A. Pérez-Omil, K. Hayek, S. Bernal, *Proceedings 12th International Congress on Catalysis*, Granada, 2000, p. 2021.
282. I. V. Yudanov, R. Sahnoun, K. M. Neyman, N. Rosch, J. Hoffmann, S. Schauermann, V. Johanek, H. Unterhalt, G. Rupprechter, J. Libuda, H. J. Freund, *J. Phys. Chem. B* **2003**, *107*, 255.
283. K. Wolter, O. Seiferth, H. Kuhlenbeck, M. Bäumer, H.-J. Freund, *Surf. Sci.* **1998**, *399*, 190.
284. G. C. Cabilla, A. L. Bonivardi, M. A. Baltanas, *Catal. Lett.* **1998**, *55*, 147.
285. W. H. Weinberg, in *Kinetics of Interface Reactions*, Springer Series in Surfaces Sciences, Vol. 8, Springer, Heidelberg, 1987, p. 94.
286. M. Morkel, G. Rupprechter, H. J. Freund, *J. Chem. Phys.* **2003**, *119*, 10853.
287. J. C. Tracy, *J. Chem. Phys.* **1972**, *56*, 2736.
288. J. B. Benziger, R. J. Madix, *Surf. Sci.* **1979**, *79*, 394.
289. M. Kiskinova, D. W. Goodman, *Surf. Sci.* **1981**, *108*, 64.
290. B. E. Koel, D. E. Peebles, J. M. White, *Surf. Sci.* **1983**, *125*, 709.
291. K. Klier, A. C. Zettlemoyer, J. H. Leidheiser, *J. Chem. Phys.* **1970**, *52*, 589.
292. R. S. Bordoli, J. C. Vickerman, J. Wolstenholme, *Surf. Sci.* **1979**, *85*, 244.
293. F. Labohm, C. W. R. Engelen, O. L. J. Gijzeman, J. W. Geus, G. A. Bootsma, *J. Chem. Soc., Faraday Trans.* **1982**, *78*, 2435.
294. H. Pfnür, P. Feulner, H. A. Engelhardt, D. Menzel, *Chem. Phys. Lett.* **1978**, *59*, 481.
295. G. Lauth, T. Solomun, W. Hirschwald, K. Christmann, *Surf. Sci.* **1989**, *210*, 201.
296. J. C. Tracy, *J. Chem. Phys.* **1972**, *56*, 2748.
297. G. Wedler, I. Ganzmann, D. Borgmann, *Appl. Surf. Sci.* **1993**, *68*, 335.
298. H. Rinne, PhD Thesis, Universität Hannover, 1974.
299. H. Conrad, G. Ertl, E. E. Latta, *Surf. Sci.* **1974**, *41*, 435.
300. R. J. Behm, K. Christmann, G. Ertl, *Surf. Sci.* **1980**, *99*, 320.
301. M. Ehsasi, K. Christmann, *Surf. Sci.* **1988**, *194*, 172.
302. G. Lauth, E. Schwarz, K. Christmann, *J. Chem. Phys.* **1989**, *91*, 3729.
303. K. H. Ernst, PhD Thesis, Freie Universität Berlin, 1990.
304. R. Miranda, S. Daiser, K. Wandelt, G. Ertl, *Surf. Sci.* **1983**, *131*, 61.
305. M. Grunze, P. A. Dowben, R. G. Jones, *Surf. Sci.* **1984**, *141*, 455.
306. M. Golze, M. Grunze, W. Unertl, *Prog. Surf. Sci.* **1986**, *22*, 101.
307. J. Lapujoulade, K. S. Neil, *Surf. Sci.* **1973**, *35*, 288.
308. K. Christmann, *Z. Naturforsch., A: Phys. Sci.* **1979**, *34*, 22.
309. J. Lapujoulade, K. S. Neil, *J. Chem. Phys.* **1972**, *57*, 3535.
310. V. Penka, K. Christmann, G. Ertl, *Surf. Sci.* **1984**, *136*, 307.
311. H. J. Robota, W. Vielhaber, M. C. Lin, J. Segner, G. Ertl, *Surf. Sci.* **1985**, *155*, 101.
312. K. Christmann, G. Ertl, T. Pignet, *Surf. Sci.* **1976**, *54*, 365.
313. B. Poelsema, K. Lenz, L. S. Brown, L. K. Verheij, G. Comsa, *Verhandl. DPG* **1986**, *5*, 1378.
314. T. E. Madey, *Surf. Sci.* **1973**, *36*, 281.
315. P. Hofmann, R. Unwin, W. Wyrobisch, A. M. Bradshaw, *Surf. Sci.* **1978**, *72*, 635.
316. P. H. Holloway, J. B. Hudson, *Surf. Sci.* **1974**, *43*, 123.
317. F. P. Netzer, R. A. Wille, *Surf. Sci.* **1978**, *74*, 547.
318. J. Benziger, R. J. Madix, *Surf. Sci.* **1980**, *94*, 119.
319. G. Ertl, M. Neumann, K. M. Streit, *Surf. Sci.* **1977**, *64*, 393.
320. T. E. Madey, J. T. Yates, *Nuovo Cimento* **1969**, *5*, 483.
321. B. J. Hopkins, S. Usamiin, in *The Structure and Chemistry of Solid Surfaces*, G. A. Somorjai (Ed.), Wiley, New York, 1968.
322. M. Bowker, D. A. King, *J. Chem. Soc., Faraday Trans. I* **1979**, *75*, 2100.
323. F. Bozso, G. Ertl, M. Grunze, M. Weiss, *J. Catal.* **1977**, *49*, 18.
324. W. M. Daniel, J. M. White, *Surf. Sci.* **1986**, *171*, 289.
325. M. Trenary, K. J. Uram, J. T. Yates, *Surf. Sci.* **1985**, *157*, 512.
326. X. Zi, L. Surnev, J. T. Yates, unpublished results.
327. T. Yamada, R. S. Zhai, Y. Iwasawa, K. Tamaru, *Surf. Sci.* **1988**, *205*, 82.
328. M. Kiskinova, A. Szabo, J. T. Yates, *J. Chem. Phys.* **1988**, *89*, 7599.
329. M. P. Kiskinova, A. Szabo, J. T. Yates, *Surf. Sci.* **1990**, *226*, 237.

330. J. L. Brand, M. V. Arena, A. A. Deckert, S. M. George, *J. Chem. Phys.* **1990**, *92*, 4483.
331. S. Johnson, R. J. Madix, *Surf. Sci.* **1981**, *108*, 77.
332. M. L. Burke, R. J. Madix, *Surf. Sci.* **1990**, *237*, 1.

5.1.2

Reactivity Index Relations in Theoretical Heterogeneous Catalysis

Rutger A. van Santen and Matthew Neurock*

5.1.2.1 Introduction

In the middle of the last century the catalysis community rallied behind different concepts in order to describe structure–reactivity relationships. The "electronic factor", for example, was considered an important parameter or index by which one could begin to correlate measured reactivity over different transition metals or alloy surfaces. In essence, it was believed that the electronic local density of states at the Fermi level, often deduced from bulk measurements could be correlated with the interaction energy of adsorbed molecules [1].

The field of surface science later demonstrated that not only were the electronic and atomic structure of surface and bulk significantly different but, more importantly, that the interaction between the adsorbate and the surface is a localized event [2]. The structures of adsorbed molecules often have great similarity with those in corresponding organometallic complexes. The structural parameters that relate the interaction energy to the detailed topology of the adsorption complex are considered to be quite important.

Whereas the proposal to classify catalytic reactions according to their structure sensitivity or insensitivity is now considered classical [3], its explanation had to wait until recently where present-day theory and computation is able to complement experimental efforts and help to establish quantitative predictions along with fundamental experiments to actually demonstrate these structure–reactivity relationships. The early concepts were mainly deduced from macroscopic observations of particle size dependence [4] (see Fig. 1), or interpretations of alloy effects in terms of the ensemble effect [7] (Fig. 2).

Within this historic context, it is somewhat ironic that the present widely accepted index used to describe the reactivity of a transition metal surface is the average position of the energy of the d-valence electron band $\bar{\varepsilon}_d$ projected onto the surface metal atoms [8]. An example of such relationship is given in Fig. 3.

This relationship of adsorption strength to electronic structure seems to suggest that we have made a U-turn back to the days of the paradigmic electronic factor days

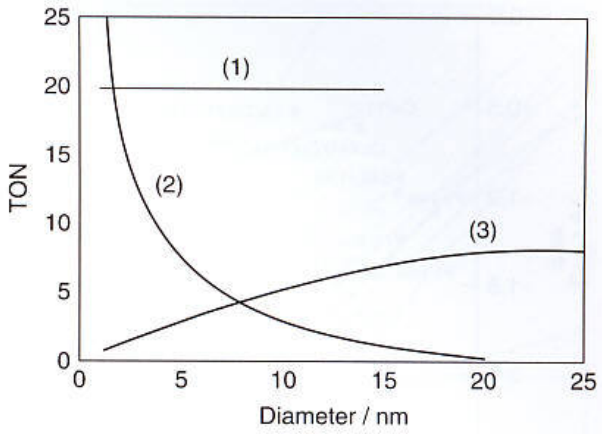

Fig. 1 Turnover number (TON) for selected reactions versus particle size. (1) Benzene hydrogenation on Pt/SiO_2. (2) Ethane hydrogenolysis on Pt/SiO_2. (3) CO hydrogenation on Ru/Al_2O_3. (From Ref. [5]).

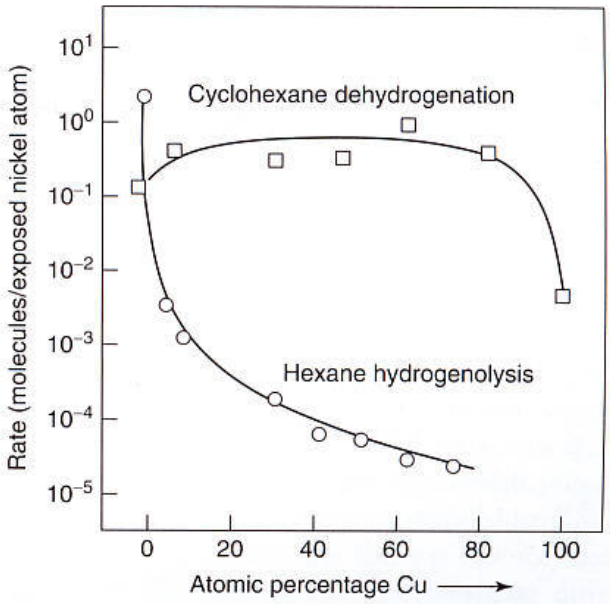

Fig. 2 Cyclohexane dehydrogenation and hexane cracking conversion as a function of the Cu/Ni ratio of the catalyst [6].

with the local density of states at the Fermi level replaced by $\bar{\varepsilon}_d$.

An important task for theory then is to elucidate the chemical reasons, why such a relationship is justified and how it fits within reactivity theories that clearly demonstrate also the importance of the degree of local environment, as coordinative unsaturation of surface atoms and their local arrangement. One of the aims of this chapter is to help elucidate the chemical bonding principles that control this relationship and to establish the conditions for which they hold.

A key concept that provides this link is the localization energy of electrons in the orbitals of a particular atom,

* Corresponding author.

References see page 1445